TECHNICAL MEMORANDUM

32

The performance of the ECMWF model in 50 day integrations

U. Cubasch

Research Department

May 1981

European Centre for Medium-Range Weather Forecasts
Europäisches Zentrum für mittelfristige Wettervorhersage
Centre européen pour les prévisions météorologiques à moyen

Abstract

A preliminary assessment is made from a number of 50 day integrations to find out the sensitivity of extended range predictions to resolution, physical parameterisation and initial data.

1. INTRODUCTION

After the first few months of operational forecasting at the ECMWF (1979) a number of systematic errors in the forecasts were found in an ensemble mean of those predictions. Since these errors are equivalent to those of a mean calculated from an extended range prediction run, but these long range integrations demanded less effort in computer time, the subsequent fine tuning of the physical parameterisation was carried out using 50 day integrations.

In this paper a re-evaluation of these 50 day integrations is carried out to find the sensitivity of the model to changes in the parameterisation, resolution and initial data.

The results can be summarized as follows:

The systematic error (the overdevelopment of pressure systems) is hardly dependent on the physical parameterisation package.

This systematic error appears not to be dependent on an increased vertical resolution but seems to amplify with increased horizontal resolution.

The systematic error shows the same order of magnitude in both spectral and gridpoint model.

All models adjust after about 20 days to a mean model climate whose atmosphere is colder (except for GFDL physics) and dryer than in the analysis.

The impact of initial data is still perceptible in a 24 day mean taken from day 24 of the integration period. Differences in the height field between individual forecasts reach in the mean the same order of magnitude as differences of each run to observed.

The initial data seem not be be responsible for the systematic error

The rainfall distribution shows a high sensitivity to the initial humidity field.

2. A COMPARISON OF THREE PARAMETERISATION SCHEMES

2.1 Introduction

Each development of a new parameterization of subgrid scale atmospheric processes involves a comparison of this new scheme against the old one. The first operational EC parameterization scheme was thoroughly tested against the one developed by GFDL (Hollingsworth et al 1979), but only for the forecast period of 10 days.

The revision of the EC parameterization scheme end of 1979 resulted in the 2. operational physical package currently used in the operational model. The following paper will try to highlight some of the differences between these parameterization schemes as found in an extended prediction run for 50 days.

2.2 Description of the experiments

Three 50-day integrations, starting on the initial date 16.1.79 with the identical dataset (INES), also using the same adiabatic spectral model (resolution: horizontal: T40, vertical 15 levels), but with three different physical parameterization schemes, have been performed.

These three parameterization schemes were:

Exp.1 First operational physical (details in Hollingsworth et al,1979)) (EC I)

Exp.2 Second operational physics (details in Tiedtke et al, 1979) (EC II)

Exp.3 GFDL - Physics (details also in Hollingsworth, et al,1979) (GFDL)

While the difference between the first and second operational EC physics lies in the formulation of the vertical exchange, the GFDL physics approach is less sophisticated and represents an earlier state of parameterisation.

2.3 Time evolution of meteorological parameters

Due to a loss of data the curve for Exp. 2 has had to be reconstructed from a similar run using a different initial dataset for the same date. We find in the global average precipitable water content (which is a function of the humidity) (Fig. 1) in the first 10 days of the integration a sharp increase in the humidity caused by a deficiency of the dataset used. It then settles for each experiment at its own individual level which is highest for Exp. 3 and lowest for Exp. 1. The difference in humidity between the first and second operational physics is about 20%.

The temperature evolution (Fig. 2) starts with a remarked drop in the first 10 days and then stays on a lower level than observed. The GFDL physical atmosphere (Exp.3) is only about $2^{o}K$ lower than observed, while both EC

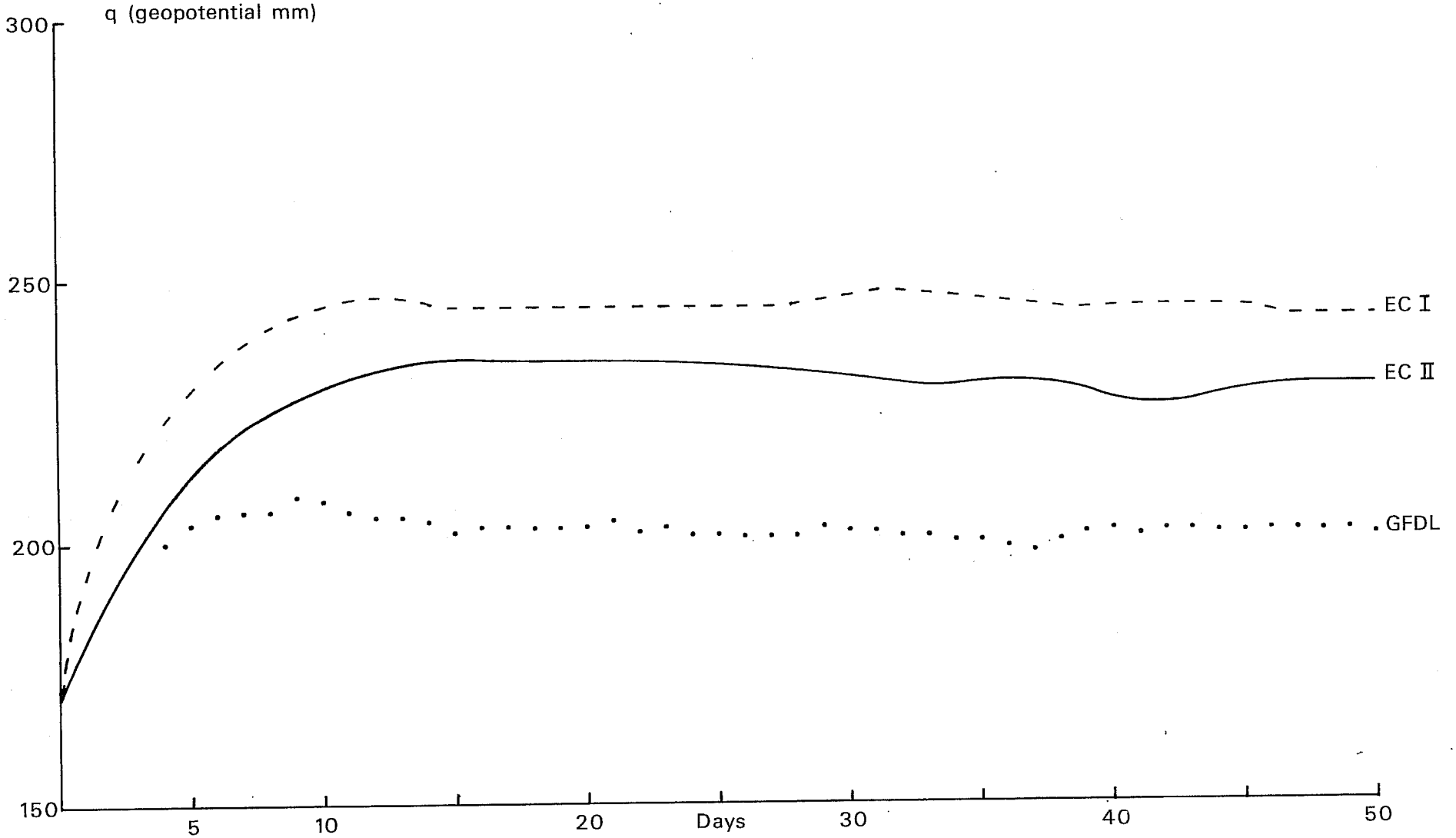

Fig. 1 Time evolution of globally averaged precipitable water

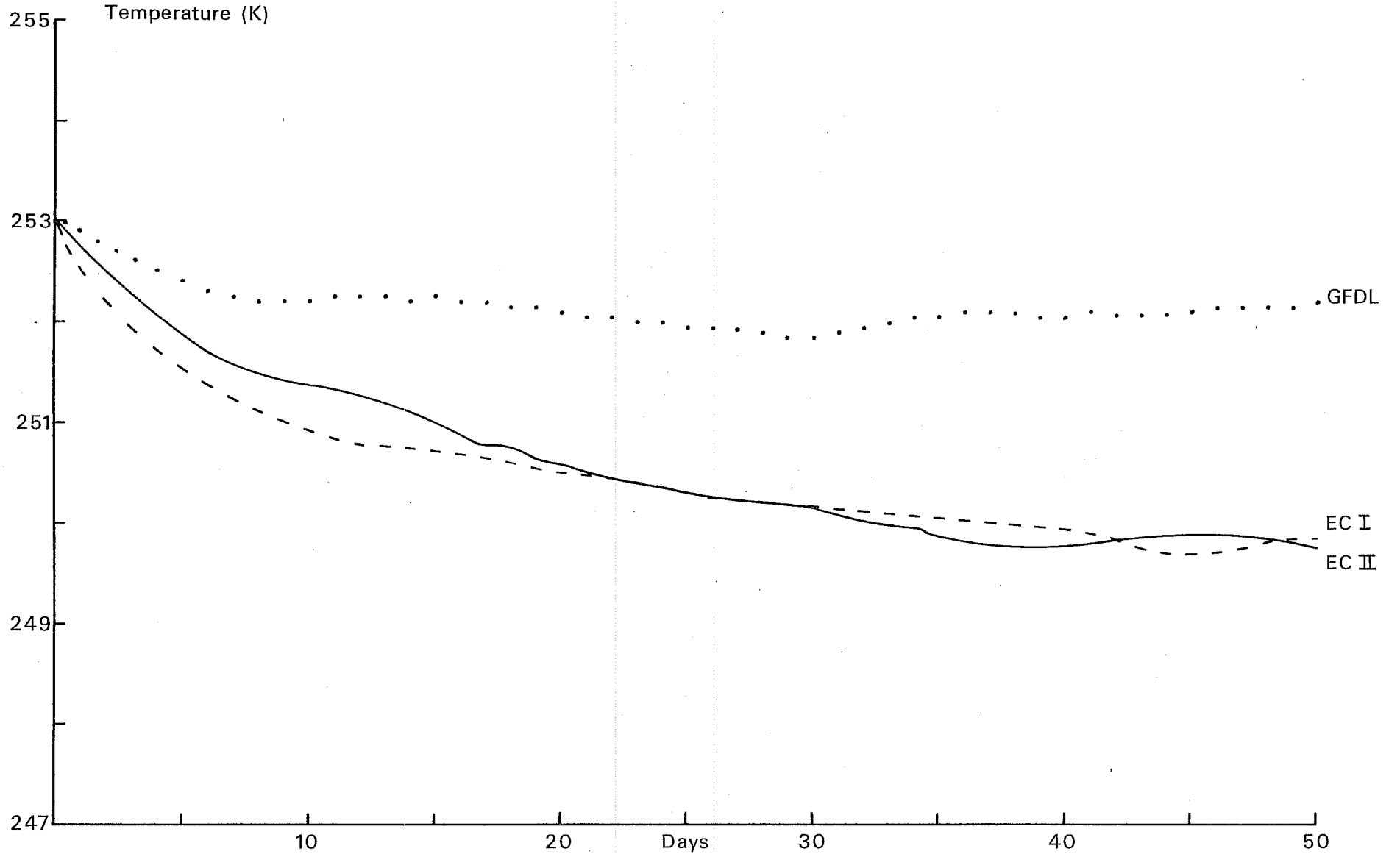

Fig. 2 Time evolution of the globally average temperature

physics cool the atmosphere with about $4^{o}K$/50 days. The switch from the first to the second operational physics brings no improvement to the temperature pattern. Also in the time evolution of the kinetic energy (Fig. 3) we find a close agreement between Exp. 1 and Exp. 2, but the level of this energy is lower than observed. Exp. 3 on the other hand almost keeps the observed level of kinetic energy.

2.4 Synoptical evolution

The mean synoptic (Fig. 4) situation for February 1979 at 1000 mb is dominated by one low south of Greenland and two others in the North Pacific Region, one of them on the coast before Alaska and the other one near the Bering Strait. This pattern is coarsely reproduced in all experiments but neither the positions nor the central pressure is well simulated. The split of the Pacific low is only reproduced by Exp. 2. The high over Greenland in Exp. 3 seems to be caused by deficiencies in the plotting package.

The variance by transient waves (Fig. 5) as means of 24 days in 100 mb height puts the centres of mean activity over the Pacific, the North Atlantic and the Balticum. These variance centres are generally smaller than analysed and too weak.

The 500 mb height field (Fig. 6) shows a wavenumber two pattern with the low over Siberia and North America and a ridge on the Bering Strait. Over Europe we observe a split in the flow-pattern with one branch reaching to the Sahara and one going north to Scandinavia.

The whole flow-pattern is only poorly reproduced in the experiments. The high in the Bering Strait is only weakly simulated in Exp. 3. The split of the flow over Europe is not present at all in Exp. 3 and only just evident in Exp. 1 and Exp. 2.

The difference from climate (Fig. 7) of 500 mb height shows for all experiments a negative height deviation over the oceans, while both EC schemes (Exp. 2, Exp. 3) produce a positive one over North America and the polar region.

The spectrum of height (Fig. 8) reveals that the old EC parameterization scheme seems to favour wavenumber 4 and 5, while the new one exaggerates wavenumber 2, but produces a too weak wavenumber 1, which, on the other hand is too strong with the GFDL physics.

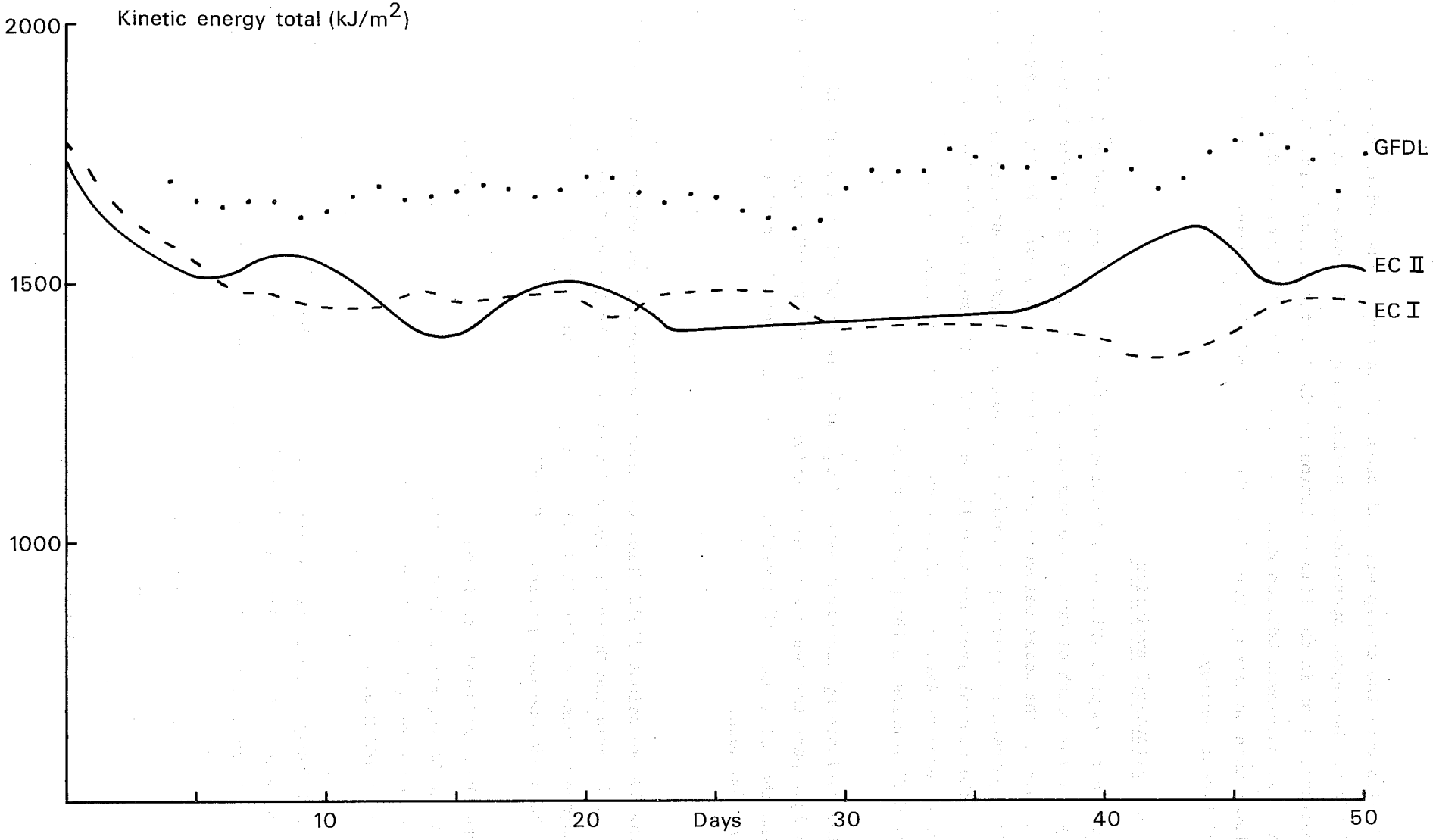

Fig. 3 Time evolution of the globally averaged kinetic energy

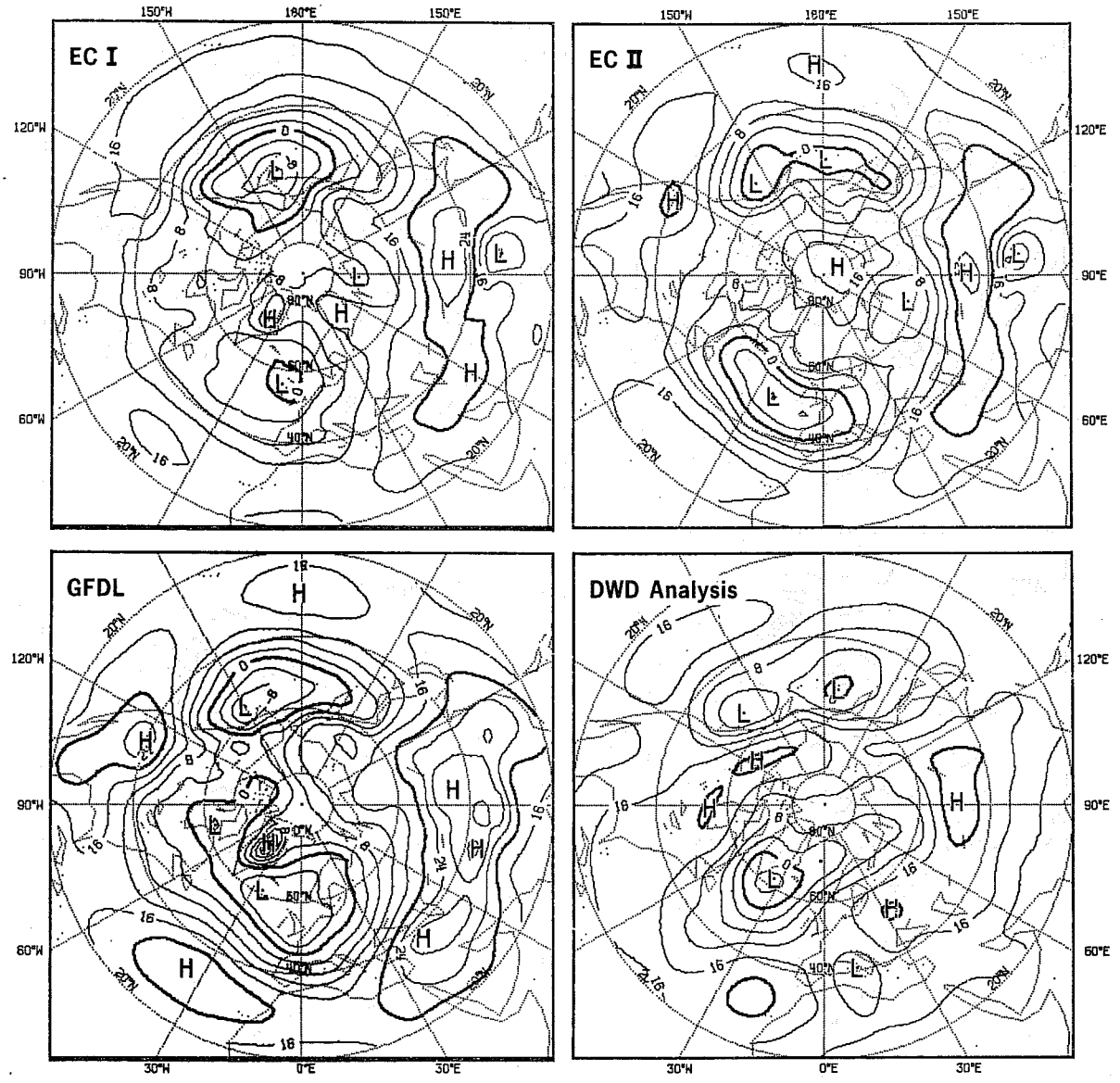

Fig. 4 24 day mean 1000 mb height field (contouring interval: 40m).

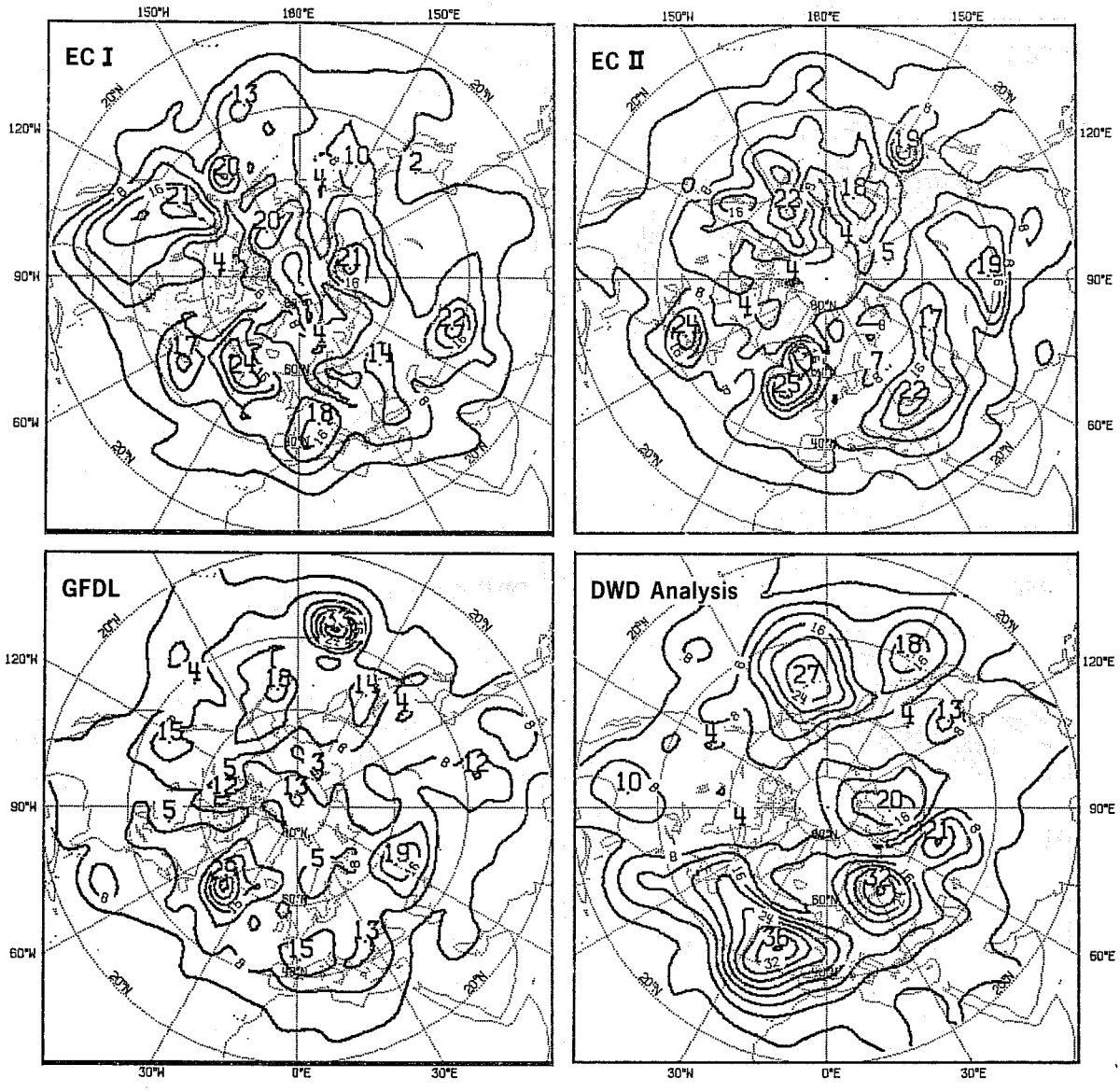

Fig. 5 24 day mean of the variance by transient waves in 1000 mb height.

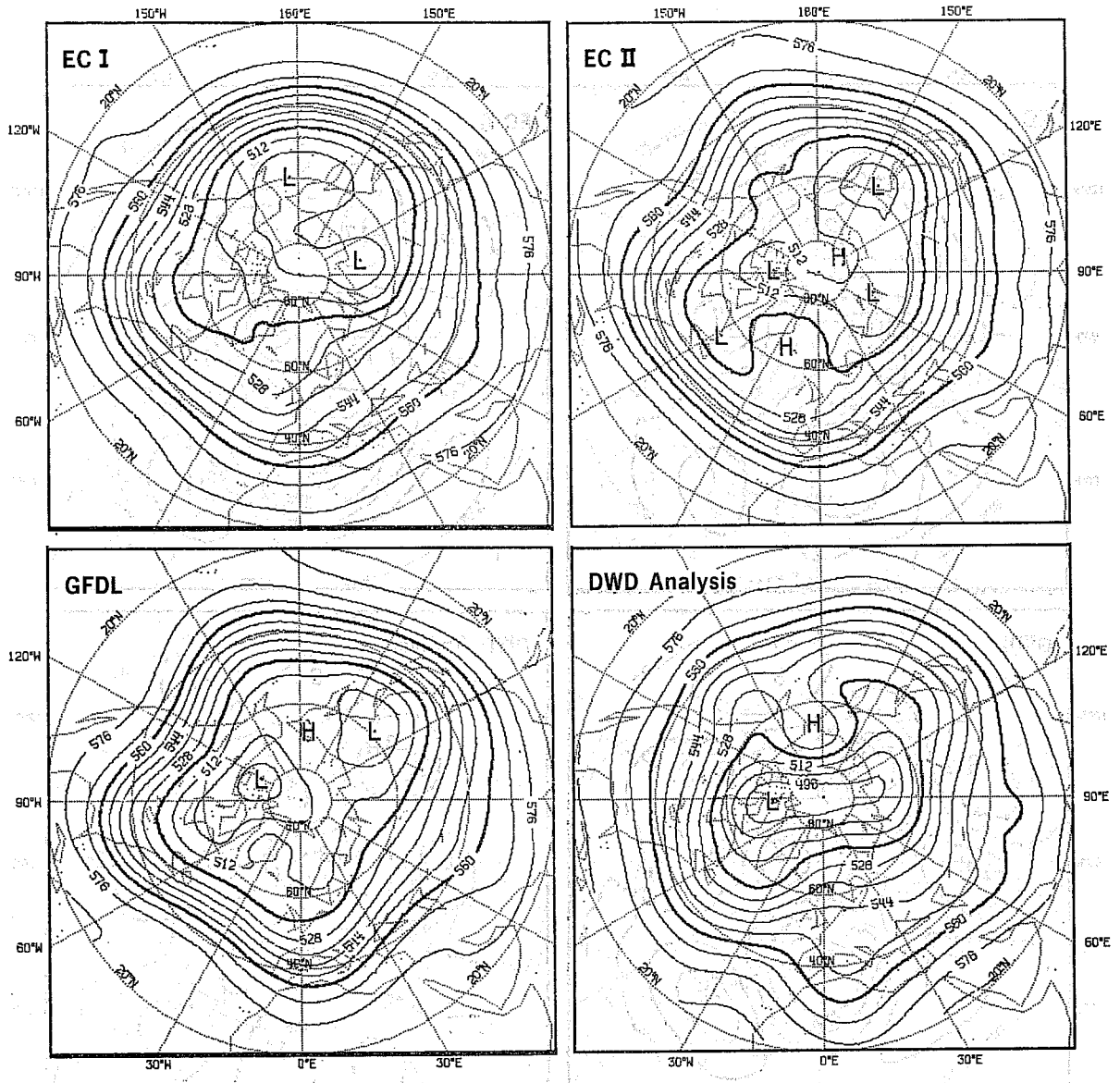

Fig. 6 24 day mean 500 mb height field (contouring interval: 80m).

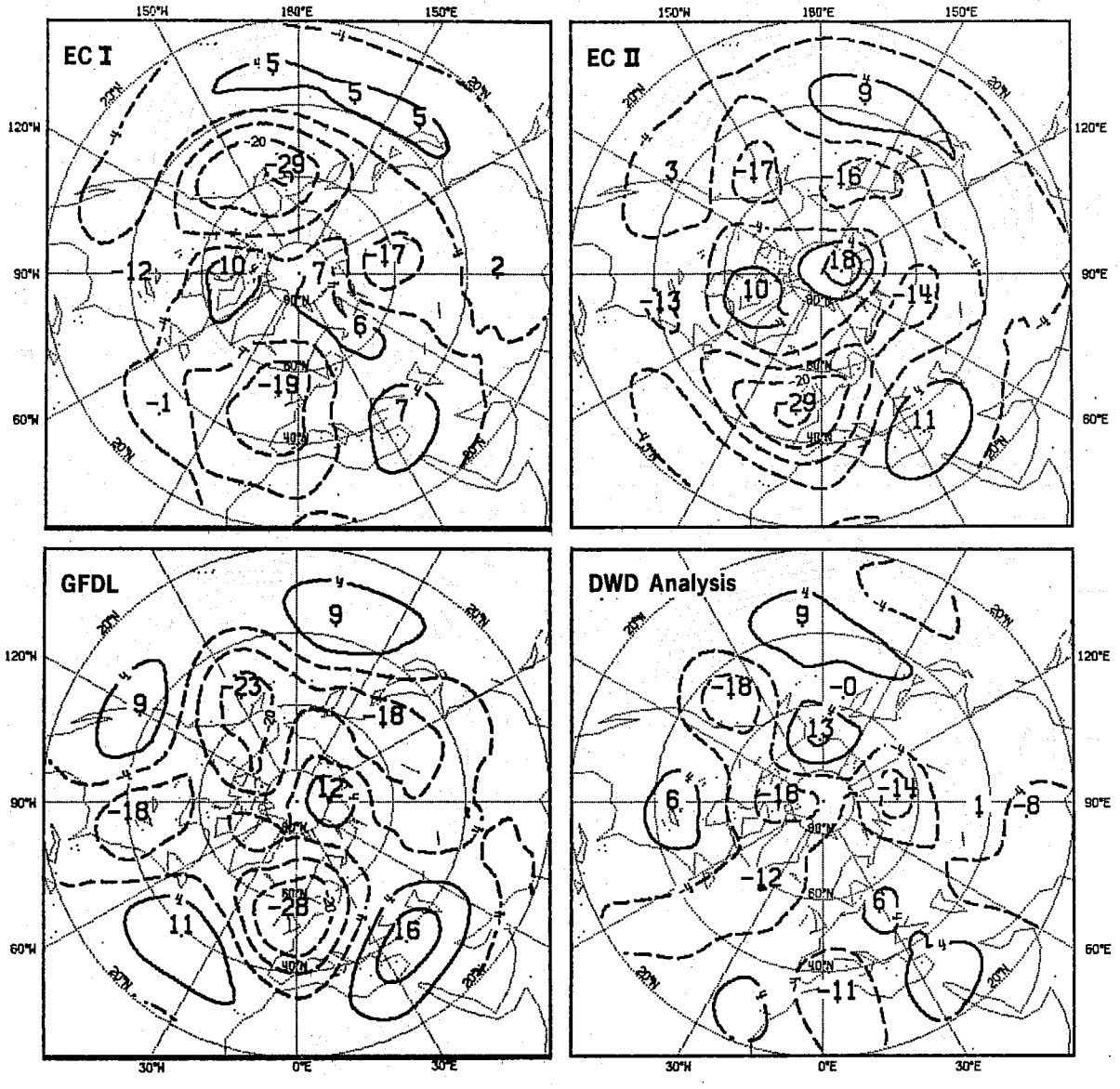

Fig. 7 The difference of the 500 mb mean height field to climate.

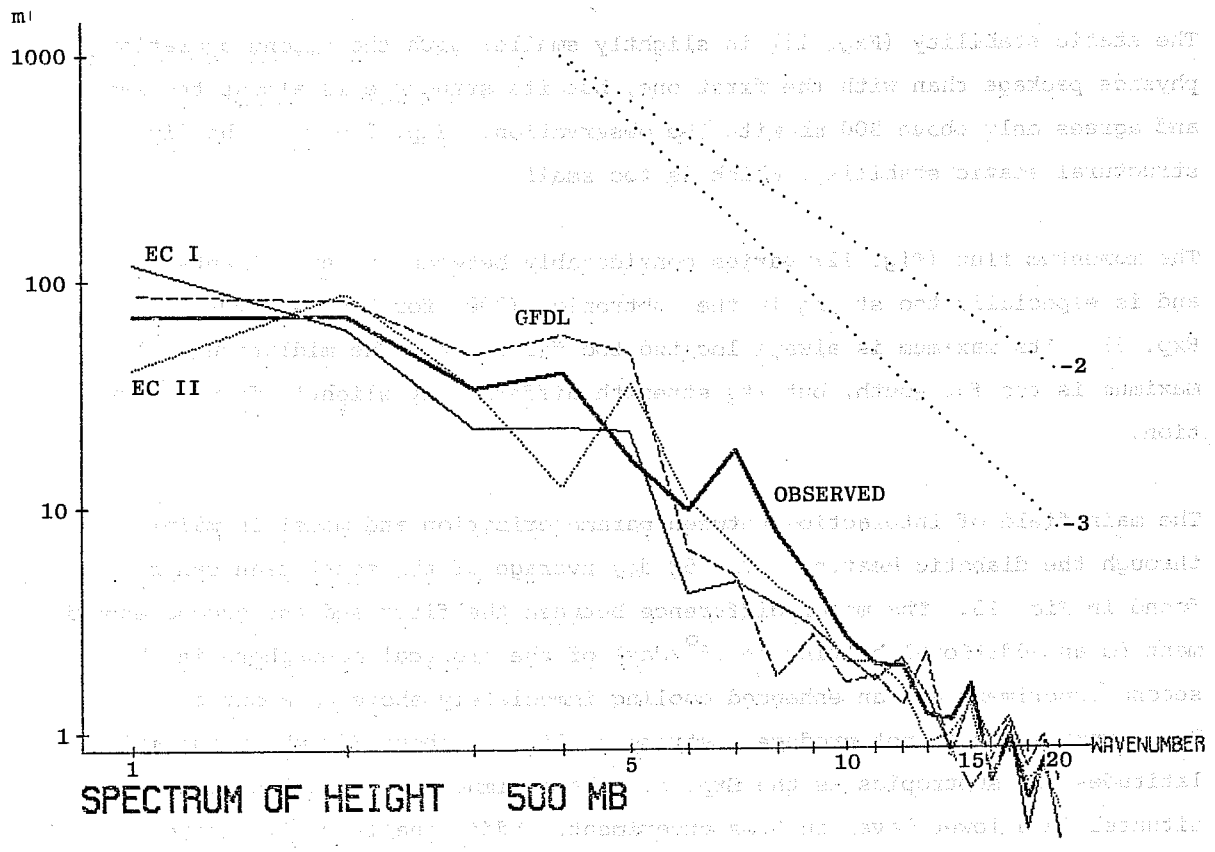

Fig. 8 The spectrum of height in 500 mb (standing waves).

The zonal mean of zonal wind (Fig. 9) displays in all three experiments a jet with reasonable strength but which is shifted too far north and, in both EC schemes,is situated at too high an altitude. A meridional crosssection of the deviational zonal mean temperature from observed (Fig. 10) shows the whole troposphere to be too cold in all experiments. The boundary layer in higher latitudes is about 6 - 8^{o} too warm. The stratosphere is generally too cold with the more recent EC physics giving results about 50% colder one than the other parameterization schemes.

The static stability (Fig. 11) is slightly smaller with the second operational physics package than with the first one, but its structure is almost the same and agrees only above 500 mb with the observation. Exp. 3 gives a hardly structural static stability, which is too small.

The momentum flux (Fig. 12) varies considerably between the experiments and is especially too strong in the subtropics (200% for Exp. 2, 300% for Exp. 3). Its maximum is always located too far north. The midlatitudinal maximum is too far south, but its strength differs only slightly from observation.

The main field of interaction between parameterization and model is mainly through the diabatic heating. The 50 day average of the zonal mean can be found in Fig. 13. The major difference between the first and the second experiment is an additional heating (+ .5^{o}/day) of the tropical atmosphere in the second experiment and an enhanced cooling immediately above at about σ = .3. Both experiments do not produce a strong cooling in about 800 mb in the midlatitudes and subtropics as the Exp. 3. The maximum of tropical heating is situated in a lower level in this experiment. Additionally we find here a large cooling in the boundary layer.

The eddy available potential energy (Fig. 14) reflects these heating differences. The abundant available potential energy in the stratosphere in Exp. 1 has been halved in Exp. 2 (which agrees better with observed) while the amount in the troposphere has slightly increased, but not enough compared to the analysis. The GFDL experiment meets about the right level of available potential energy in the troposphere (though not in the right locations), but predicts more than twice the observed value in the stratosphere.

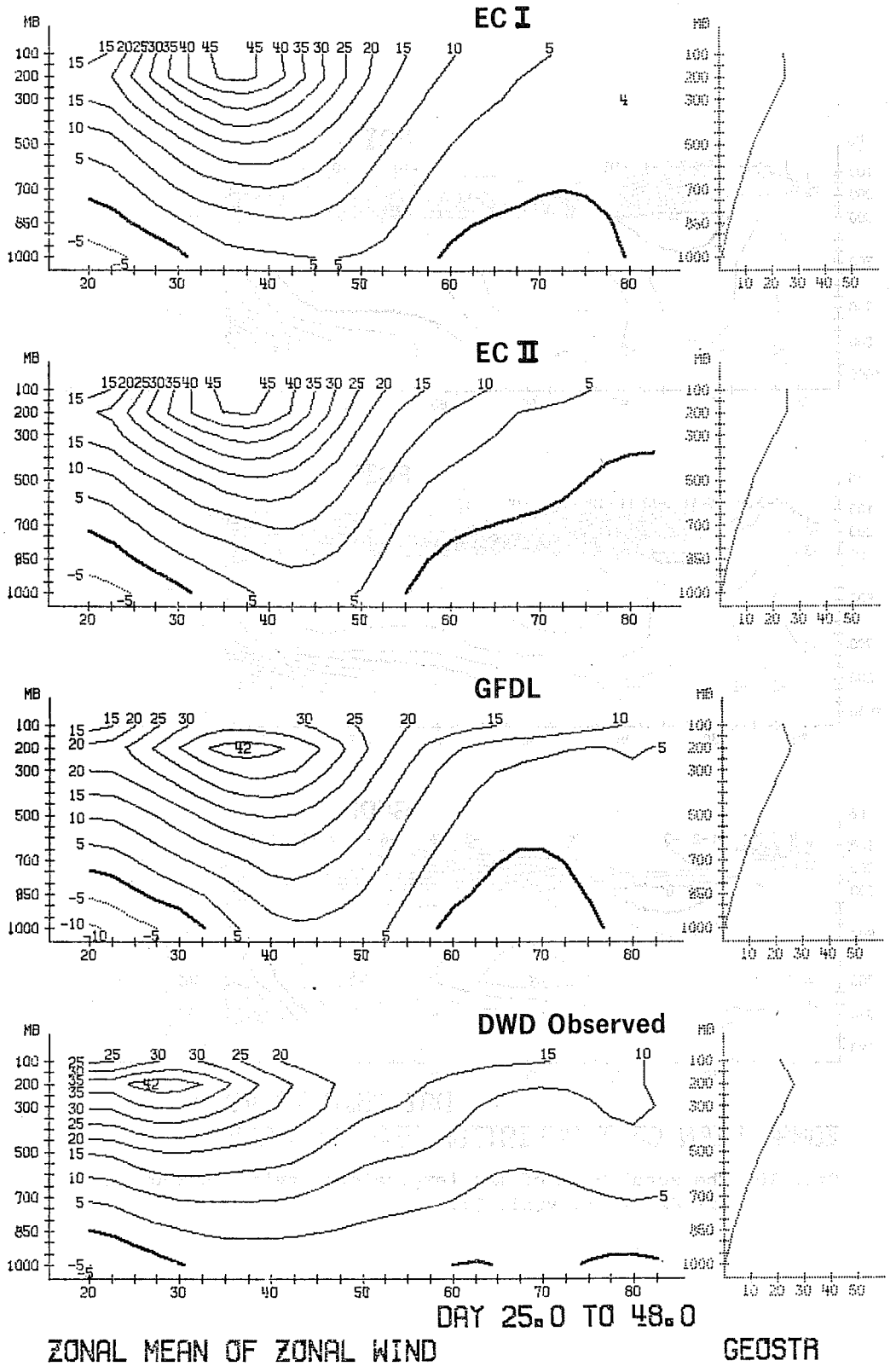

Fig. 9 The zonal mean of the zonal wind (24 day mean).

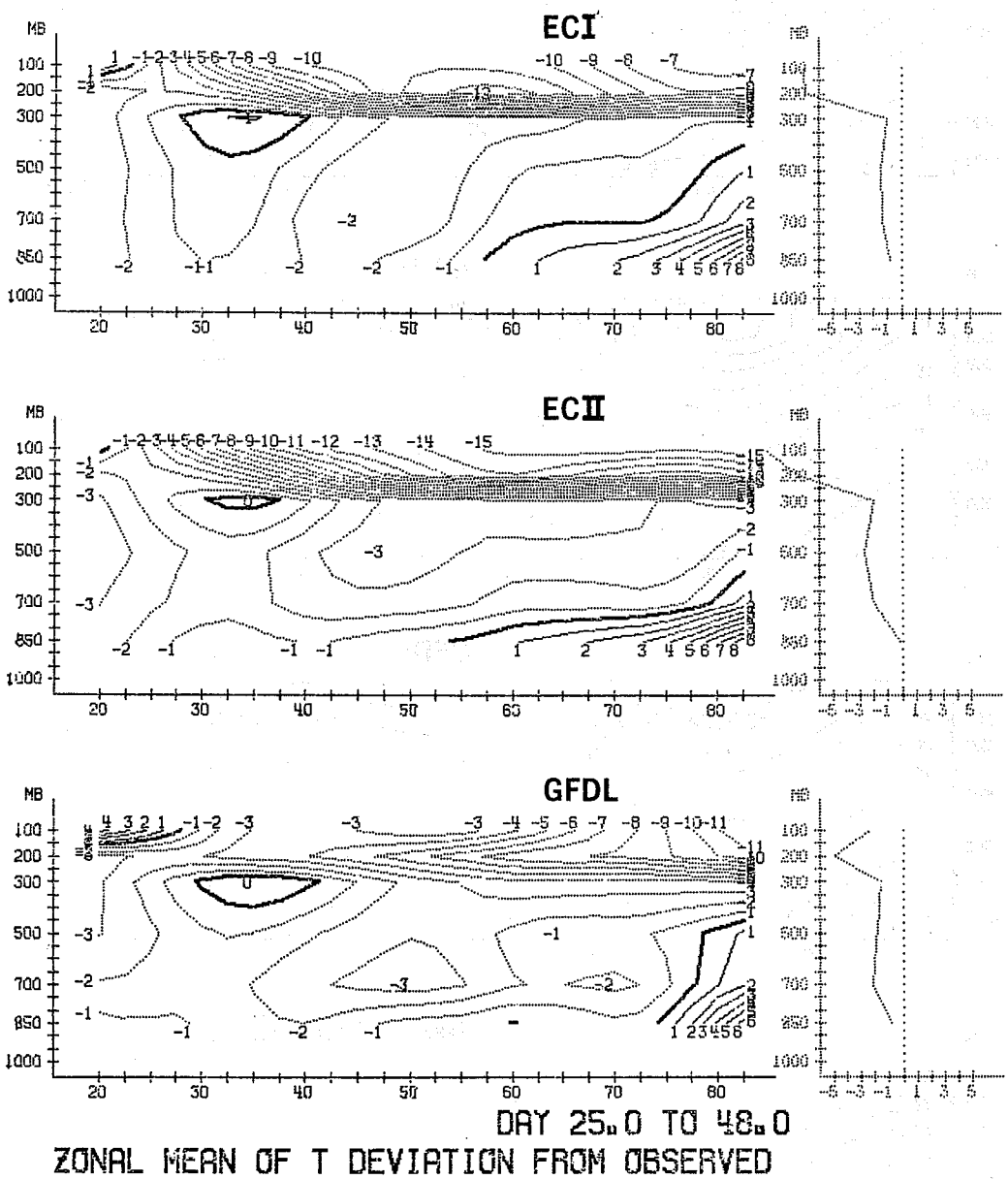

Fig. 10 The zonal mean of the temperature deviation from observed (24 day mean, unit: K).

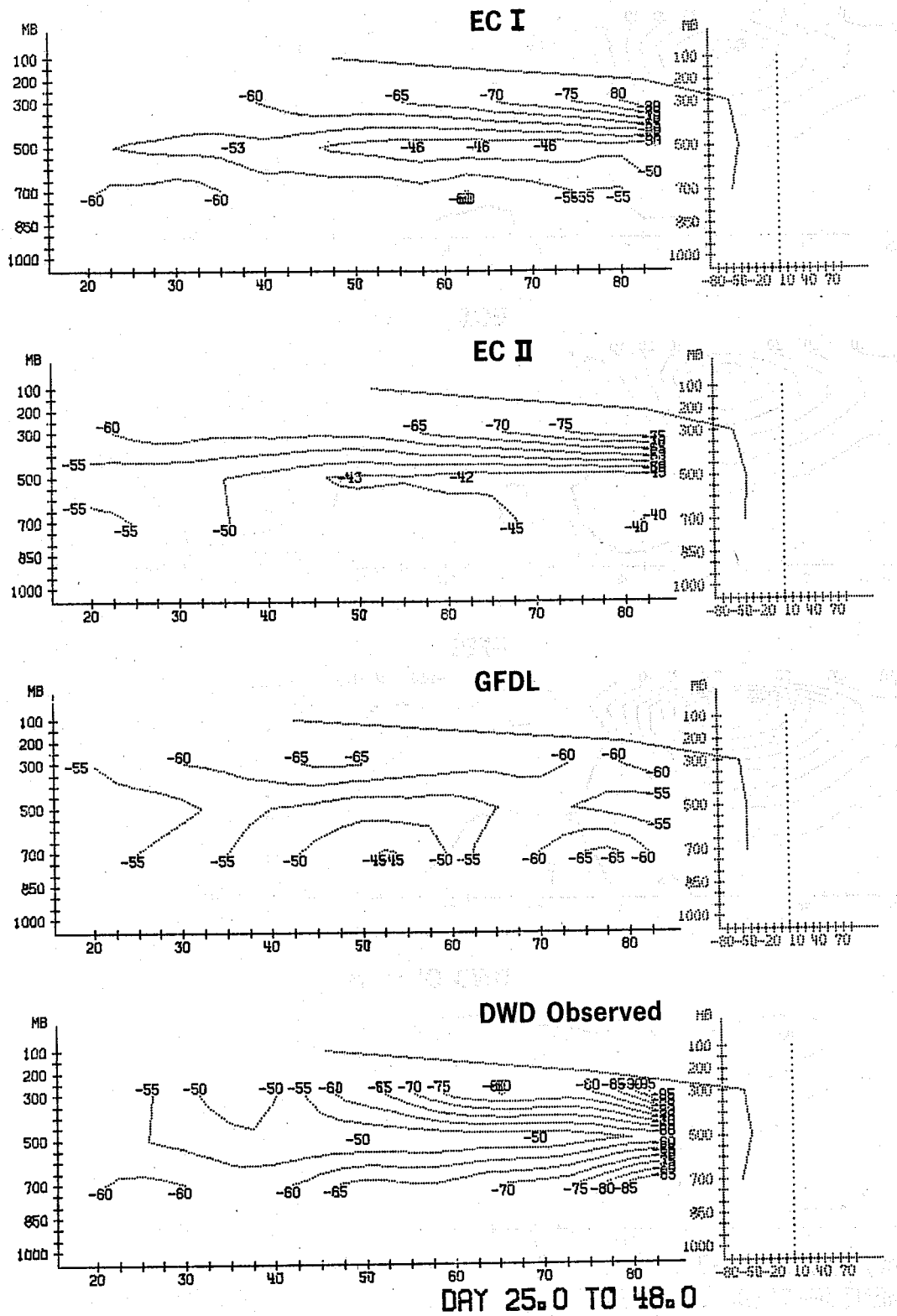

Fig. 11 The 24 day mean static stability (unit: K/ bar).

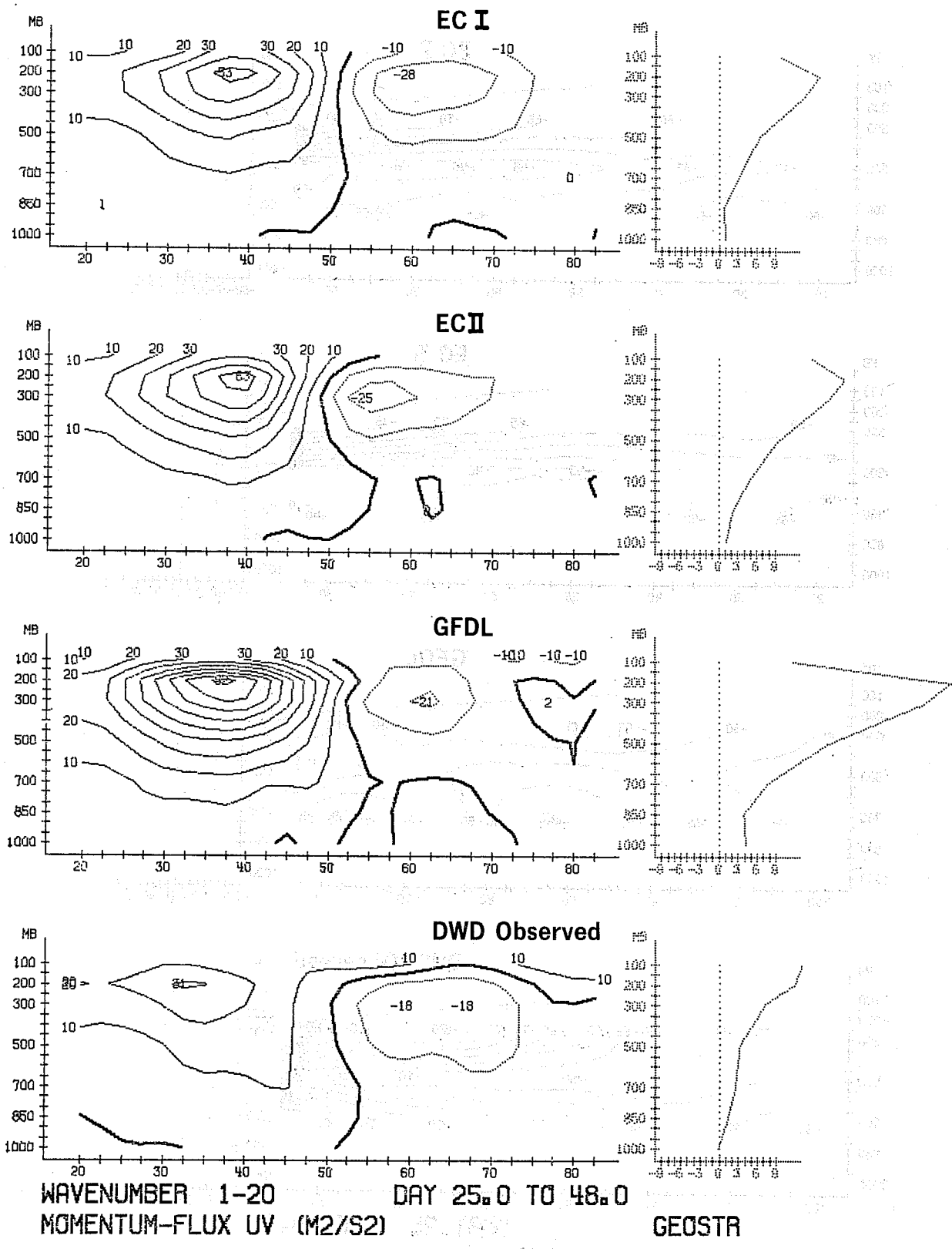

Fig. 12 The 24 day mean momentum transport (wave number 1...20, unit: m^2 / s^2).

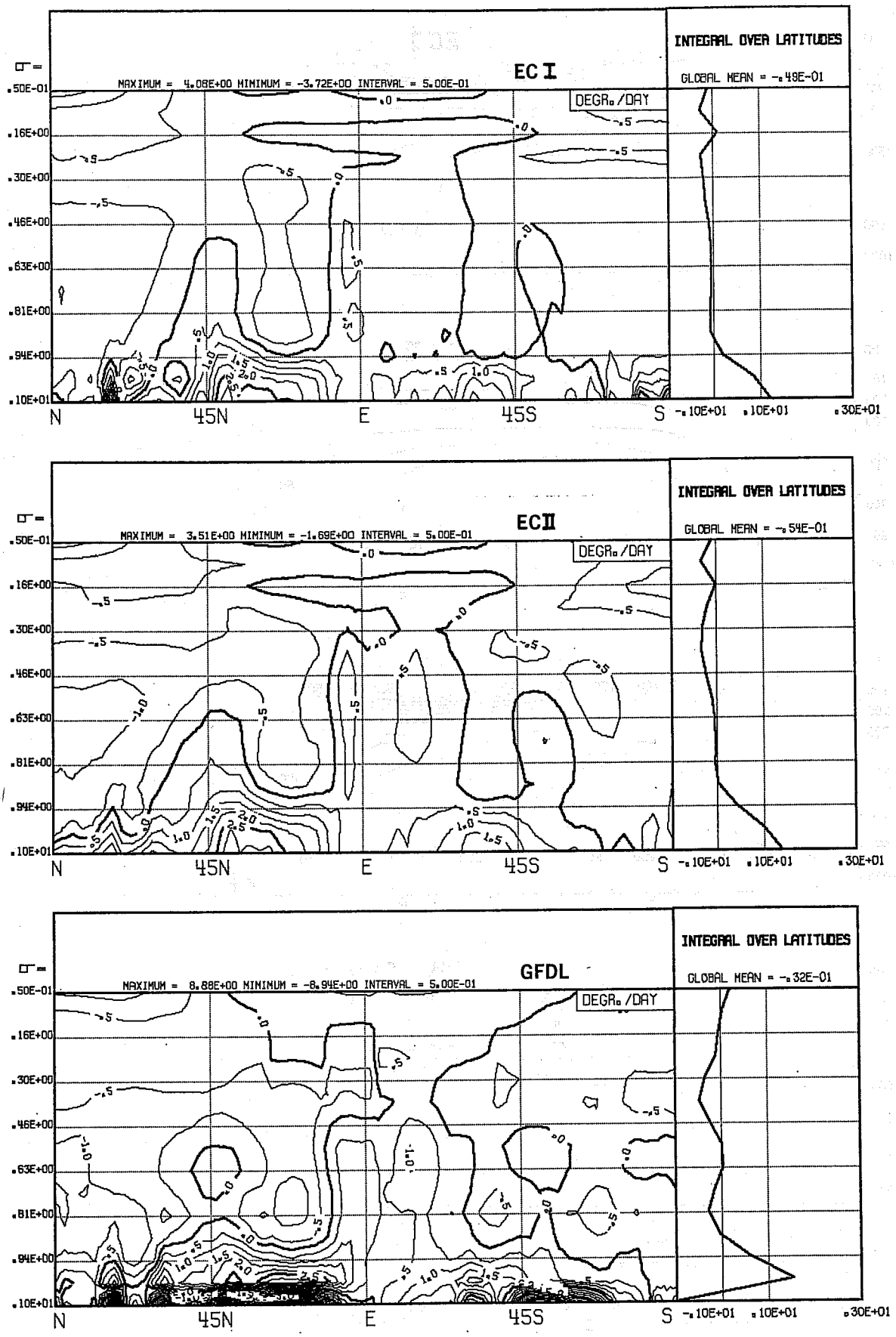

Fig. 13 The 50 day mean diabatic heating as function of latitude and height.

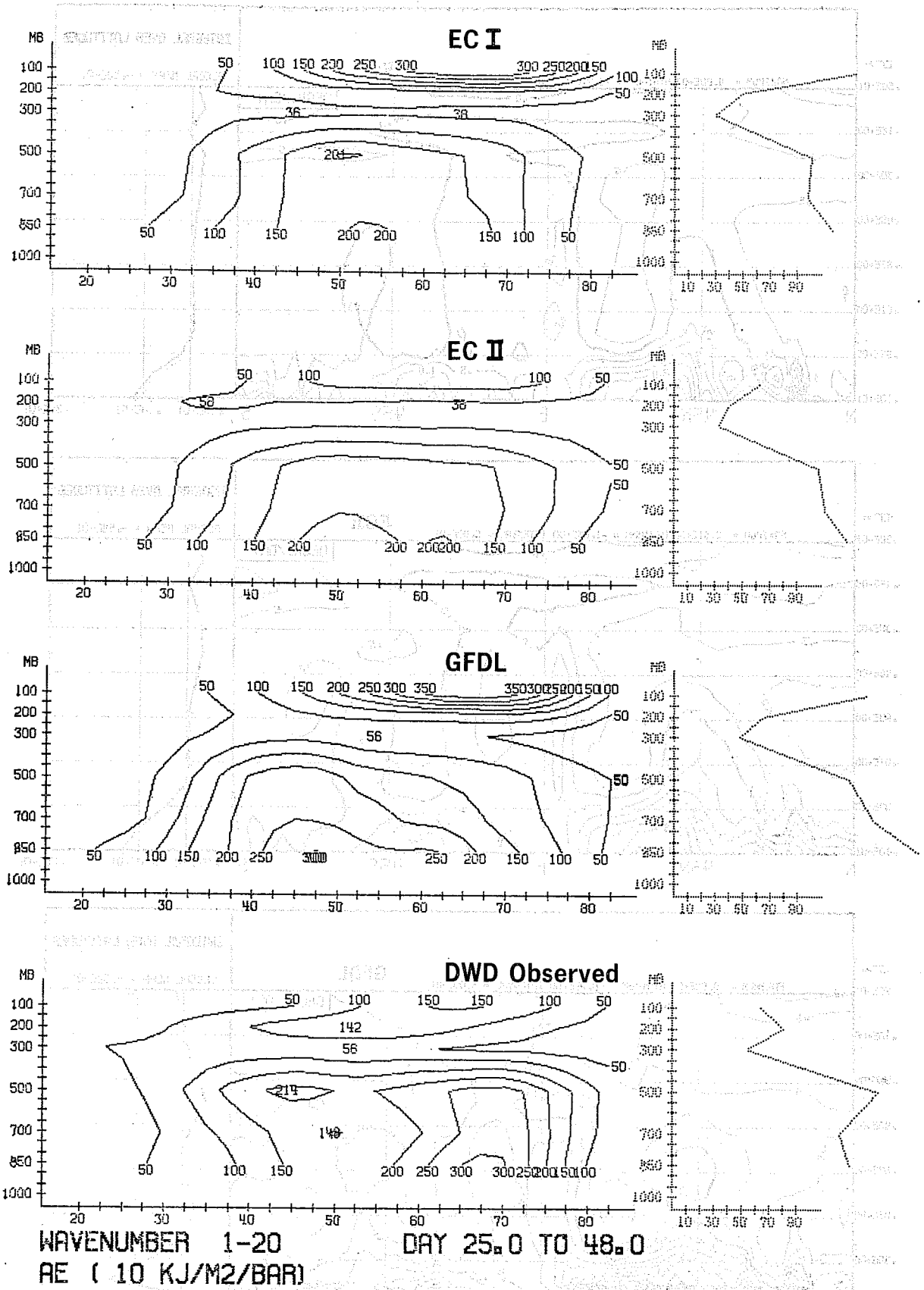

Fig. 14 The 24 day mean available potential energy (wavenumber 1...20, unit 10*kJ $m^{-2}bar^{-1}$).

The kinetic energy in wavenumber 1 - 20 (Fig. 15) is in the first two experiments confined to a comparatively narrow region at about 40^{o}N, while the analysis seems to extend this tropospheric maximum over all latitudes. The maximal strength is for these experiments about 10% too strong, while the third run even overestimates the strength by about 30%. The kinetic energy in the boundary layer is too strong in the second and third experiments.

The predicted rainfall (Fig. 16) is more pronounced in the second experiment than in the first one, particularly over the Indian Ocean and also in the North Atlantic. The third experiment produces hardly any rainfall at all in the Congo region but a lot near the equator near Panama.

2.5 Summary and conclusion

The improvement from the first to the second operational physics can be found mainly in a more realistic heating and moistening. Both these experiments have still more similarity between them than with the GFDL run, whose heating distribution leads to an overestimation of the eddy available potential and kinetic energy. The pattern of the systematic error in the height field does not show much response to changes in the parameterization.

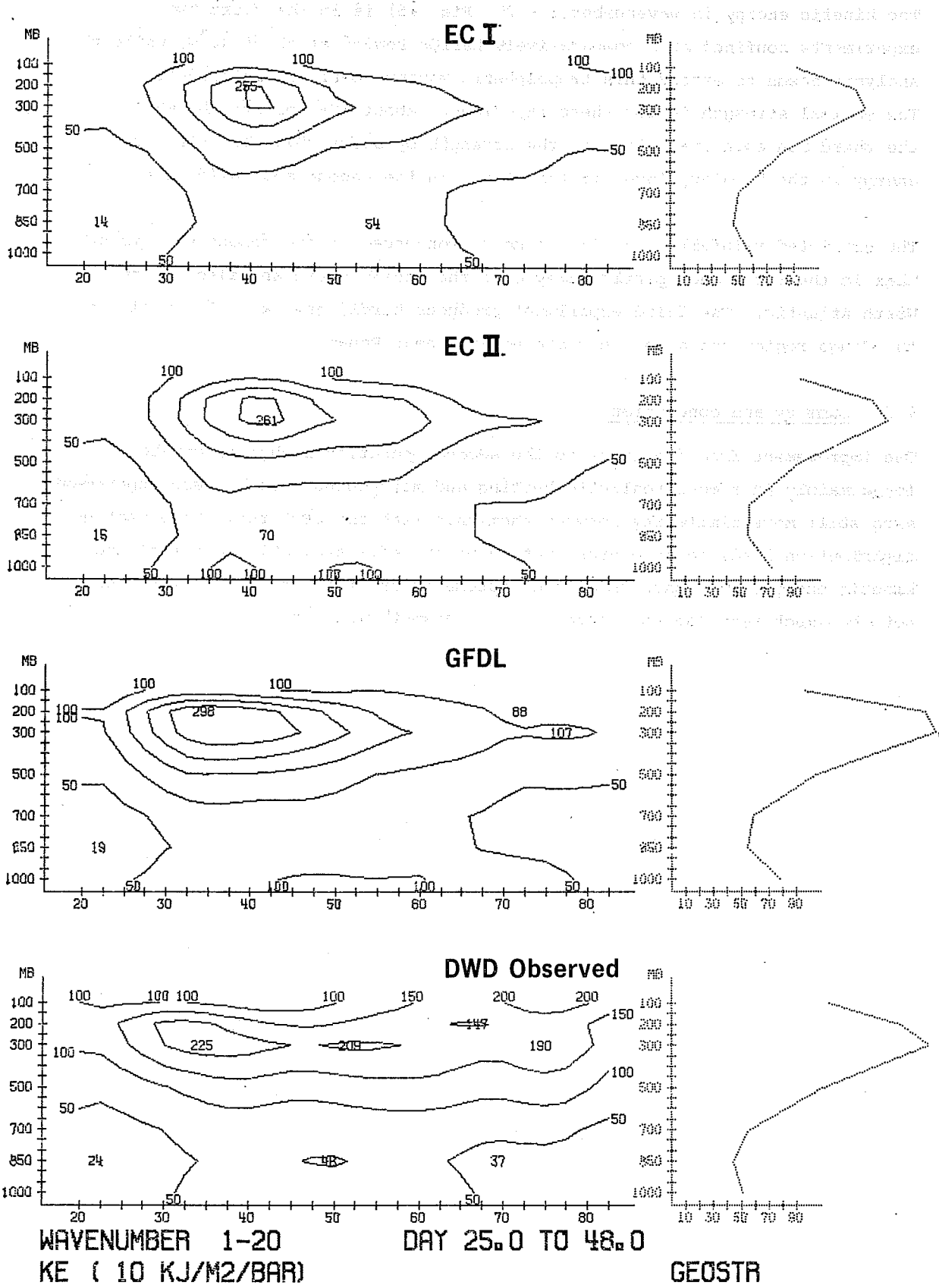

Fig. 15 The 24 day mean kinetic energy (wavenumber 1...20, unit 10*kJ $m^{-2}bar^{-1}$).

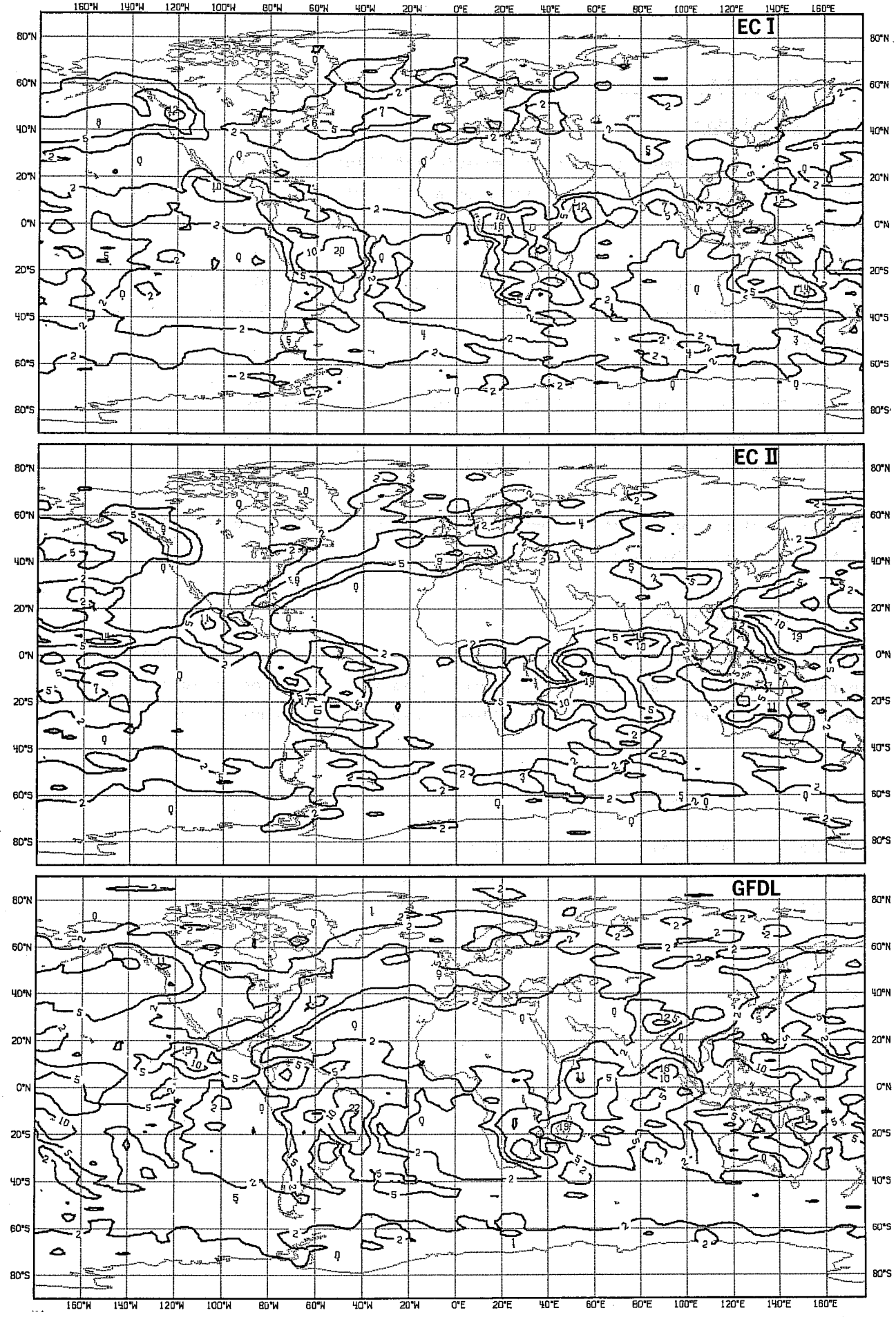

Fig. 16 The 30 day mean precipitation (convective and large scale, unit: mm/day).

3. THE IMPACT OF HORIZONTAL AND VERTICAL RESOLUTION

3.1 Introduction

One of the basic assumptions in atmospheric modelling is that with an increase of resolution the performance of a model will be improved, since quantities and their derivatives can be represented more accurately.

This has been discussed in several papers (Manabe et al, 1970, 1979) and Williamson (1978) found that he could achieve the same improvement by changing the horizontal diffusion.

The performance of the EC model for a medium range forecast as a function of resolution has been discussed in Bengtsson (1979) with the clear result that the forecast quality improves with resolution.

In this Section the impact of horizontal and vertical resolution on 50 day integrations will be discussed.

3.2 The experiments

Six experiments are compared, all using the 16.1.79 as initial day. The parameterisation of sub grid scale processes is that of the operational ECMWF model (Tiedtke et al, 1979). The following cases were integrated over 50 days.

Exp.	Mod. type	resolution	
		horizontal	vertical
T21L15	spectral	triangular 21	15 levels
T40L9	spectral	triangular 40	9 levels
T40L15	spectral	triangular 40	15 levels
T40L20	spectral	triangular 40	20 levels
T63L15	spectral	triangular 63	15 levels
N48L15	gridpoint	196 x 196 points global	15 levels

The nine level version (2 exp.) uses the GFDL distribution of levels, (Hollingsworth et al (1979), the 20 level version has 5 levels more in the stratosphere than in the operational model. The experiments have been verified against the DWD analysis.

3.3 Evaluation

The time evaluation of the total global mean kinetic energy (Fig. 17) shows a drop in the first 4 days of all experiments which is continued in the spectral integrations up to day 8, while the grid point model subsequently increases its kinetic energy until it reaches a steady state at about day 20. The spectral models stay on a lower level than the initial data. The level of kinetic energy finally reached in the spectral integrations is a function of resolution. The difference between highest and lowest measured kinetic energy is about 20%.

The ratio between zonal and eddy kinetic energy (Fig. 18) ("zonality") seems not to be a direct function of resolution. The highest variability can be found within the spectral T40L9 and T40L15 integration, while the T21L15 and the T63L15 produce more eddy than zonal kinetic energy. (The zonality is at day 40: 0.8 for T63L15 and 1.8 for T4019!) The 24 day mean 1000 mb height field (Fig. 19) displays in all 5 experiments an overdevelopment of the depression over the Atlantic and Pacific ocean.

Since the tendency exists to deepen these depressions with increased resolution, we find the results of Manabe et al (1979) confirmed.

Less distinct are the trends concerning the variance by transient waves in 1000 mb (Fig. 20). While the gridpoint model produces the main areas of high variability over the oceans correctly the spectral models produce very small scale variability features so that here the low resolution experiments T40L9 and T21L15 have to be considered best.

An increase of resolution also seem to worsen the mean 500 mb flow pattern (Fig. 21) whose observed dumb bell shape is not predicted in any of the experiments. Instead we find with increasing resolution the high over the European continent replaced by a trough. The high pressure observed in the North Pacific has never been simulated by any model. We find therefore in the difference to climate at 100 mb (Fig. 22) a negative pressure anomaly in the Pacific and Atlantic region, separated by too high pressure over the North American continent. Except for T40L15 and T21L15 the oceanic height error varies only marginally with resolution (10%) but the position shifts.

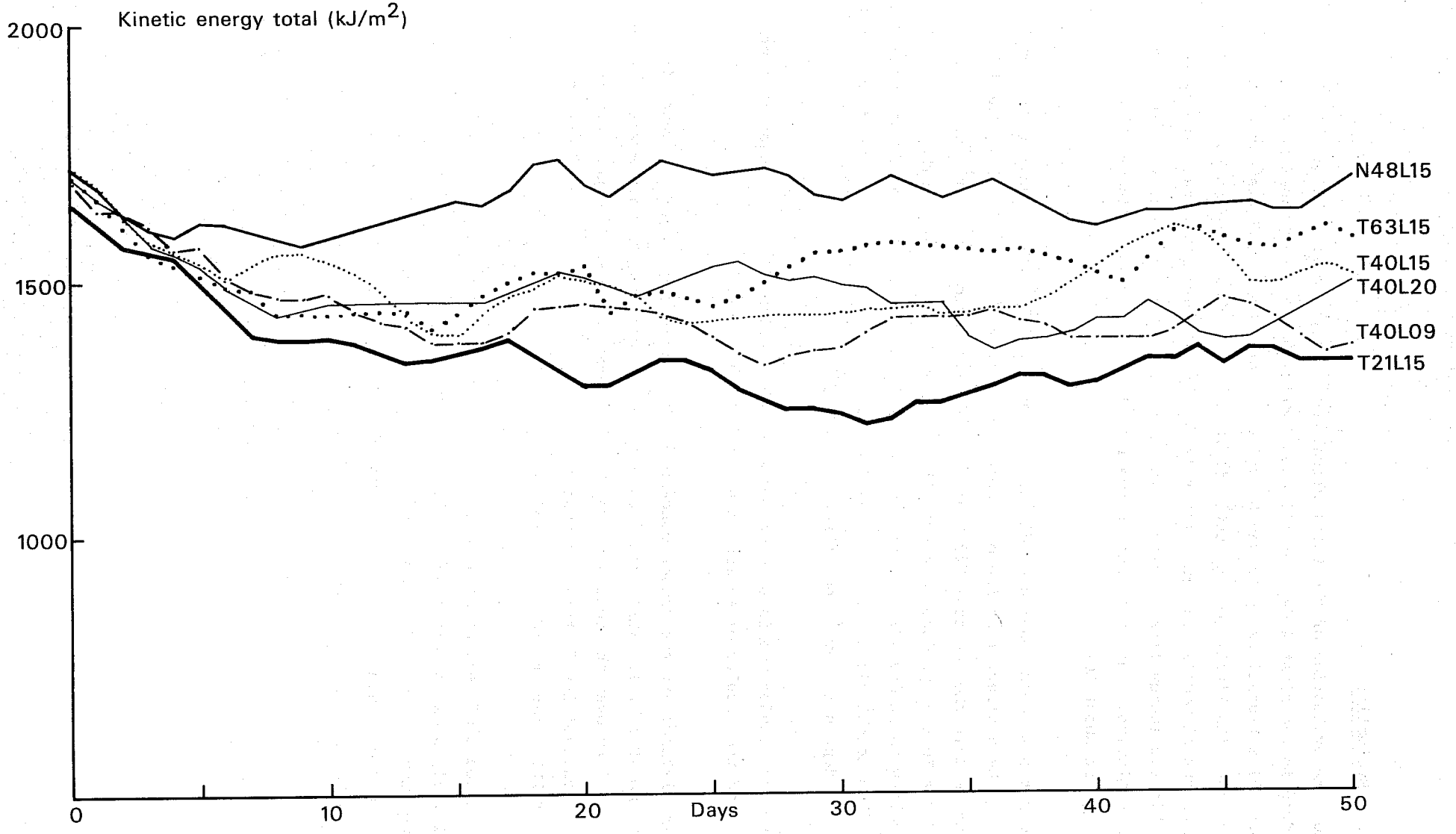

Fig.17 The time evolution of globally averaged total kinetic energy

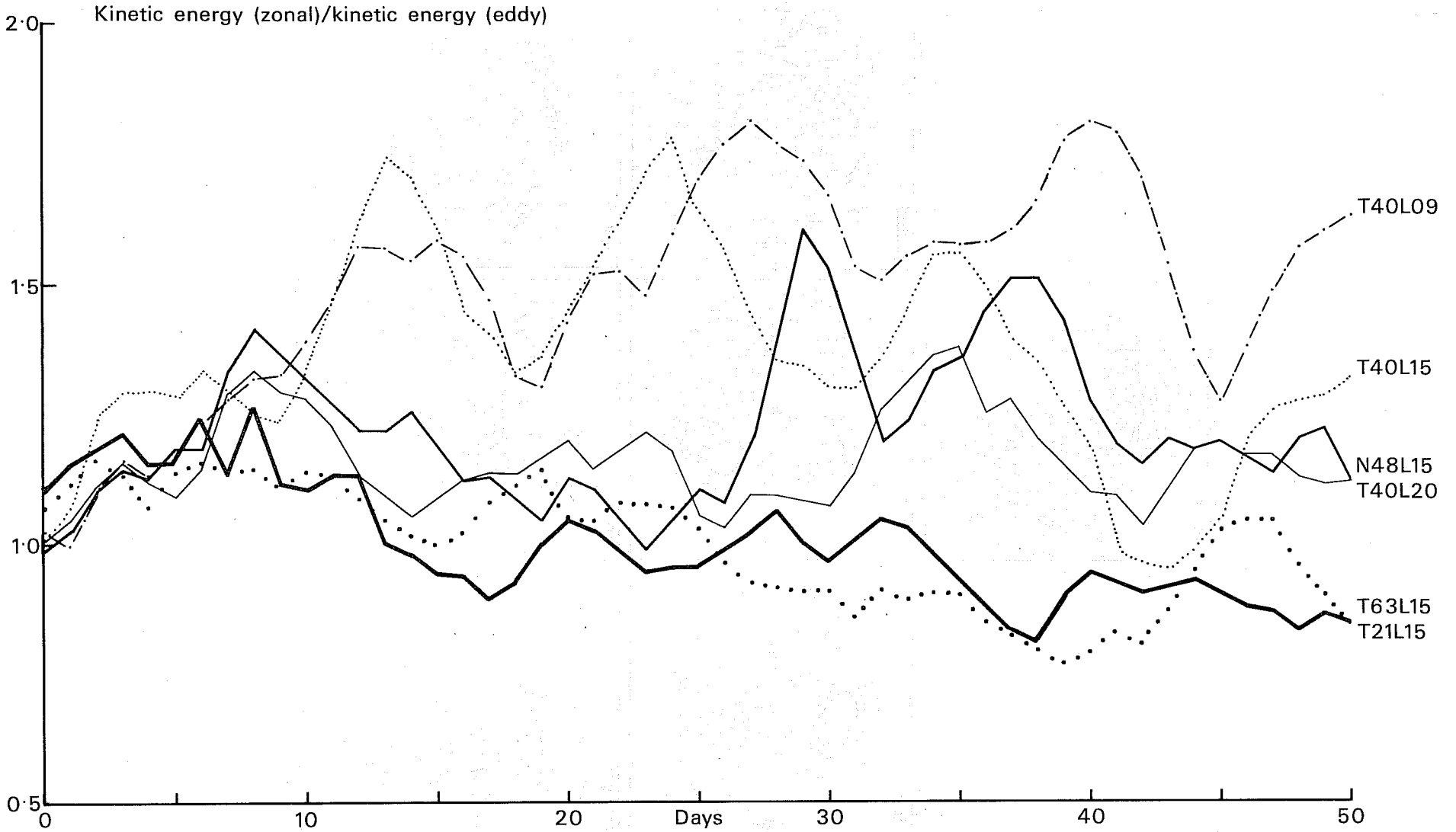

Fig. 18 The time evolution of the ratio between zonal and eddy kinetic energy

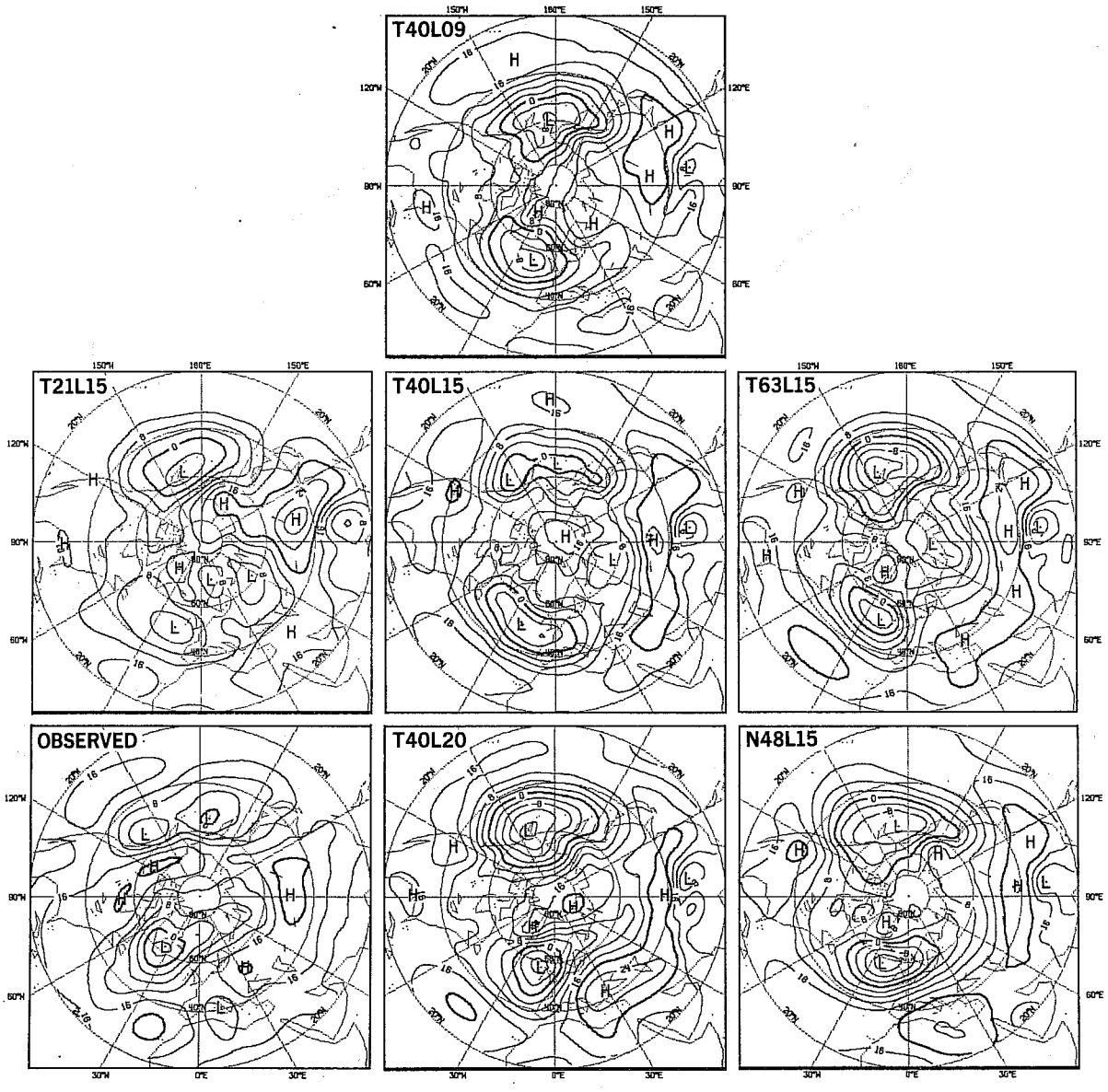

Fig. 19 The 24 day mean 1000 mb height field (contouring interval 40m).

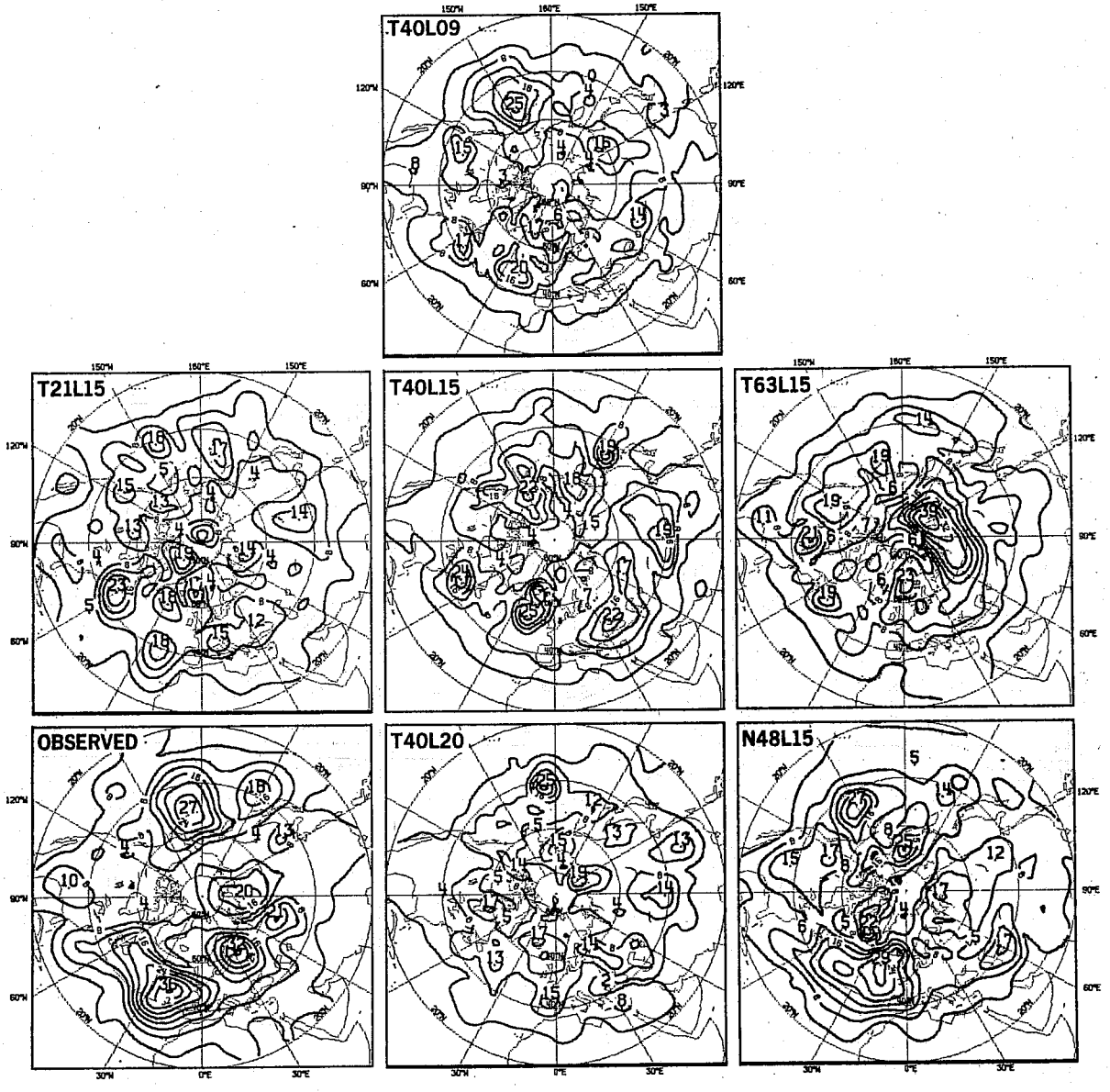

Fig. 20 The 24 day mean variance by transient waves in 1000 mb height.

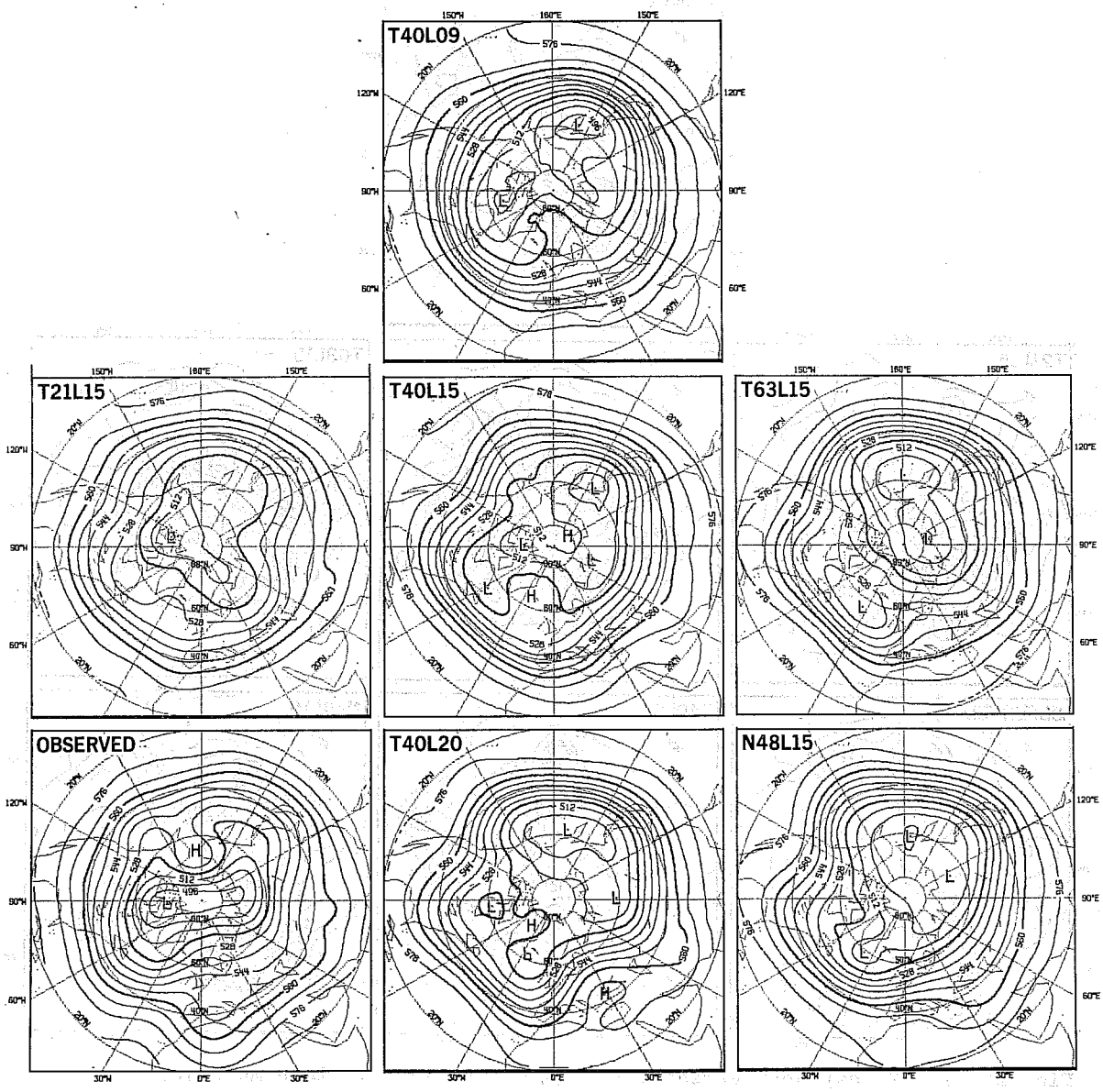

Fig. 21 The 24 day mean 500 mb height field (contouring interval: 80m).

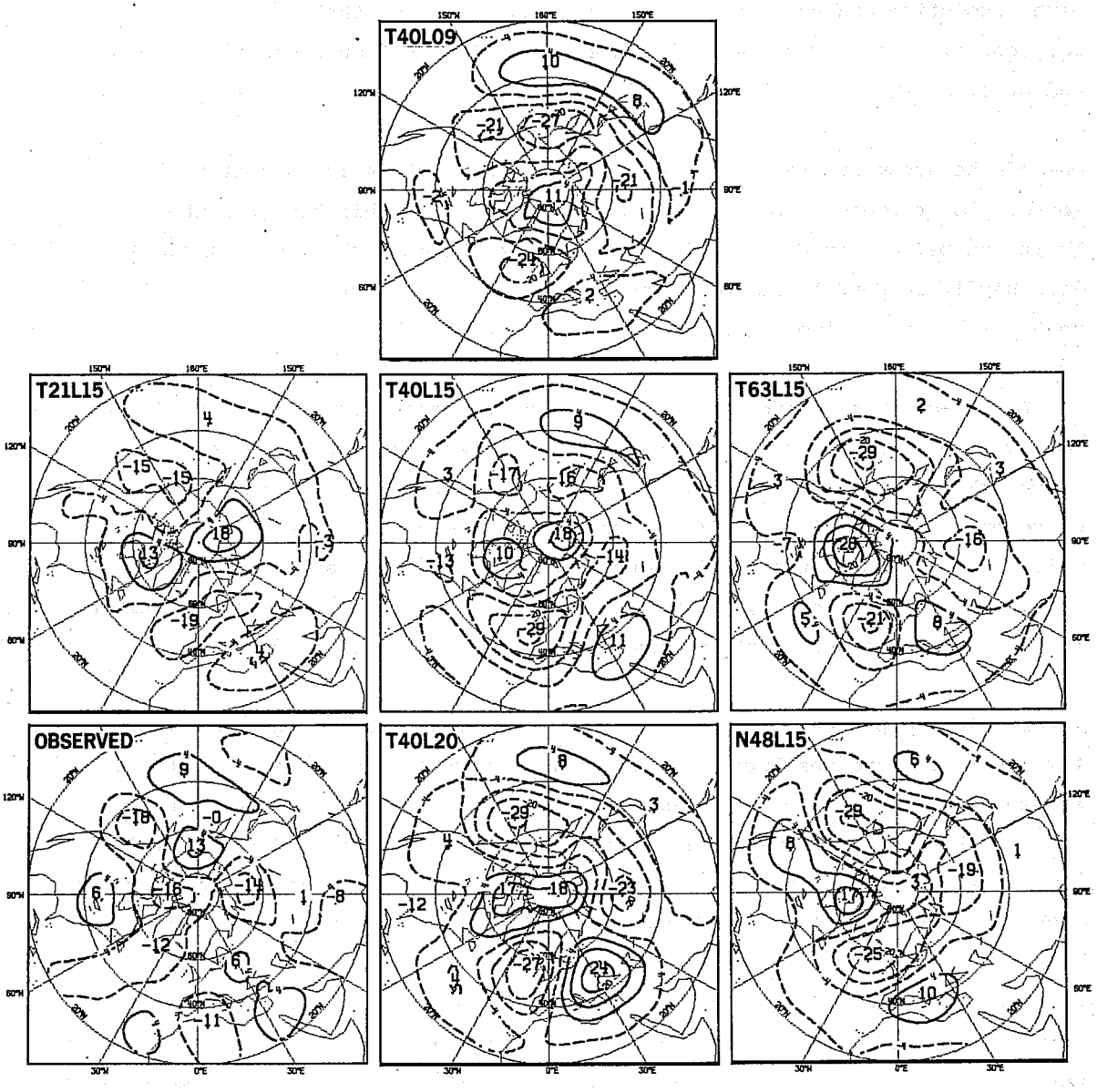

Fig. 22 The difference to climate of the 24 day mean 500 mb height field.

A meridional cross section of the zonal mean zonal wind (Fig. 23) proves one of the main deficiencies of the model, the northward shift of the jet, to be independent of the chosen resolution, although its strength varies with resolution and seems to be a function at least of the horizontal coarseness. Also the meridional temperature distribution seems to be independent of a particular resolution (Fig. 24).

One of the arguments for a refinement of the resolution is that it would improve the representation of the momentum transfer within the atmosphere. As it can be seen in Fig. 25 this is not true, because the momentum transport does hardly respond to improved resolution and is (except for the very low resolution TL115) almost twice as high as observed.

The Lorenz-cycle of energy carried in the model atmosphere is studied in the following meridional cross sections. The available potential energy (wavenumber 1-20) Fig. 26 seems in the troposphere as well as in the stratosphere only vaguely linked with the resolution and agrees in no experiment too well with the observation. The conversion between zonal and eddy available potential energy, Fig. 27, shows a clear dependence on resolution, but already in the lowest resolution this conversion term is overestimated.

A very clear dependence can be found between the kinetic energy in wavenumber 1-20 (Fig. 28) and resolution in horizontal as well as vertical direction. No experiment is able to reproduce the horizontal extent of the maximum through the whole tropopause as observed, but rather each produces a limited core at about 40°N. The strength of this cell is too weak in the experiments with the lowest resolution and too strong in all the others. The increase of kinetic energy with increasing resolution leads therefore to a worsening of the representation of this parameter by finer resolution. The conversion between zonal and eddy kinetic energy (Fig. 29) also increases with resolution, but starts already at too high values, so that this conversion gets worse with increasing resolution.

In the mean rainfall over 30 days (Fig. 30) increase of resolution lead to stronger, locally more confined rainfall maxima.

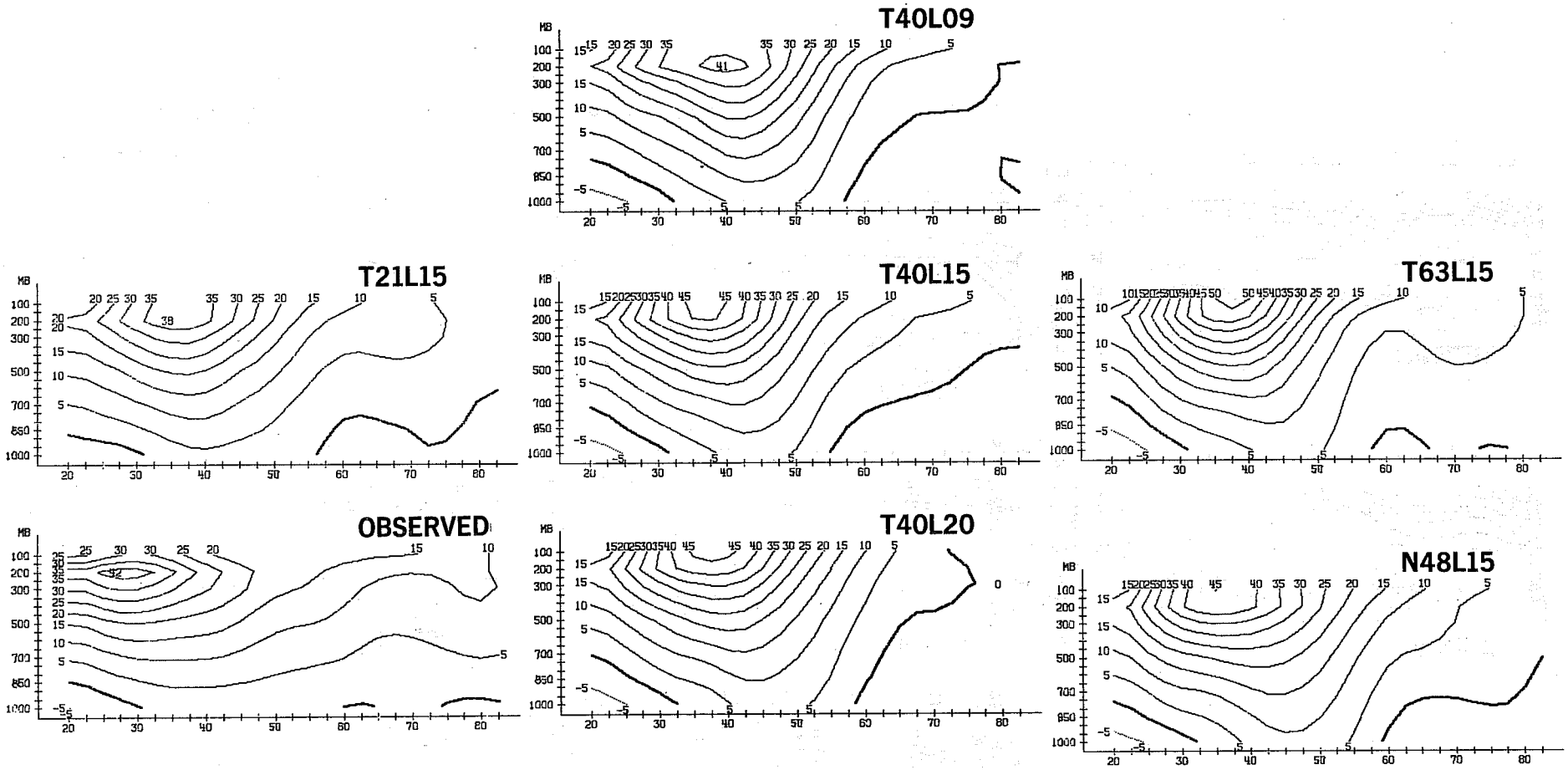

Fig. 23 The 24 day mean of the zonal mean of the zonal wind (unit: m/sec).

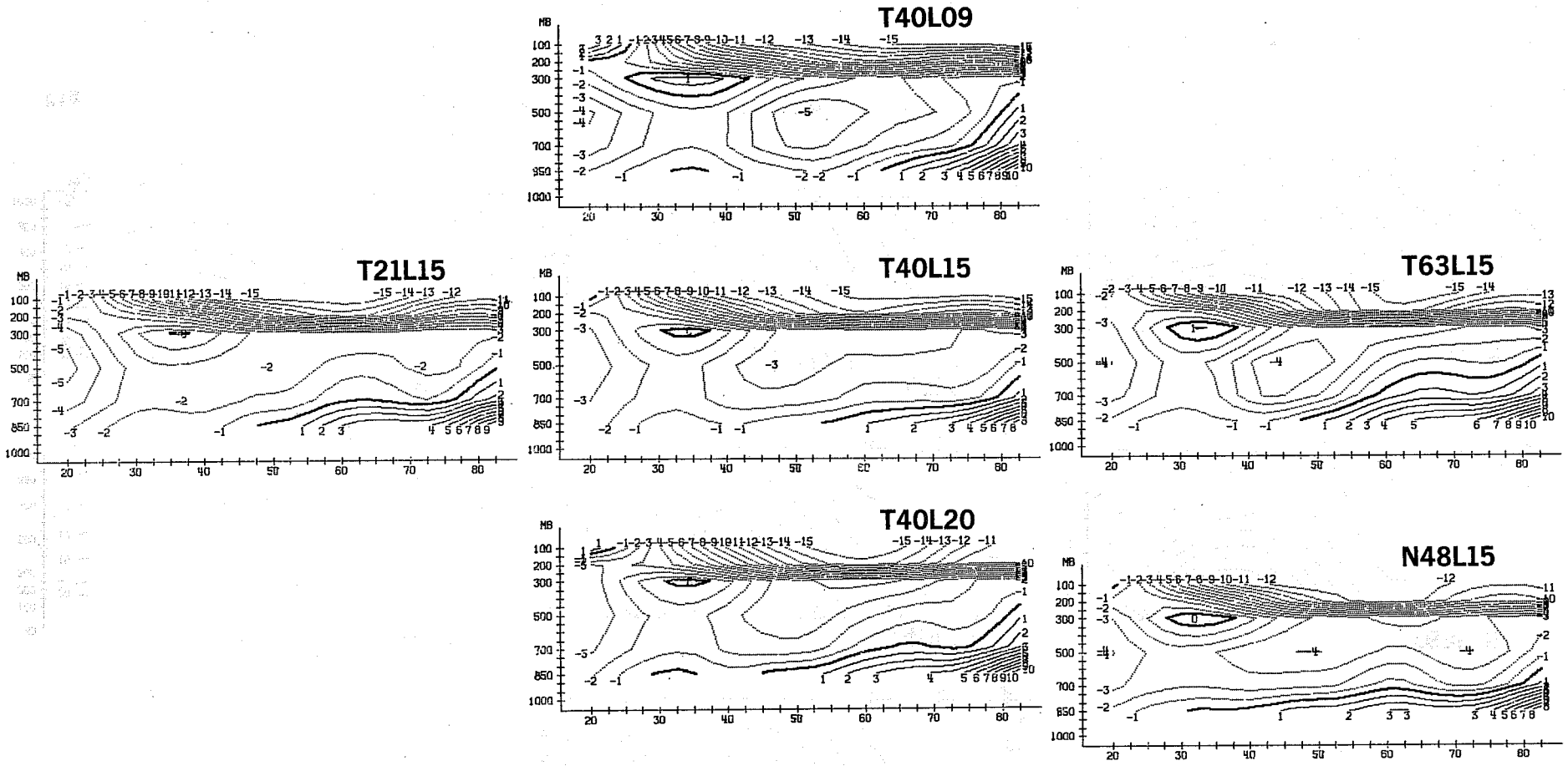

Fig. 24 The 24 day mean zonal mean temperature deviations from observed (unit: K).

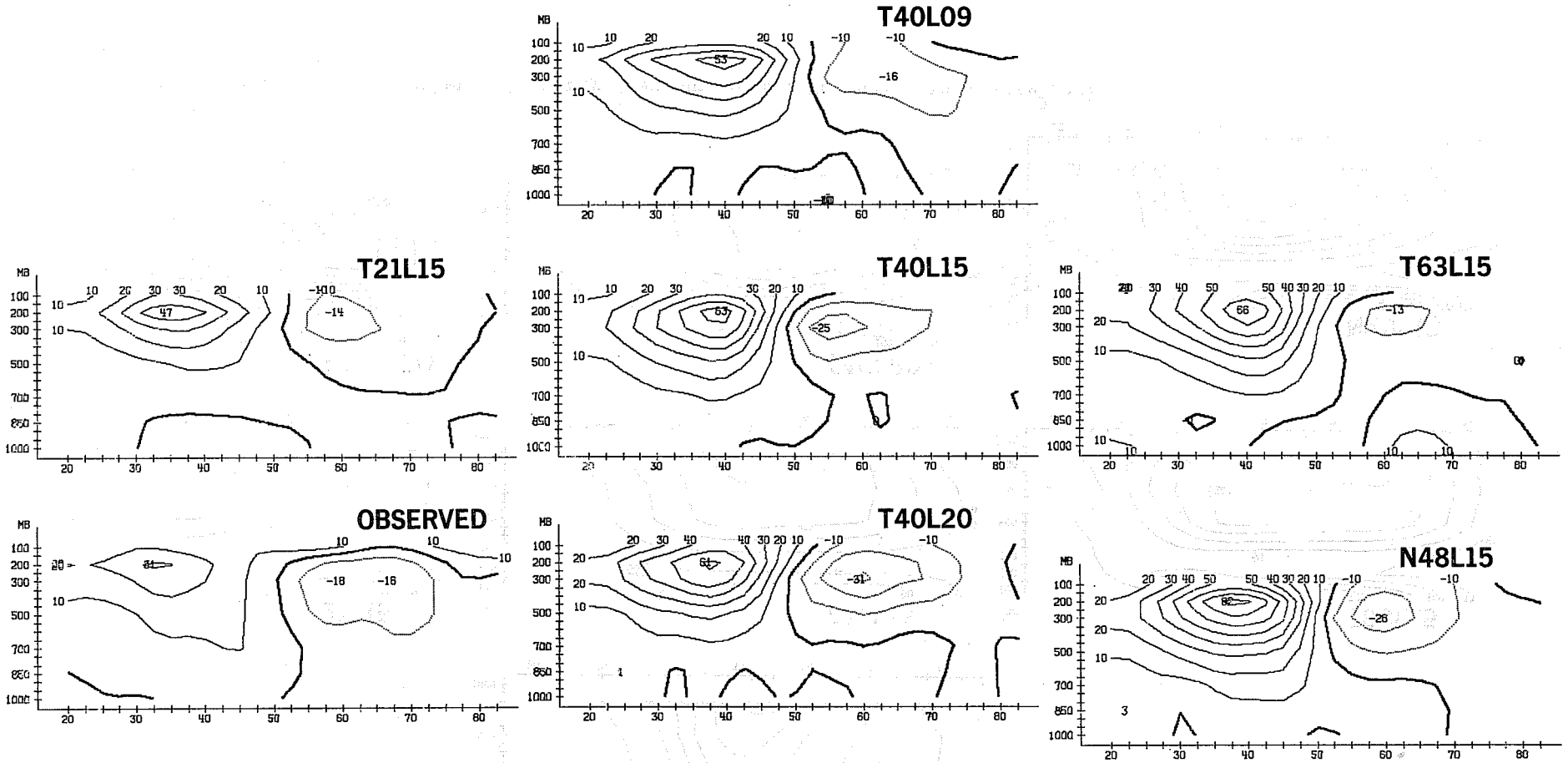

Fig. 25 The 24 day mean momentum flux (wavenumber 1...20, unit: m^2/sec^2).

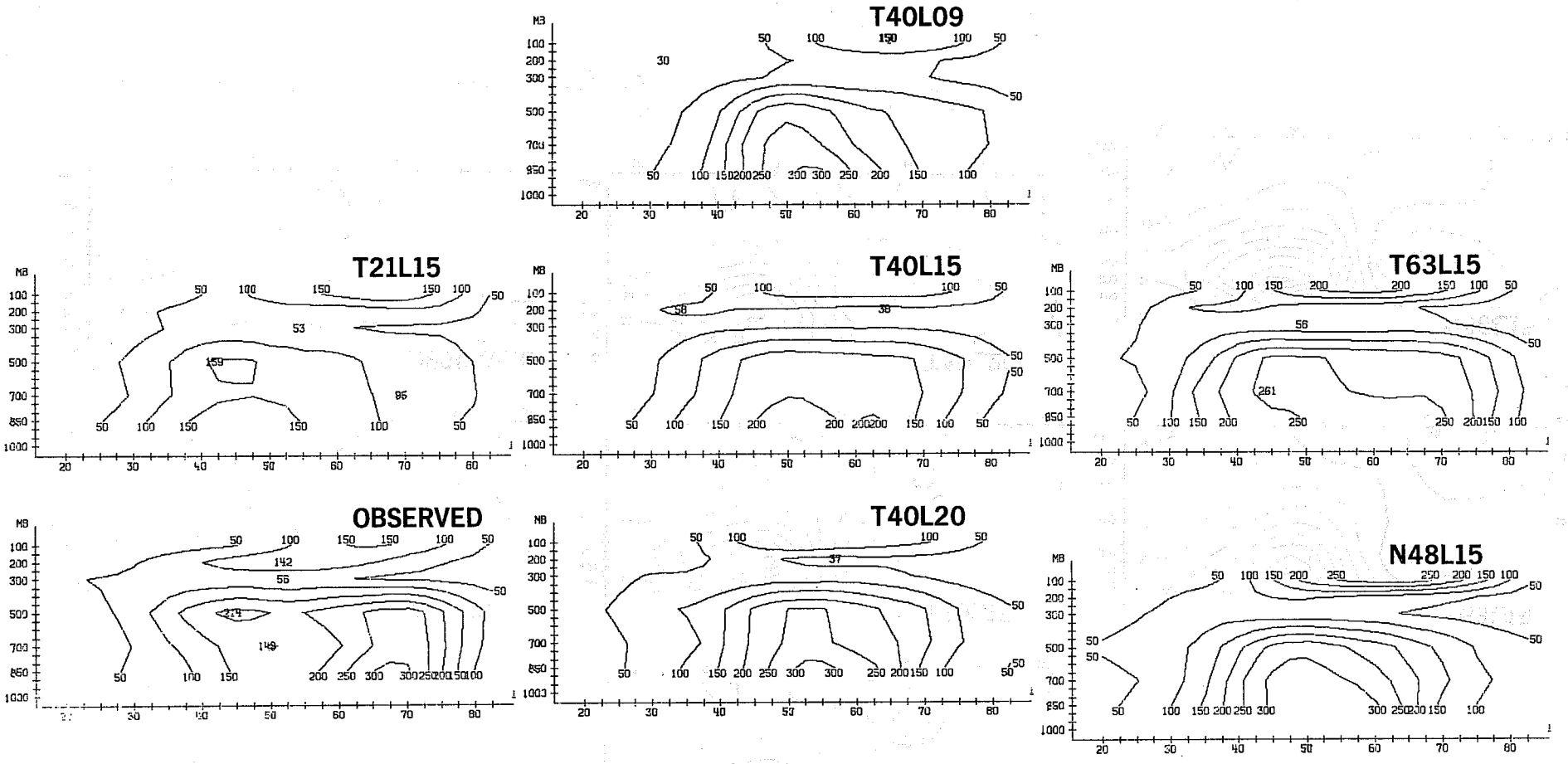

Fig. 26 The 24 day mean available potential energy (wavenumber 1...20, unit: 10 x kJ/m^2/bar)

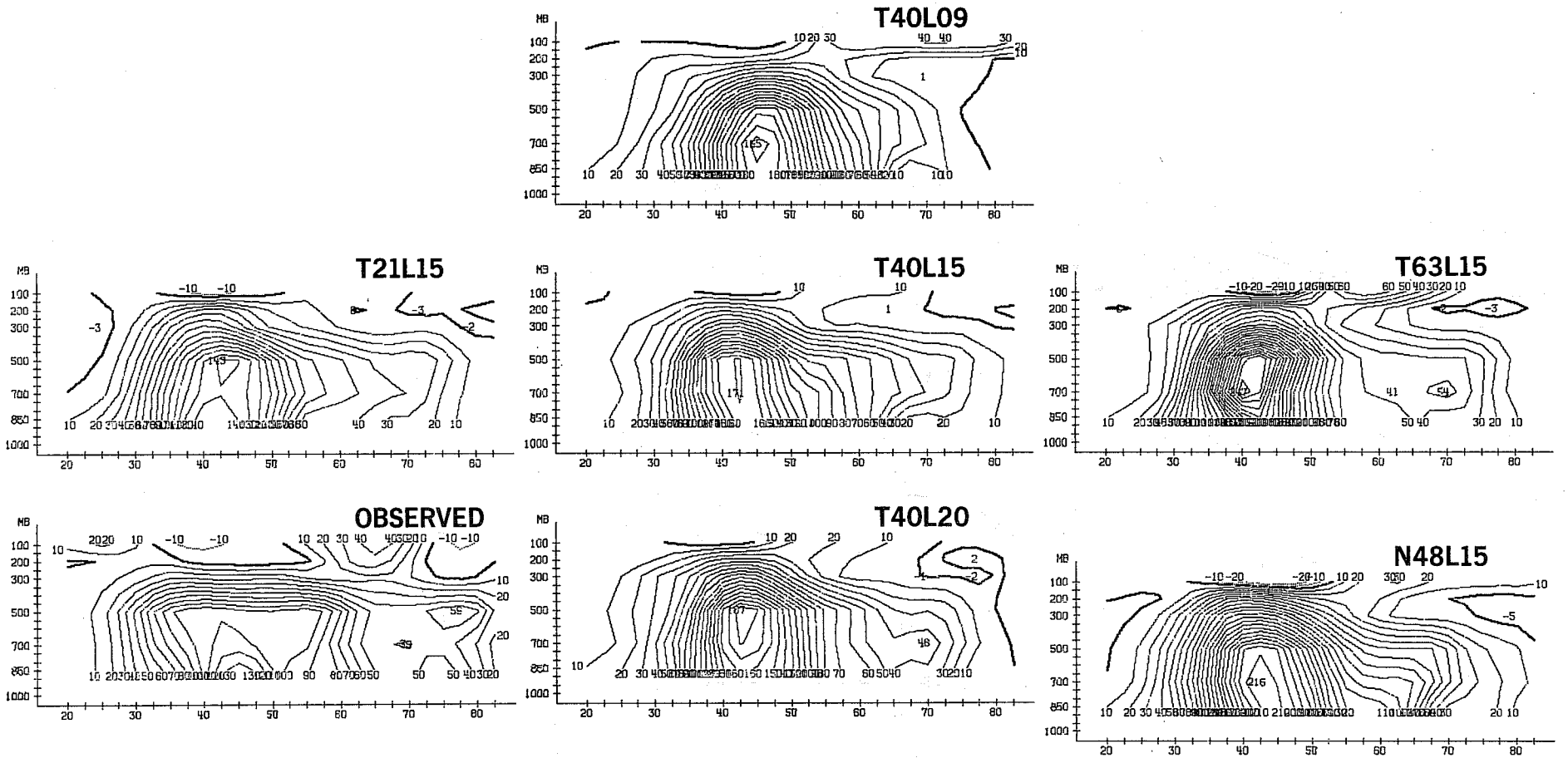

Fig. 27 The 24 day mean conversion of available potential energy (wavenumber 1...20, unit: 1/10 Watt/m^2/bar).

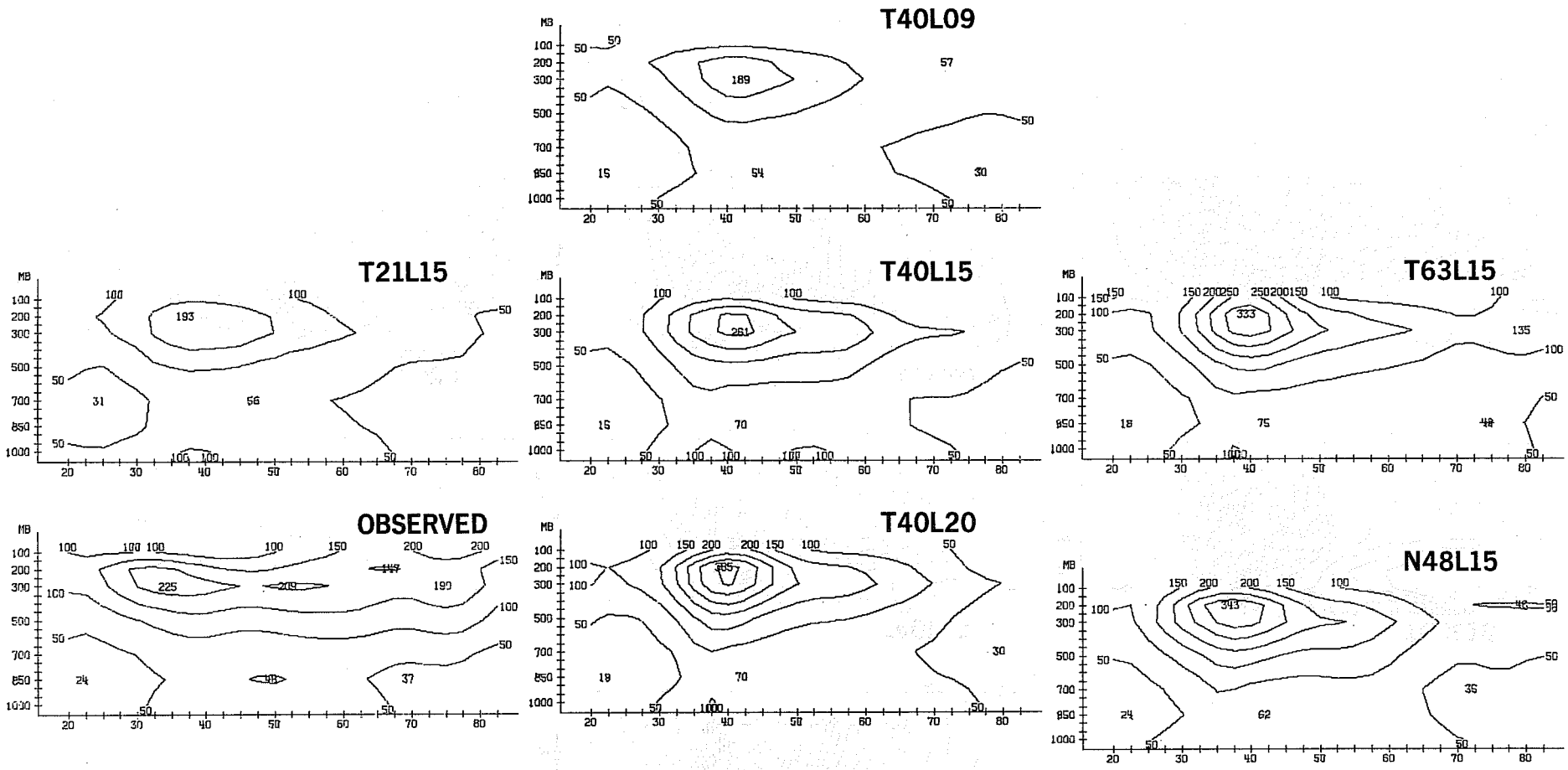

Fig. 28 The 24 day mean kinetic energy (wavenumber 1...20, unit 10 kJ/m^2/bar).

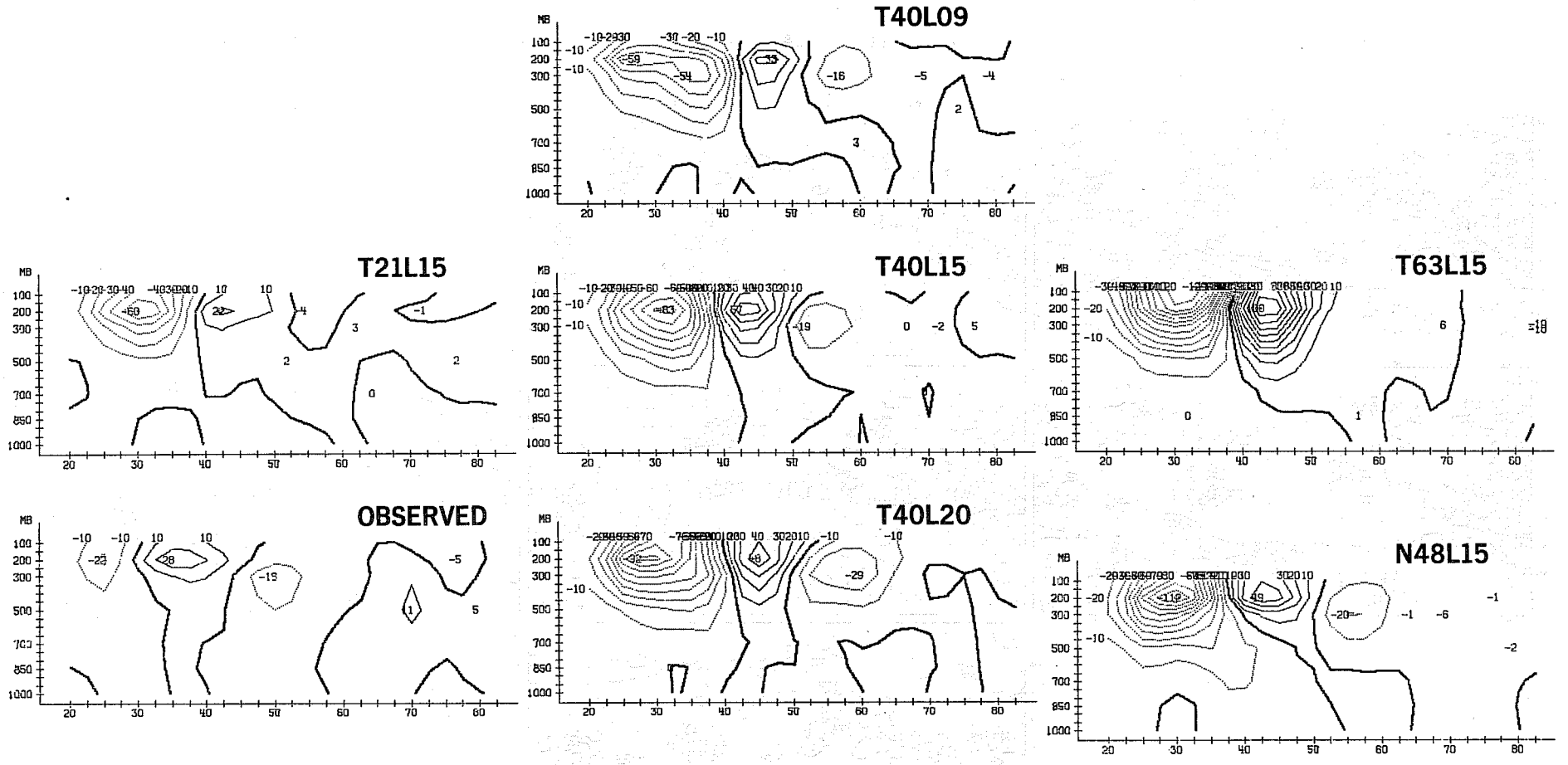

Fig. 29 The 24 day mean conversion of kinetic energy (wavenumber 1...20, unit: 1/10 Watt/m^2/bar).

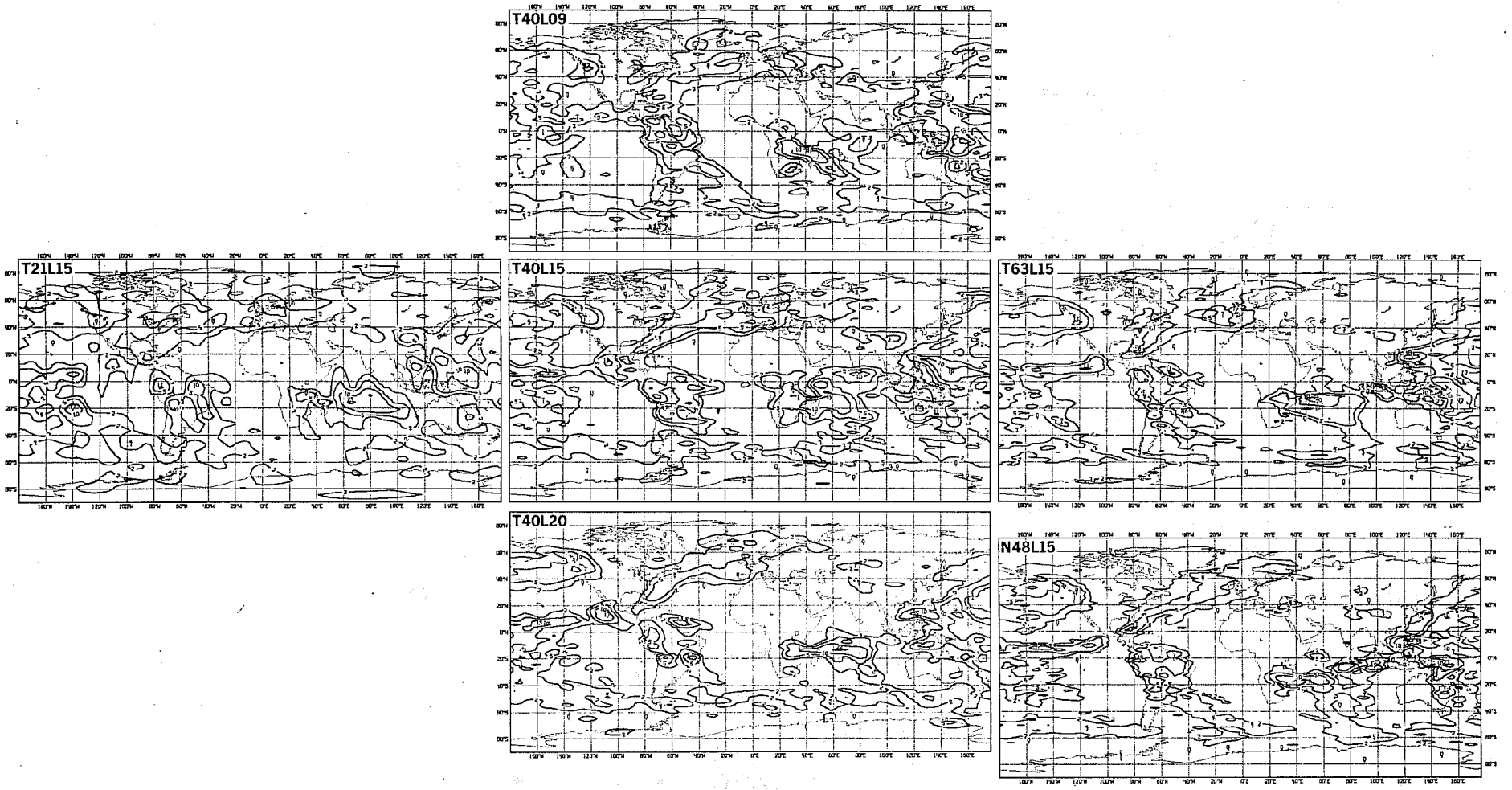

Fig. 30 The 30 day mean precipitation (convective and large scale, unit: mm/day).

3.4 Summary

A comparison of six 50 day integrations shows only a slight dependence of the height error on the horizontal resolution.

The energetics seem to be a direct function of resolution, but since they are overestimated already with low resolution models they get worse with an increase in the resolved scale.

The performance of the gridpoint model equals that of the spectral models. Since a low resolution model (T21L15) gives a slightly better result for some parameters and duplicates many of the errors inherent in the higher resolution results, its use for experimental extended range predictions appears worthwhile. The performance of the gridpoint model (N18L15) and the high resolution spectral models (T40L20, T63L15) is fairly similar.

4. THE RESPONSE TO CHANGES IN THE KARMAN CONSTANT

4.1 Introduction

The Karman constant was introduced as a proportionality factor to describe the height dependency of the mixing length which is used to describe the surface drag. Since the vertical diffusion (τ) is dependent on the square of the mixing length, we find (for neutral to slightly unstable stratification)

$$\tau \sim k^2 \, | \underline{V}_n | \, \underline{V} \qquad (1)$$

The value of the dimension less Karman constant k can vary between .22 and .61 (Sutton, 1953). More recent publications, like Businger (1971), whose boundary layer scheme has been adopted for the EC model, proposed .35, while Pruitt et al (1973) calculates from measurements values of .39 and .44 and recommends a value of .40. The difference between the values of Businger and Pruitt made it worthwhile to test both within the forecast model.

4.2 Description of the experiments

The spectral model with a vertical resolution of 15 levels and a horizontal representation of 40 zonal waves has been used to carry out two 50 day integrations.

Exp. 1 k = .35 for vertical diffusion of u, v, T, q

Exp. 3 k = .40 for vertical diffusion of u, v, T, q

The initial data (16.1.79) were prepared during the first FGGE end-to-end test (INES). The results have been averaged from day 24 to 48 of the integration period and verified against the DWD analysis.

4.3 Evaluation

The curves for the time evolution of the global mean precipitable water (Fig.31) start in both experiments with a too low value (a known deficiency of the dataset) but increases very rapidly to the final values at day 10. This value is about 4% higher for the experiment with the higher value for the Karman constant.

The global mean temperature (Fig. 32) drops rapidly both experiments in the first days of the forecast period, after about day 10 the cooling rate decreases. At day 50 exp. 2 is about .3^{o}K warmer than exp. 3. The higher Karman constant seem therefore to enhance the heat exchange of the sea surface with the atmosphere.

The mean pressure pattern at 1000 mb (Fig. 33) (time averaging interval shown in Fig.31 shows two distinct areas of low pressure over the North Pacific and the North Atlantic, separated from high pressure cells over North America and Sibera. This pressure pattern has been reproduced in both experiments, but the North Atlantic and the Pacific low is by far too deep in the second experiment. The mean 500 mb height for the same period (Fig. 34) displays a dumb-bell like shape with a low over Siberia and Canada in the analysis. Of special interest from the Centres point of view is also a split of the zonal flow over Europe. The low over Canada is quite well predicted in the second experiment, while it is shifted to the east in the first one. The Siberian low is situated too far west almost over the Pacific. The flow pattern over Europe is only badly met in both experiments. A remarkable distinction between exp. 1 and exp. 2 is the extensive development of a ridge over the Rocky Mountains. The variance by transient waves (Fig. 35) in 1000 mb seem to be considerably enhanced by the higher Karman constant, (exp. 2) and also the position of those centres are better than in exp. 1, but it is still about 30% too low compared with the analysis.

In the zonal mean of zonal wind (Fig. 36) averaged from day 25 to 48 of the prediction period the maximum of the wind is shifted to the north in both experiments. While this jet stream is rather narrow and extends hardly into the stratosphere in the first experiment, it is much broader and unconfined in the second one. The easterly flow weather surface is further extended in the second experiment. The temperature deviation from (Fig. 37) observed shows an increase of the positive deviation in the boundary layer in the experiment

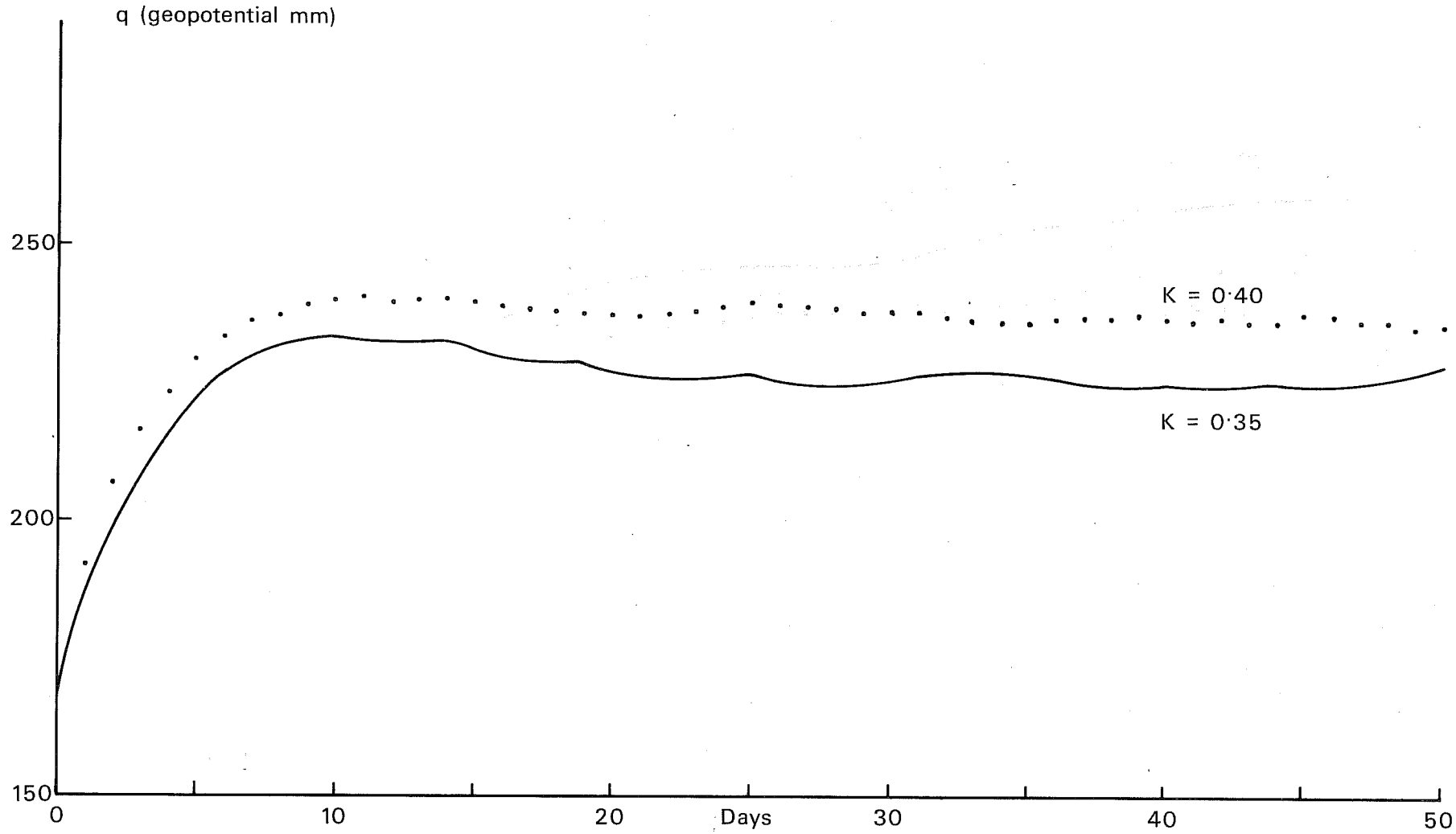

Fig. 31 The time evolution of the global mean humidity

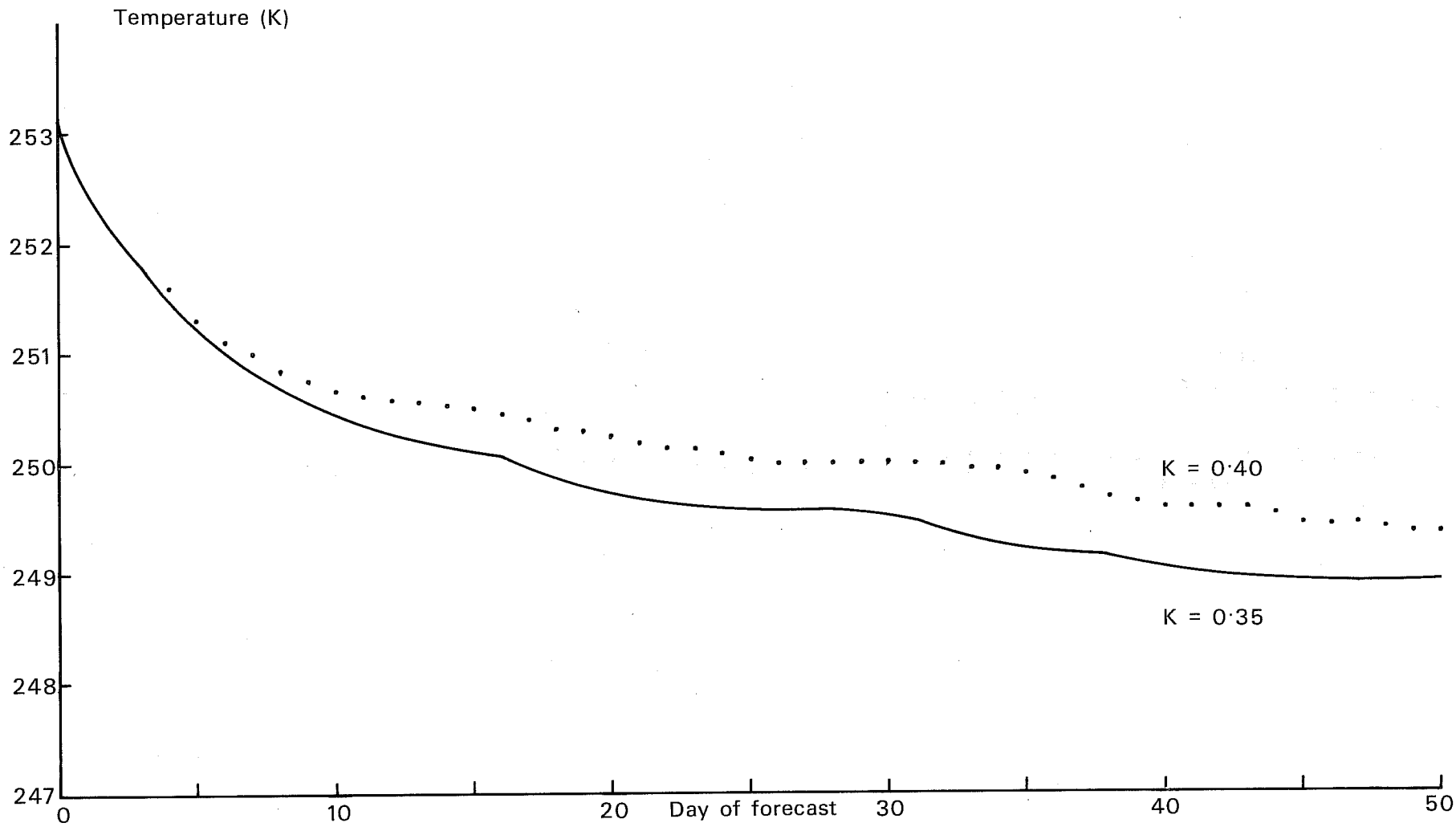

Fig. 32 The time evolution of the global mean temperature

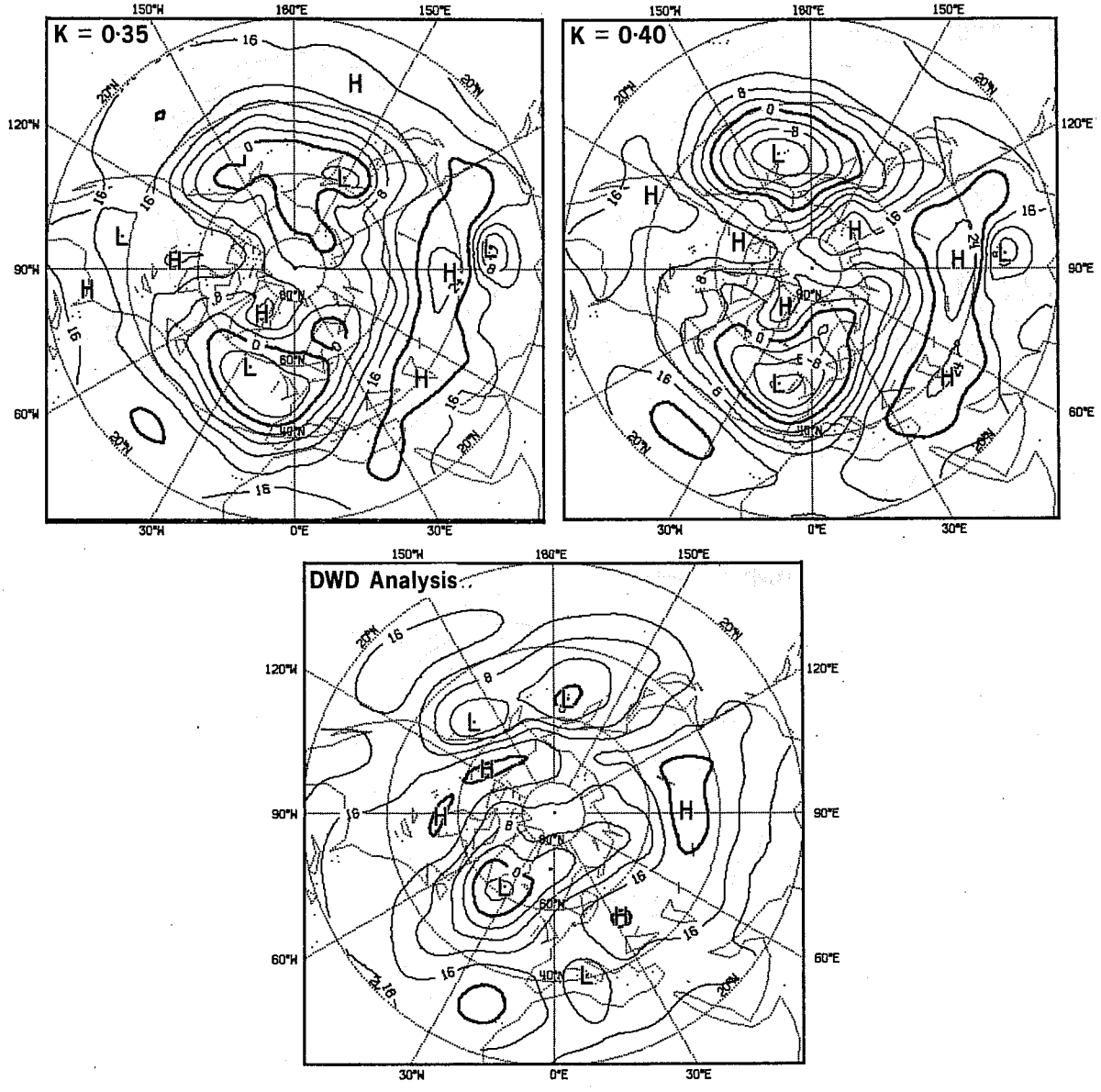

Fig. 33 The 24 day mean 1000 mb height field (contouring interval: 40m).

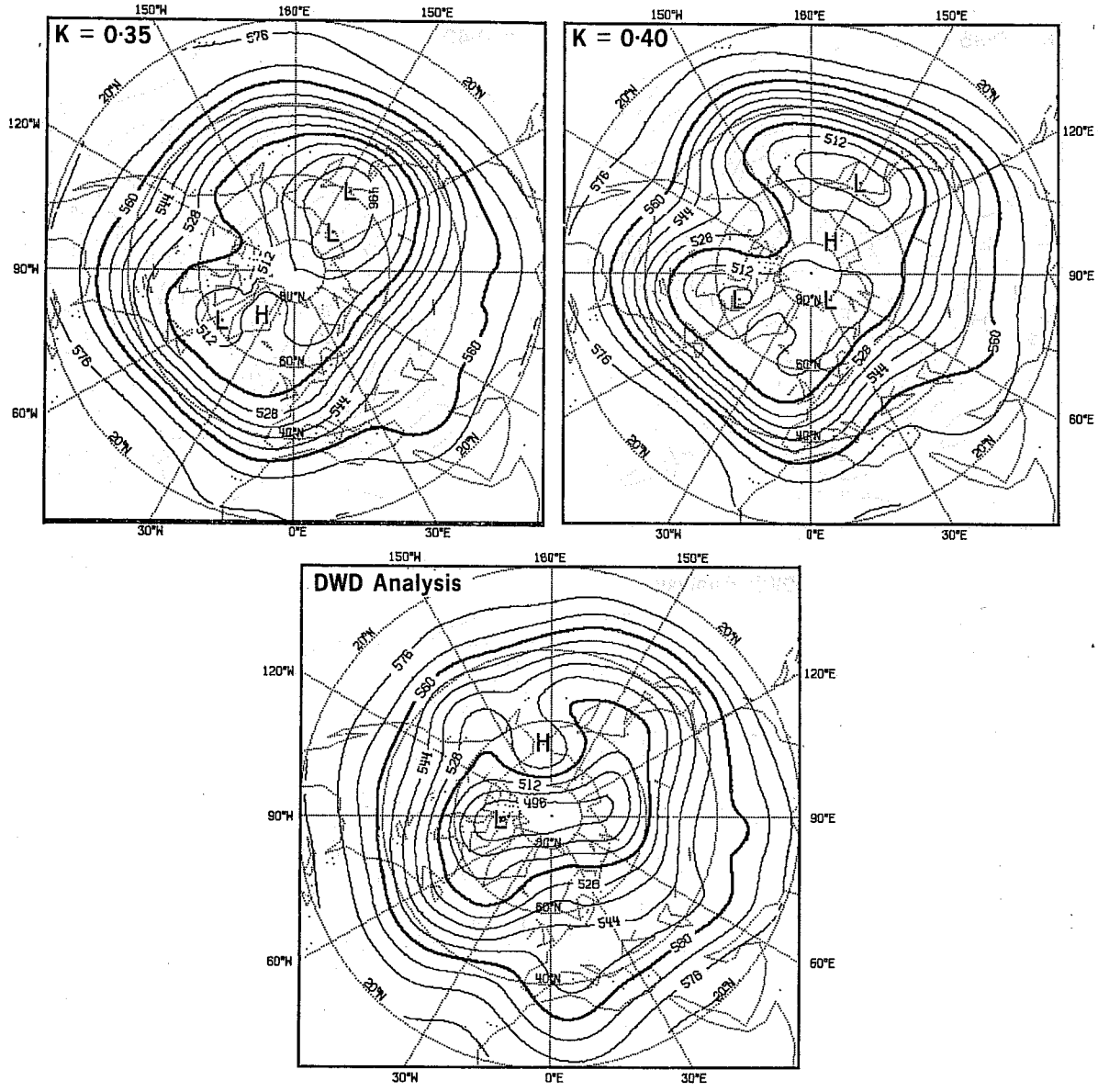

Fig. 34 The 24 day mean 500 mb height field (contouring interval: 80m).

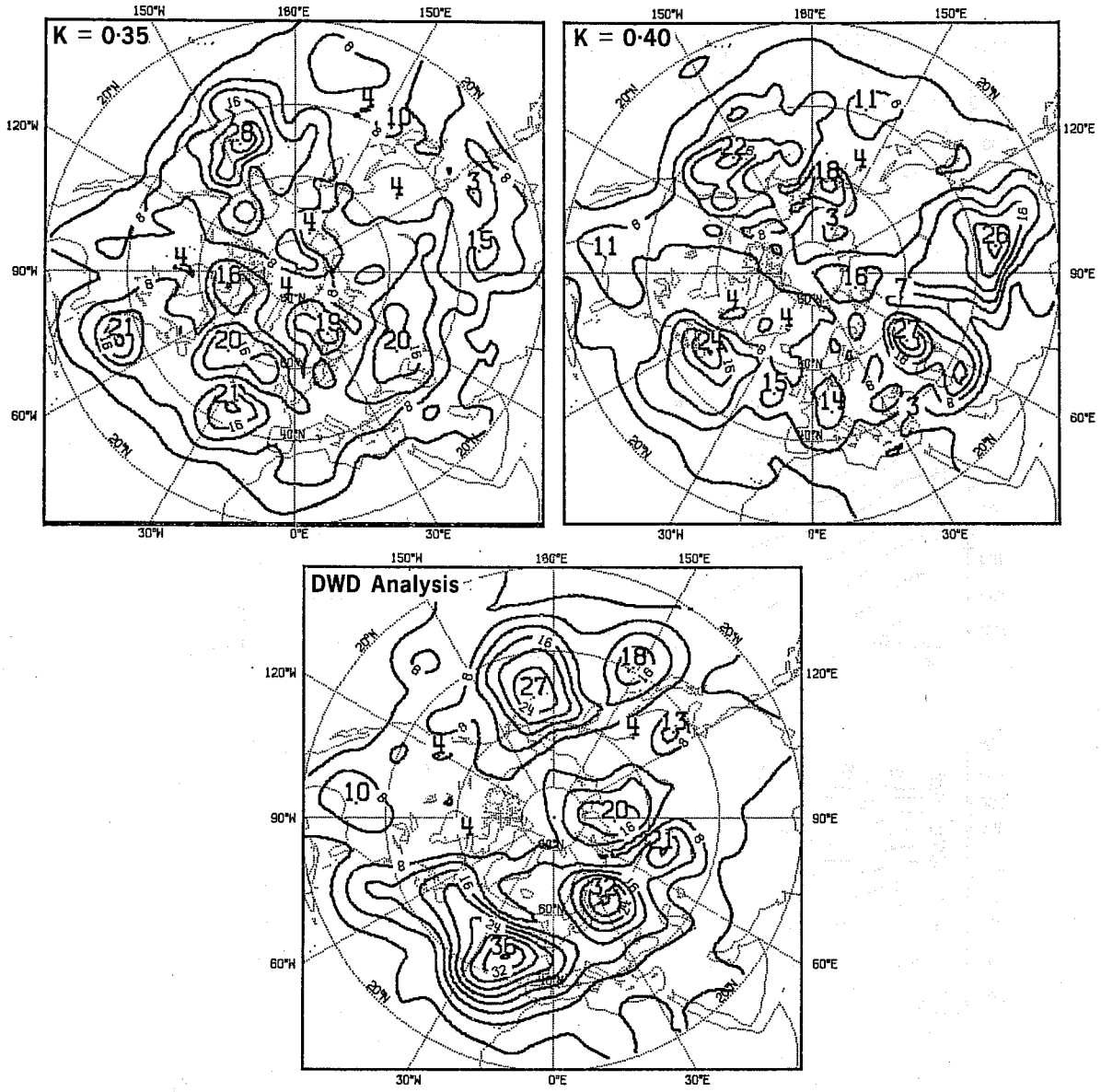

Fig. 35 The 24 day mean variance by transient waves in 1000 mb height

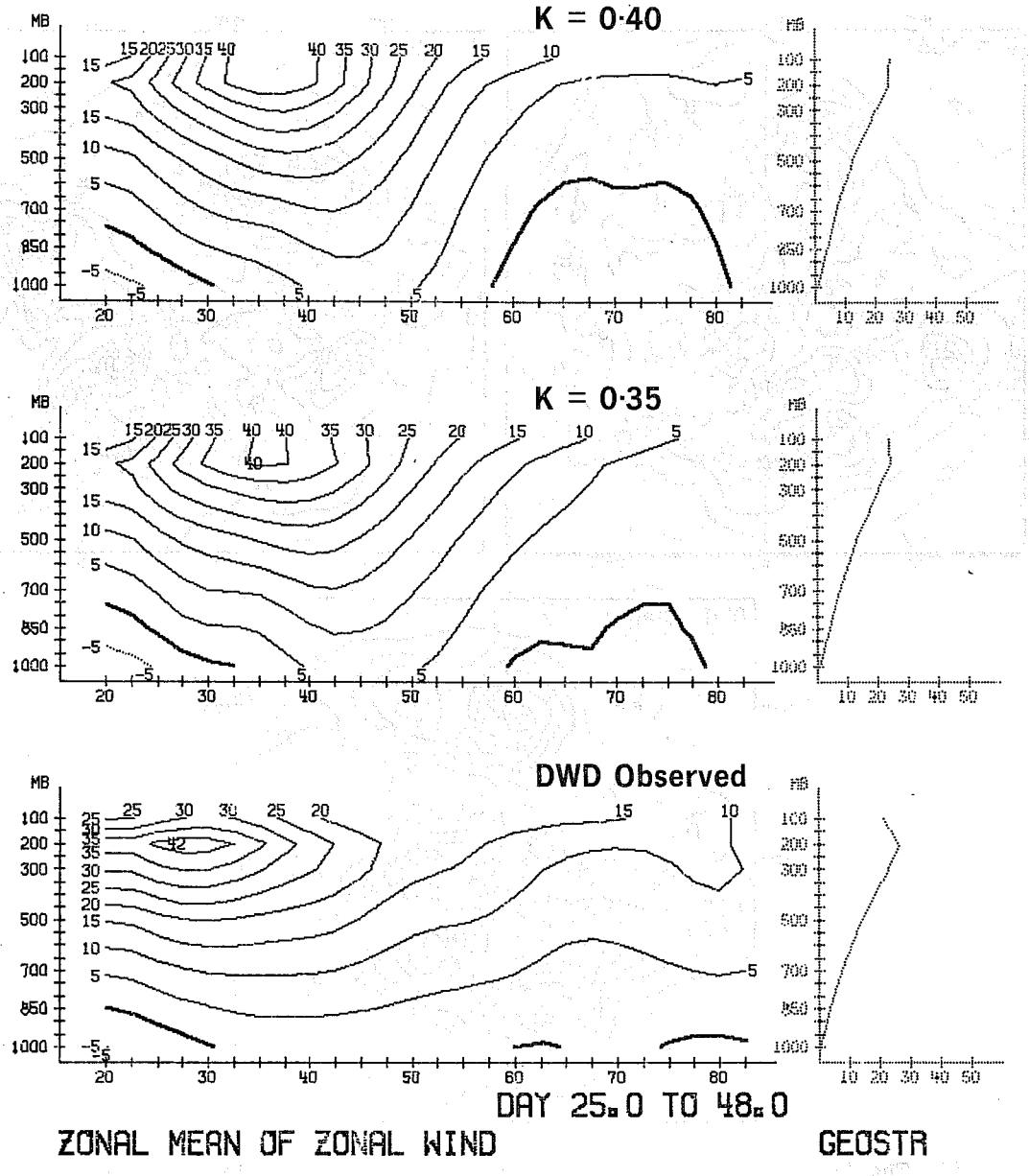

Fig. 36 The 24 day mean of the zonal mean of zonal wind (unit: m/sec).

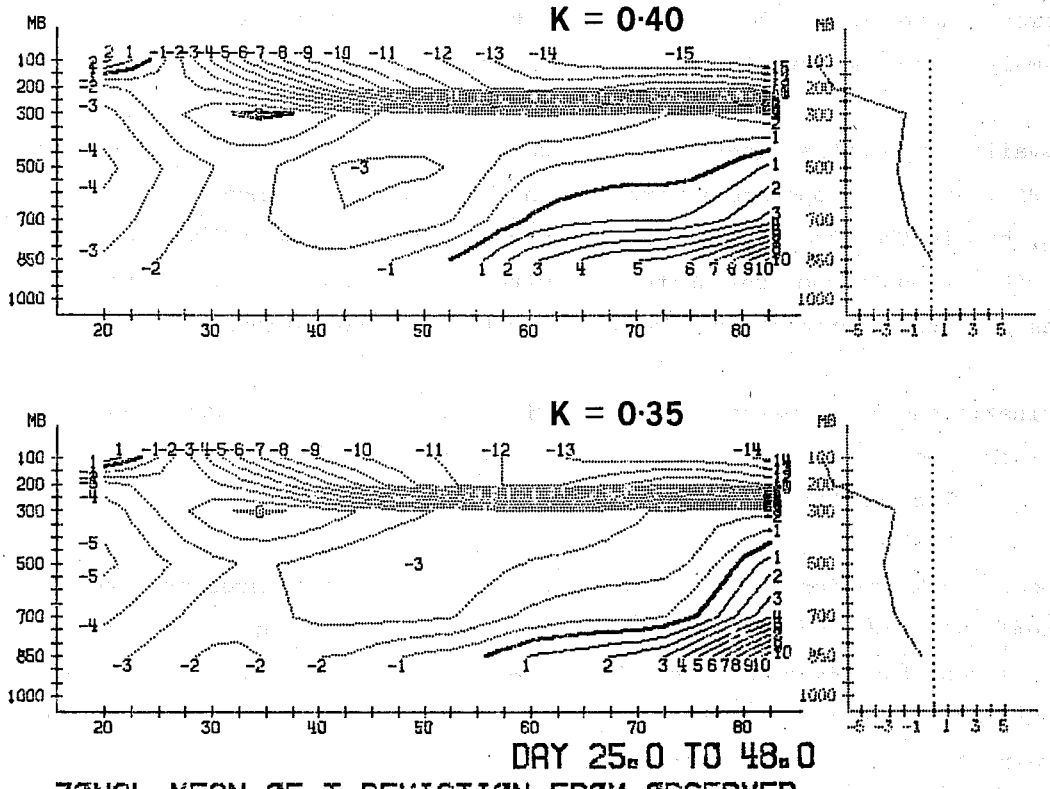

Fig. 37 The 24 day mean zonal mean of the temperature deviation from observed (unit: K).

with the higher Karman constant, but also a slightly colder stratosphere.

How has now the energetic cycle changed with the change of the Karman constant? The atmosphere is warmed by diabatic processes, whose 50 day mean is displayed in Fig. 38. The net heating is in the first experiment larger in the boundary layer in the subtropics in both hemispheres. On the other hand the rest of the troposphere is more cooled in exp. 1 than exp. 2, thus explaining the about 10% smaller cooling rate in the second experiment.

The available potential energy in wavenumber 1-20 Fig. 39 averaged over day 25 - 48 is in the troposphere stronger in the second experiment than in the first, but in the stratosphere, it has become weaker and moved to the North, where its strength compares quite well with observation. The troposphere agrees in both experiments not very well with the observations.

The kinetic energy in wavenumber 1-20, Fig. 40, averaged from day 25-48, has been increased and extended in the second experiment, but exceeds now the observed values with the factor 1.5.

The mean precipitation (Fig. 41) underwent considerable changes over the Indonesian Islands, where it dissolved in a larger number of smaller maxima in the second experiment. A remarkable feature is also the creation of a rain fall maximum east of India in the second experiment, where we observe hardly any rainfall at all in the first one.

4.4 Summary

The introduction of a higher Karman transport in the model increases temperature and humidity in the model atmosphere and creates stronger and more active pressure systems. On the other hand it does not solve the problem of the cooling in the model atmosphere and tends rather to amplify the over development of lows. The effects on the model energetics are more apparent in the higher atmosphere than in the boundary layer, where one might expect them.

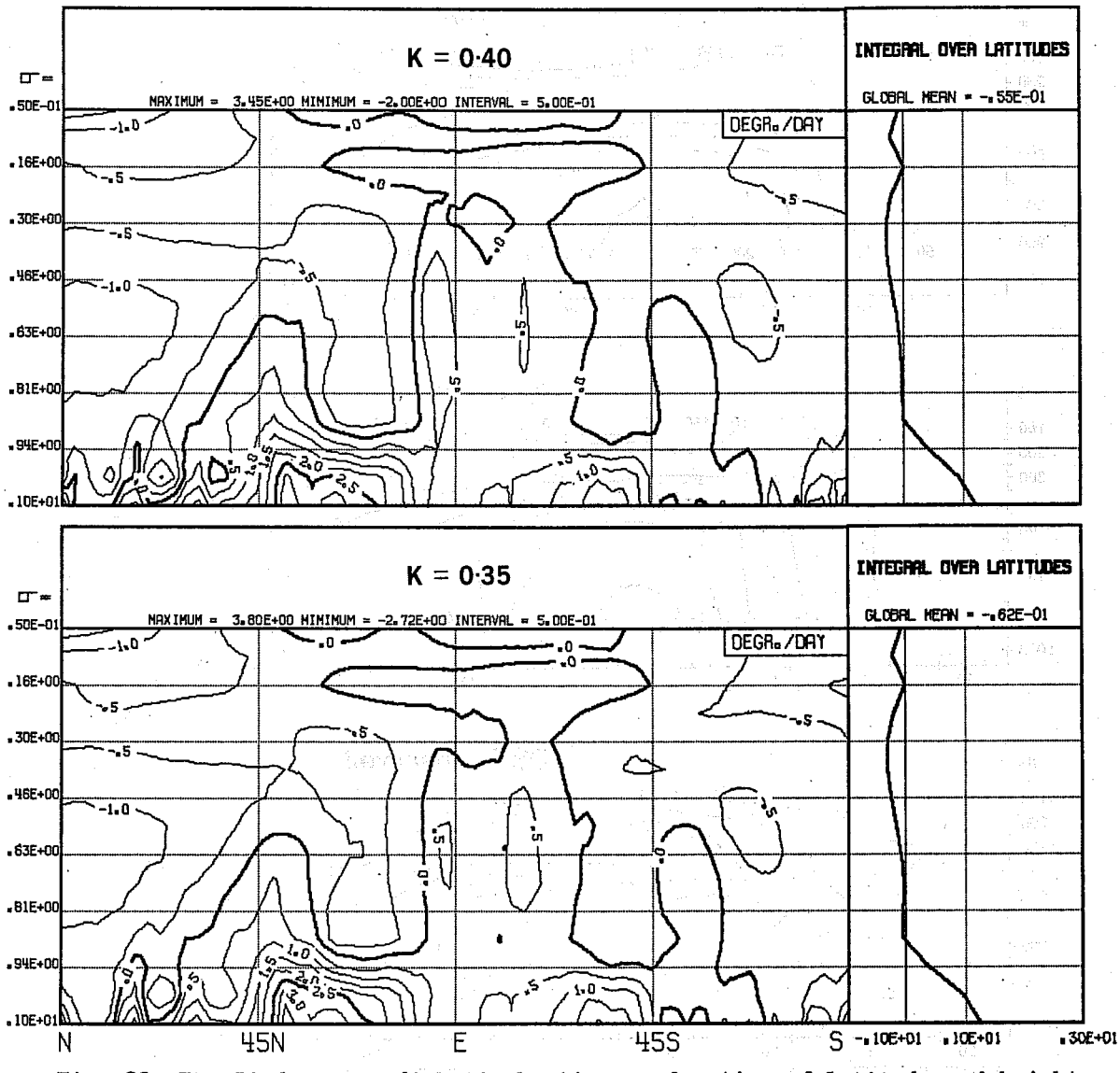

Fig. 38 The 50 day mean diabatic heating as function of latitude and height.

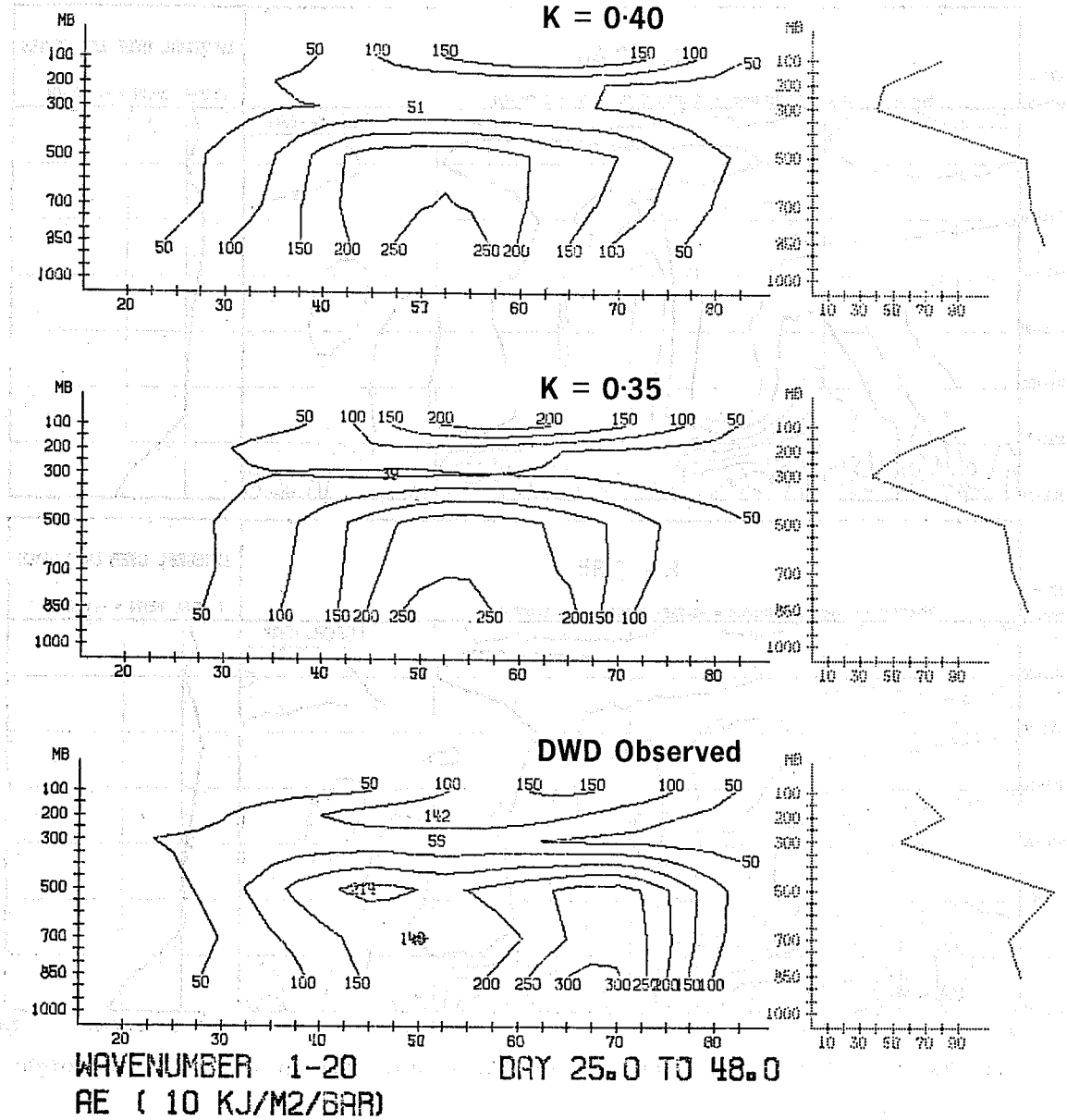

Fig. 39 The 24 day mean available potential energy (wavenumber 1-20, unit: $10kJ/m^2/bar$).

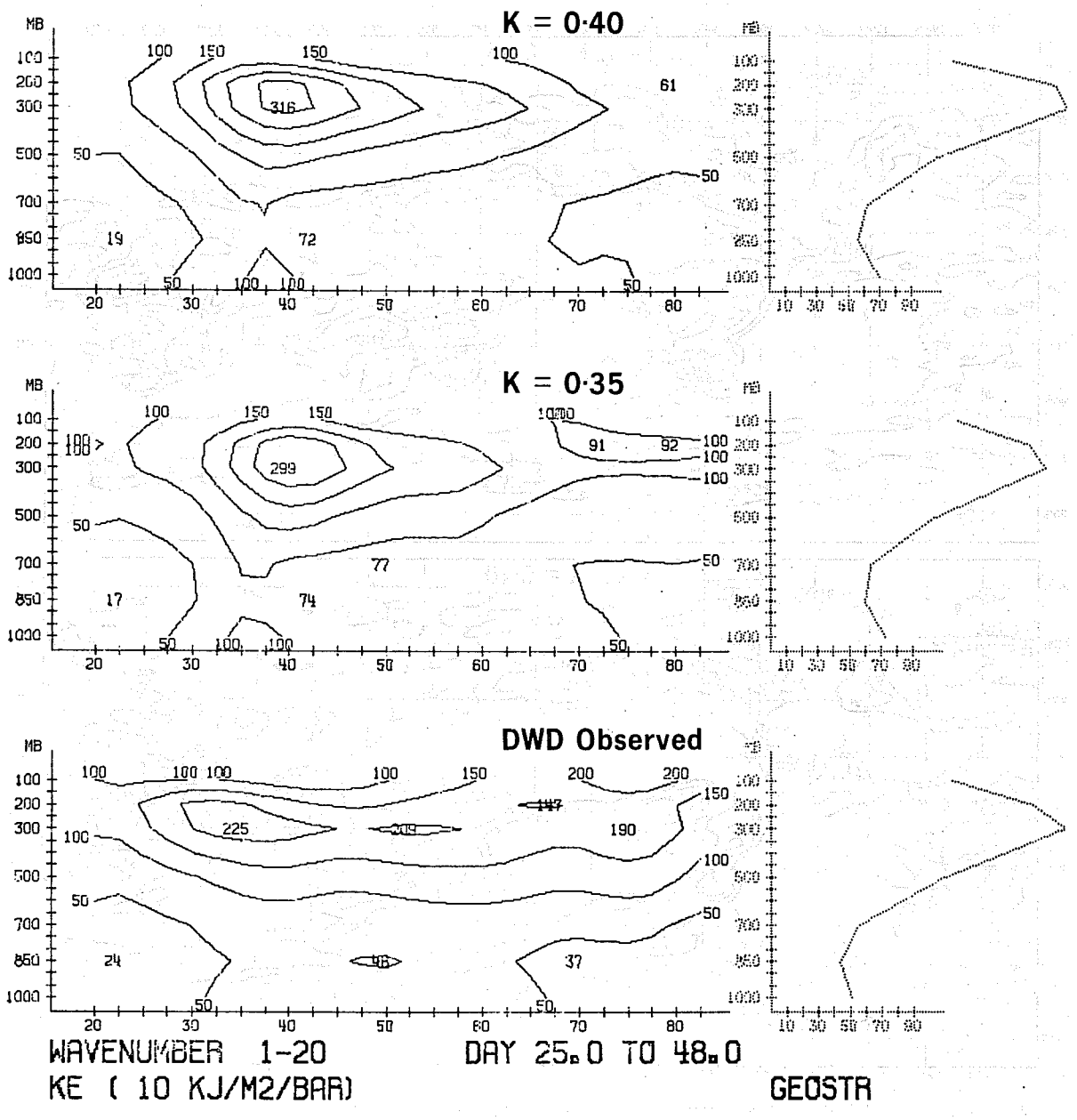

Fig. 40 The 24 day mean kinetic energy (wavenumber 1...20, unit: 10 kJ/m^{2}bar)

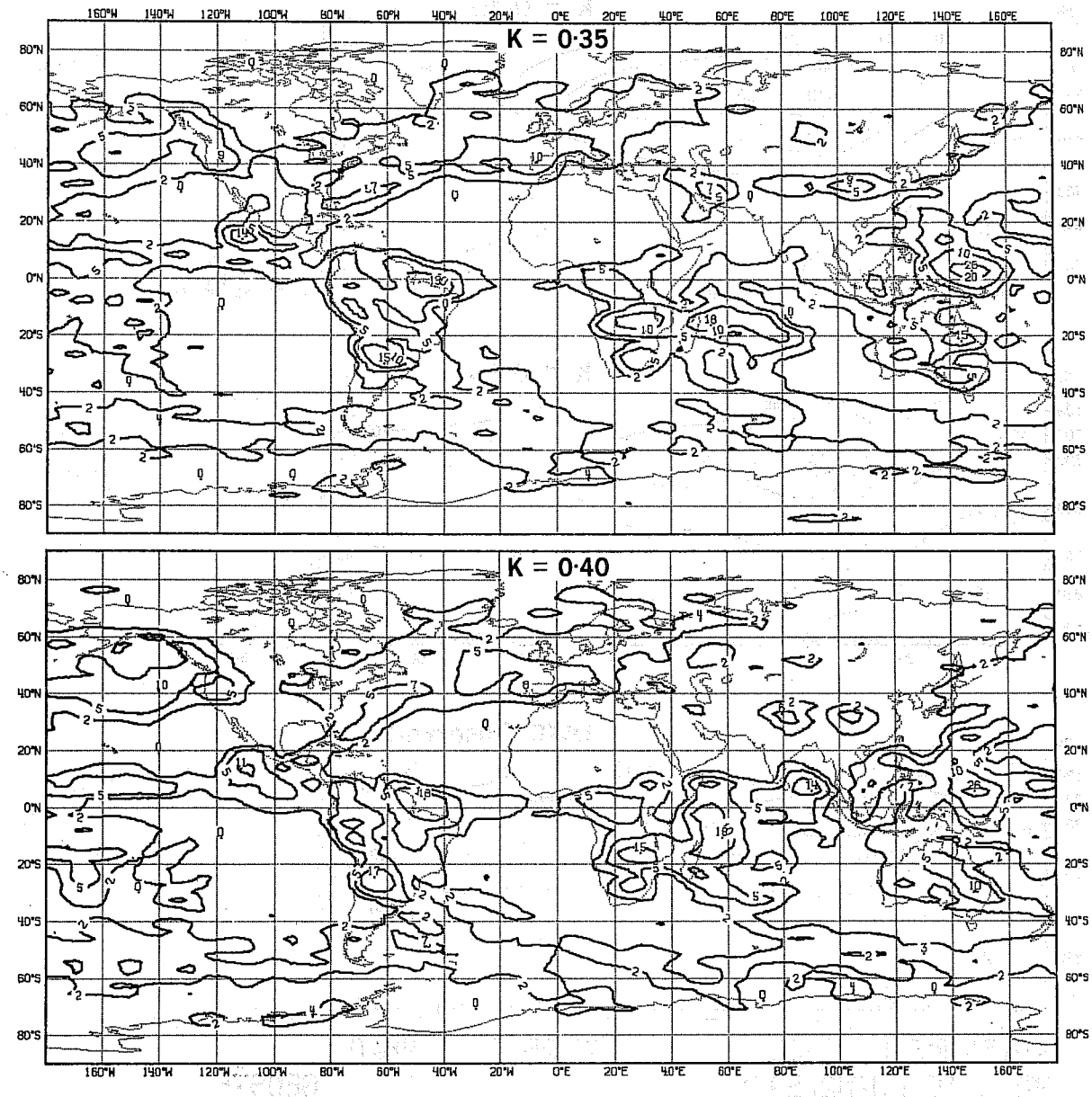

Fig. 41 The 30 day mean precipitation (convective and large scale, unit: mm/day).

5. THE RESPONSE OF THE EC MODEL TO CHANGES IN THE ANALYSIS SCHEME AND THE INITIAL DATA

5.1 Introduction

A recent paper by Arpe (1980) describes considerable differences in the analysis of a number of national weather centres. But not only among different weather centres, but also in the EC analysis one can find some differences in the analysis corresponding to a number of corrected programming errors. Since one can expect more corrections of errors in the EC analysis scheme, this study might give some hints to which extent they will influence the dynamics of the model.

Additional to three runs with FGGE datasets one integration, (made available by the French Met. Office) starting from an atmosphere at rest is included in this evaluation to find out up to which prediction time the initial data dominate the model atmosphere.

5.2 The experiments

All experiments have been carried out using a T21L15 spectral model (Baede et al, 1979), and the ECMWF physical parameterisation package. As initial date the 16.1.79 was chosen and the results were compared with the DWD analysis. All initial datasets were created from the FGGE group and represent a historical development in the FGGE analysis. Following experiments were performed.

Exp.1 first FGGE end-to-end test dataset (INES)

Exp.2 as Exp.1, but better humidity field (ITUACMOLD)

Exp.3 operational FGGE dataset, but influence function "upside down" (ITUAPAOLD)

Exp.4 background field as Exp.2, but atmosphere set to a state of rest (this run was made available by the French Met. Office). (REST)

5.3 Results

Although all experiments start at day 0 from a different mean precipitable water content value (which is a measure for the humidity) (Fig.42) they converge after day 30 to a mean value of 23.8 potential mm. Experiment 2 and 3 which start from the most realistic humidity value, show in the first 2-3 days a sharp increase in humidity which drops afterwards and meets the curve of Exp. , which starts at a too low humidity at about day 12. The spinup cannot be observed in Exp. 1 (too low humidity) and Exp. 4 (no humidity at all). The forecast, which starts at zero humidity and from an atmosphere at rest, reaches the curves of the other forecasts between day 25 and 30 and runs then among them.

Also the experiments 1, 2 and 3 start at almost the same temperature (Fig. 43), the one of Exp. 1 drops more rapidly in the first 10 days. This is probably caused by the humidity deficit in this run, because the atmosphere loses sensible heat, which is used to evaporate water until the equilibrium state is reached. The same explanation can be given for Exp. 4 where the drop in potential energy is used to start up a reasonable atmospheric circulation. Despite the different angle of temperate drop all the curves meet together at about day 15 (the temperature loss for Exp. 1, 2 and 3 was to that time about 2. - 2.5^{o}) and steadily converging to each other they end up with a final temperature of 249.2 $^{o}K \pm 0.25$ at day 50. Forecast experiments done up to day 100 suggest that the temperature decrease from day 50 onwards is only marginal.

The globally averaged total kinetic energy (Fig. 44) seems to be fairly similarly reproduced in the runs with the FGGE data (exp. 1, 2, 3).

In the first 8 days one can see a sharp drop in the kinetic energy, which is even stronger for Exp. 1 due to the wrong humidity, but after day 15 they have reached their final value of about 1300 $kJ/m^2 \pm 75$. The curve of the run starting at an atmosphere at rest joins the curves of the other runs at day 39 and and runs then together with them.

Also in the diagram displaying the ratio between zonal and eddy kinetic energy (Fig. 45) one can see the close link between Exp. 1,2, and 3. After a period of increasing zonality until day 8, all the curves indicate an increase of

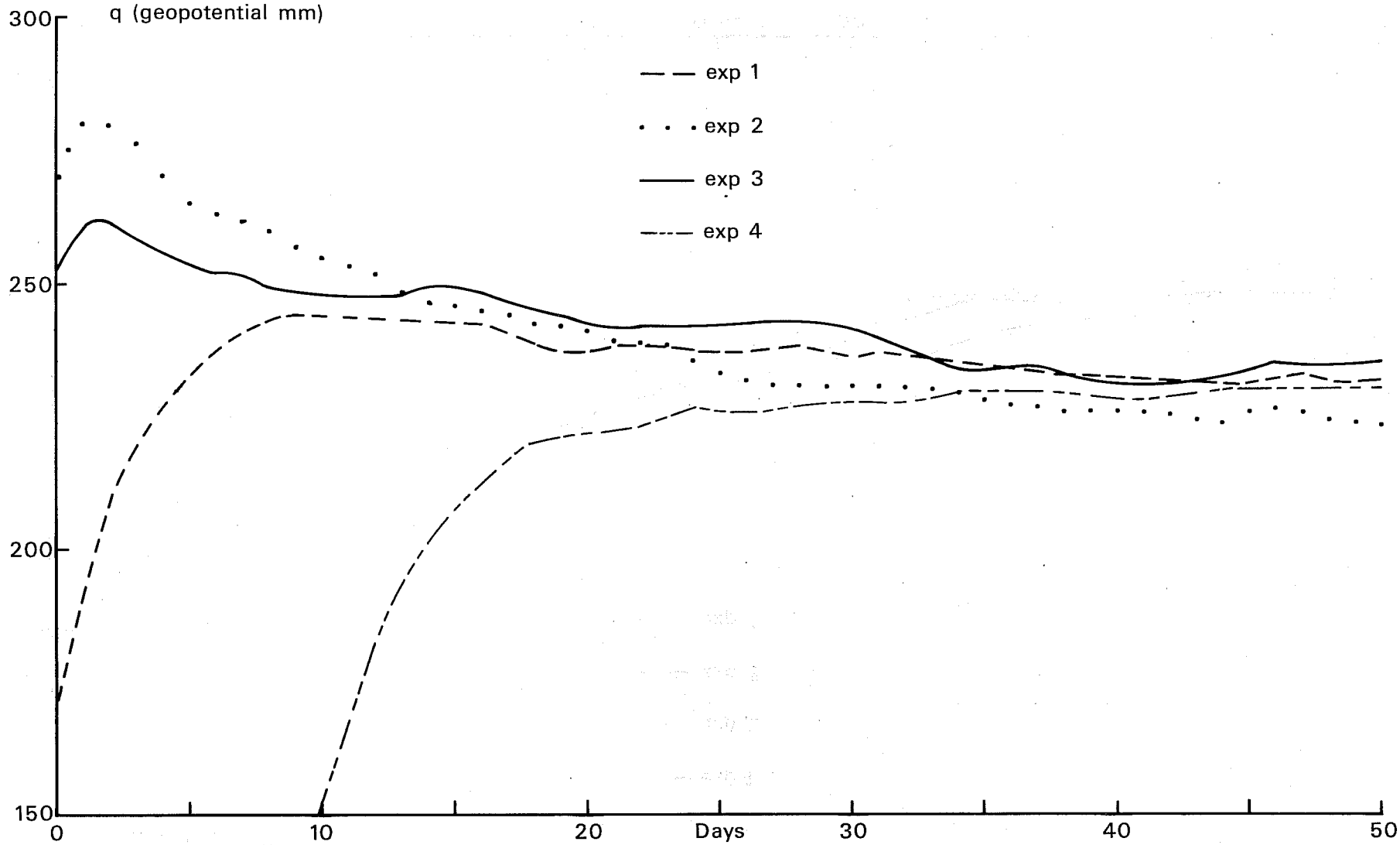

Fig. 42 The global mean precipitable water as function of prediction time

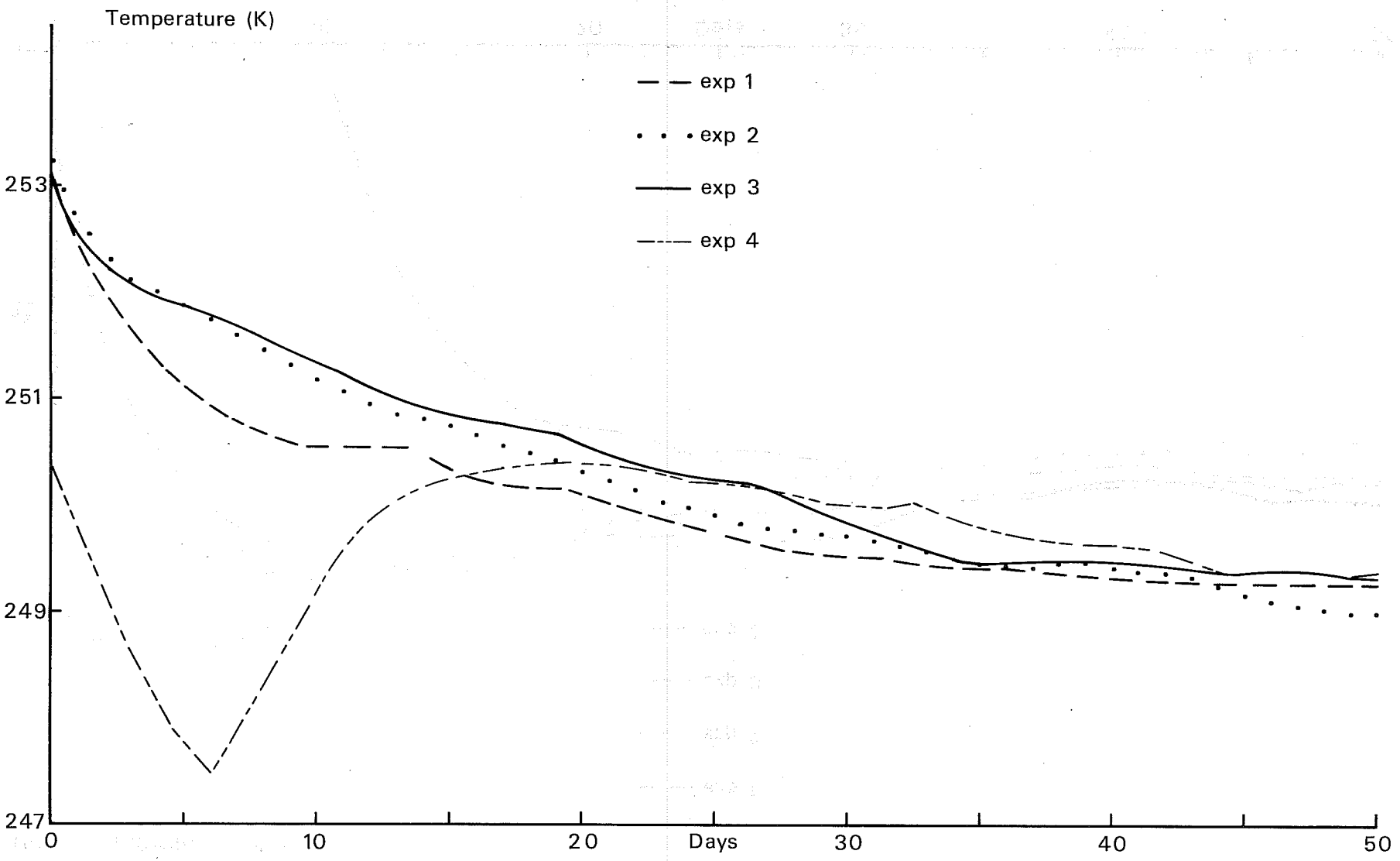

Fig. 43 The global mean temperature as function of prediction time

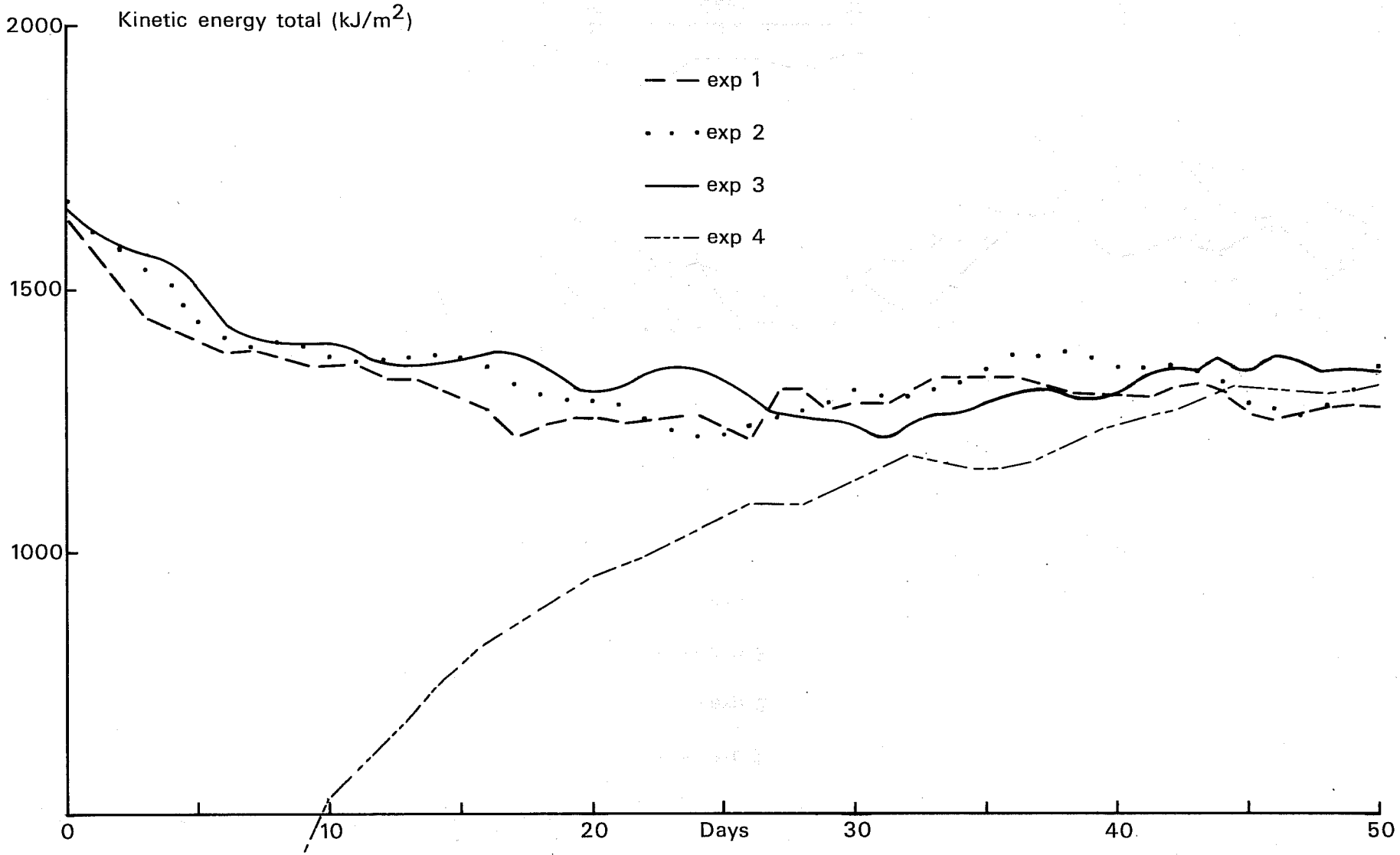

Fig. 44 The global mean of total kinetic energy as function of prediction time

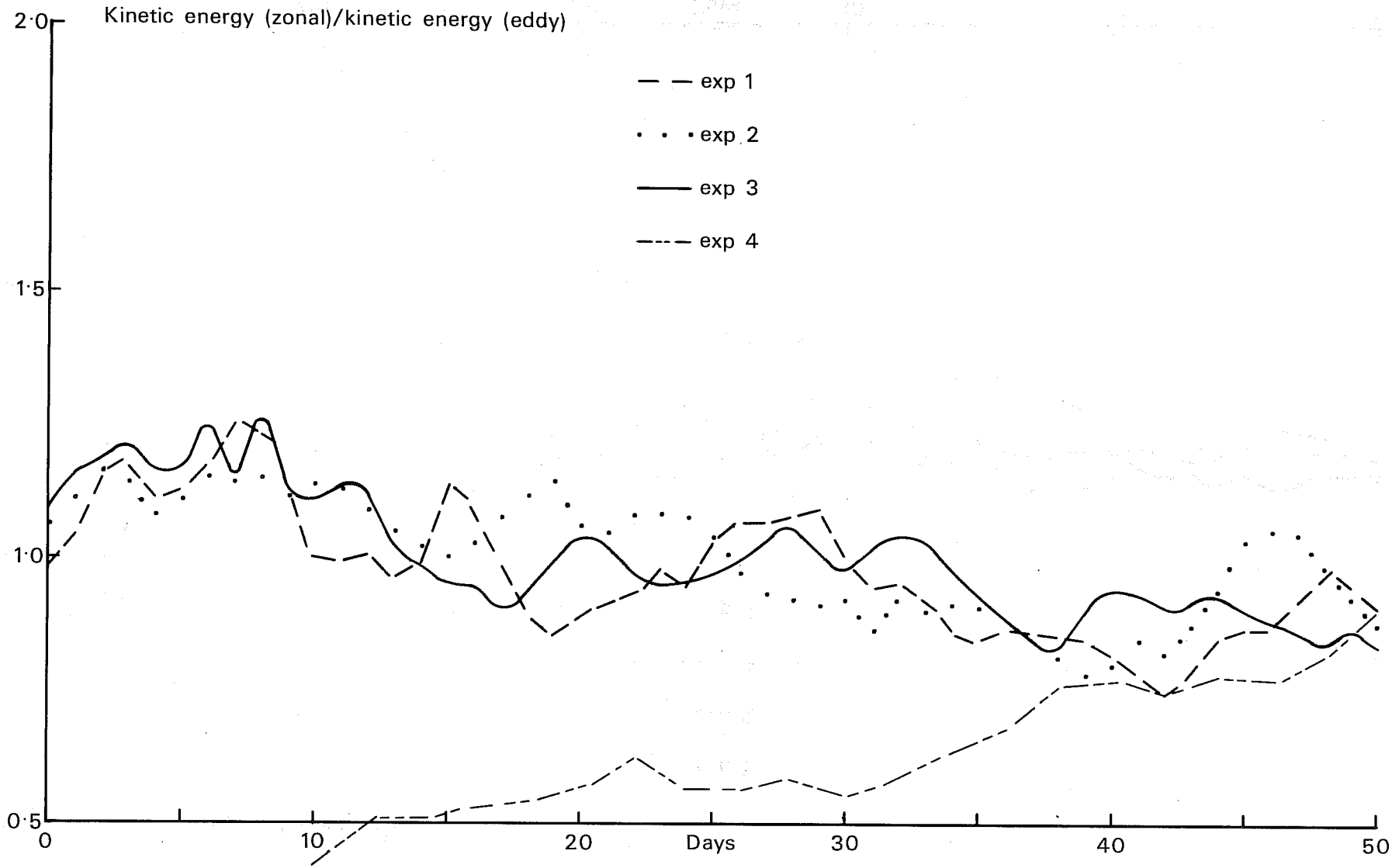

Fig. 45 The ratio of the global mean zonal kinetic energy to the mean eddy kinetic energy as function of prediction time

eddies with the final ratio of $k_z : k_e = .9 \pm .15$. The zonality for the 3. exp increases steadily till its curve meets the one of the other experiments at about day 38, where it then runs together with them.

The time evolution of the global mean of the meteorological parameters can be summarised as follows:

There exists a state of the model, where the average meteorological quantities are independent of the initial state. The time, when this state is reached, is dependent on the quantity. It is about

- 30 days for the humidity
- 20 days for the temperature
- 40 days for the kinetic energy

The variability of these parameters, once the stable state is reached, is small and smaller than the differences in the initial state.

The stable state of the model is always different from the initial data, which means that the model atmosphere and the initial data atmosphere are built up in a different way.

Other models started from atmosphere at rest give about the same adustment period (Mintz, 1964) or much longer periods up to 200 days (Manabe et al, 1965, Smagorinsky et al, 1965). These long spin up times for the GFDL model is probably a consequence of the low resolution used in those runs at the beginning (N5 - N20) and also manual corrections applied during those runs (Holloway, et al 1971).

The mean (day 24 - 48) 1000 mb height map (Fig. 46) of the DWD shows 2 distinct lows over the Pacific region and one south of Greenland. All model runs display lows in these regions, but with different intensities and location.

The run started from the atmosphere at rest shows over the Atlantic side of the hemisphere a lot of small scale features and resembles in this region very much the forecast of Exp. 3. The general air flow over Europe is in no experiment reasonably reproduced and the Mediterranean low is left out completely.

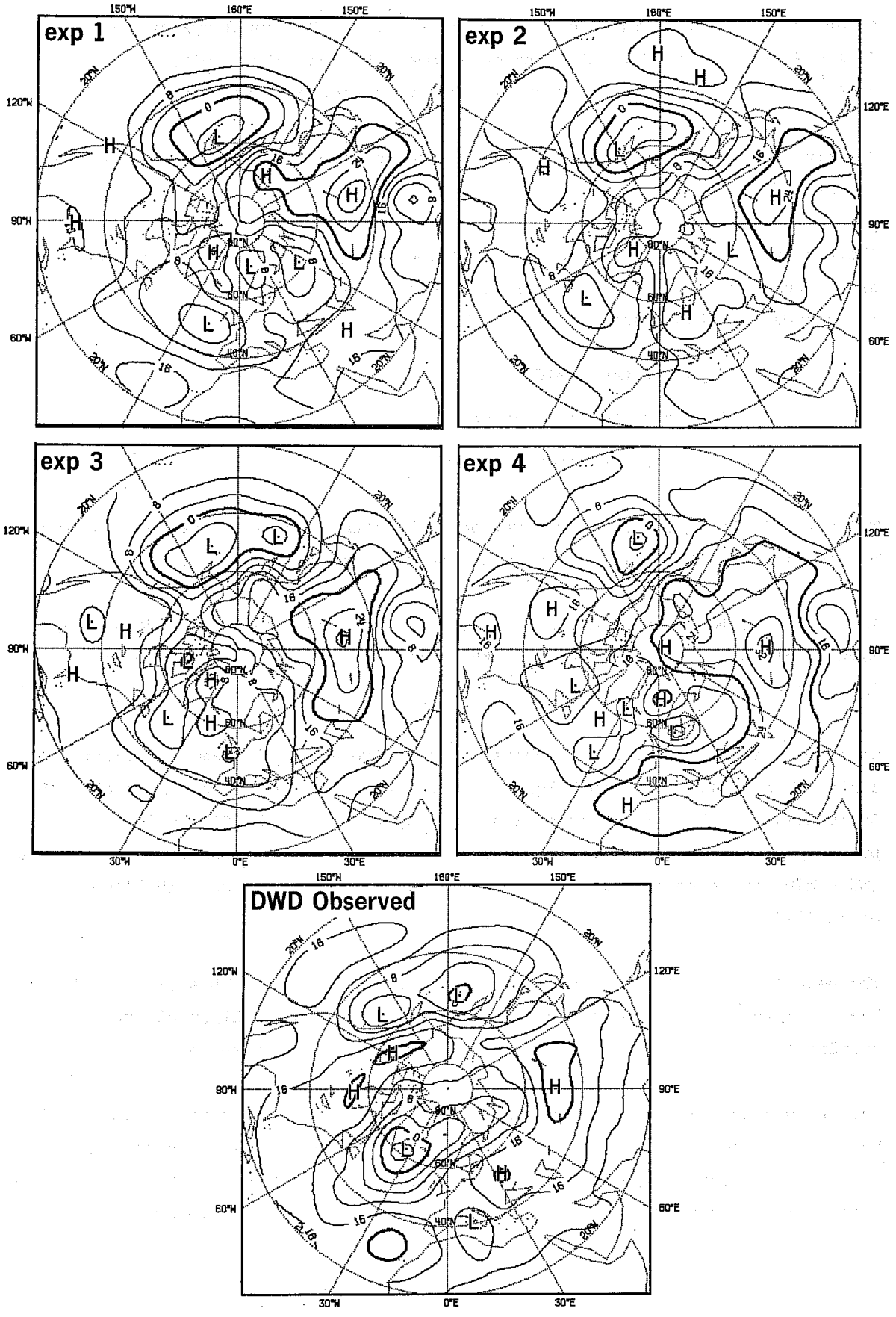

Fig. 46 The 24 day mean 1000 mb height field (contouring interval: 40m).

Table 1. The number and minimal pressure of depressions in the 24 day mean in the Atlantic and Pacific area in 1000 mb.

	Atlantic		Pacific	
	Pressure	Number	Pressure	Number
Exp. 1	1004	1	996	1
Exp. 2	1004	1	996	1
Exp. 3	1000	2	996	2
Exp. 4	1004	4	996	1
DWD	996	1	1000	2

The mean 500 mb height field (Fig. 47) displays nicely the variability of these test integrations. The polar region is in all experiments too warm but the centre of the coldest air can be found over North America (Exp. 1, Exp. 3) or Russia (Exp. 2). The difference to climate (Fig. 48) and the difference between the runs (Fig. 49) (here Exp. 2 as standard) seem to have the same order of magnitude. Moreover, the difference to climate and the difference to Exp. 2 obtain their maximum in fairly similar regions (N.W. Europe and coastal regions of the Pacific area) which indicate the strong local variability of these deviation maxima even in a 24 day mean. Since the difference to climate is similar in Exp. 4 to all other experiments, this systematic error seems to be independent of the data. The variance by transient waves (Fig. 50) reaches in Exp. 1 and 3 values up to 40 dkm, (DWD up to 50 dkm)- while exp. 2 and 4 are limited to maximal 30 dkm.

The rate of change of available potential energy (A_E) is balanced by the diabatic heating (Q) and by transformation into kinetic energy (T_K).

$$A_E + T_K + Q = 0$$

The heating function Q is dependent of the physical parameterisation, the initial data and the boundary conditions. In Exp. 4 the initial data are set to unrealistic values and one can therefore see from this experiment how much and how fast the boundary conditions and the physics force the model into its own state.

The zonal mean of available potential energy in wavenumber 1 - 20 (Fig. 51) shows for all experiments a deviation of 50% from the observed values. The stratosphere on the other hand is worse reproduced in Exp. 4 suggesting that the higher levels of the model have not yet found their final equilibrium. Also the conversion of AE (Fig. 52) is equally well treated in all experiments with the fourth experiment coming close to the observed values. The stratosphere

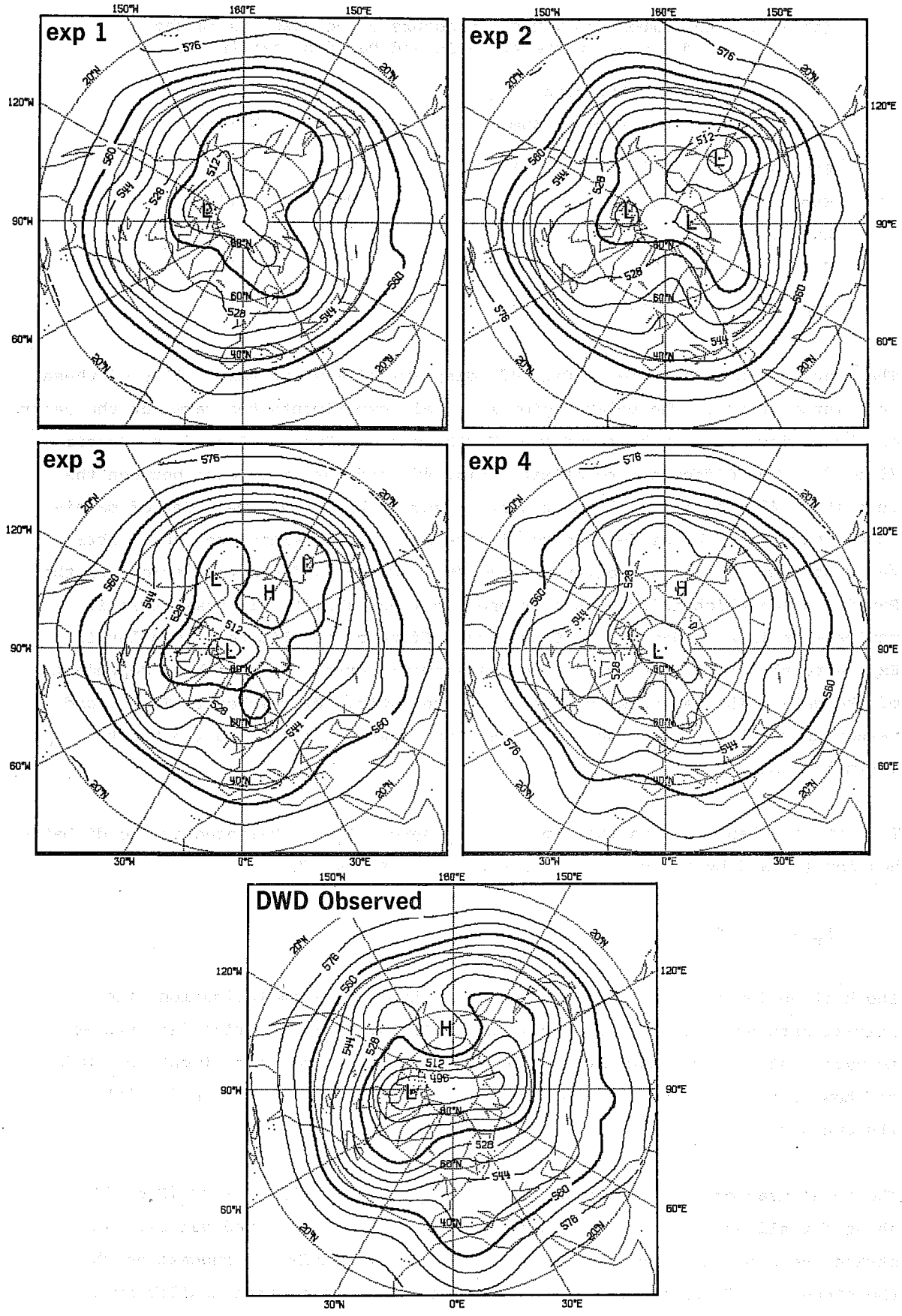

Fig. 47 The 24 day mean 500 mb height field (contouring interval: 80m).

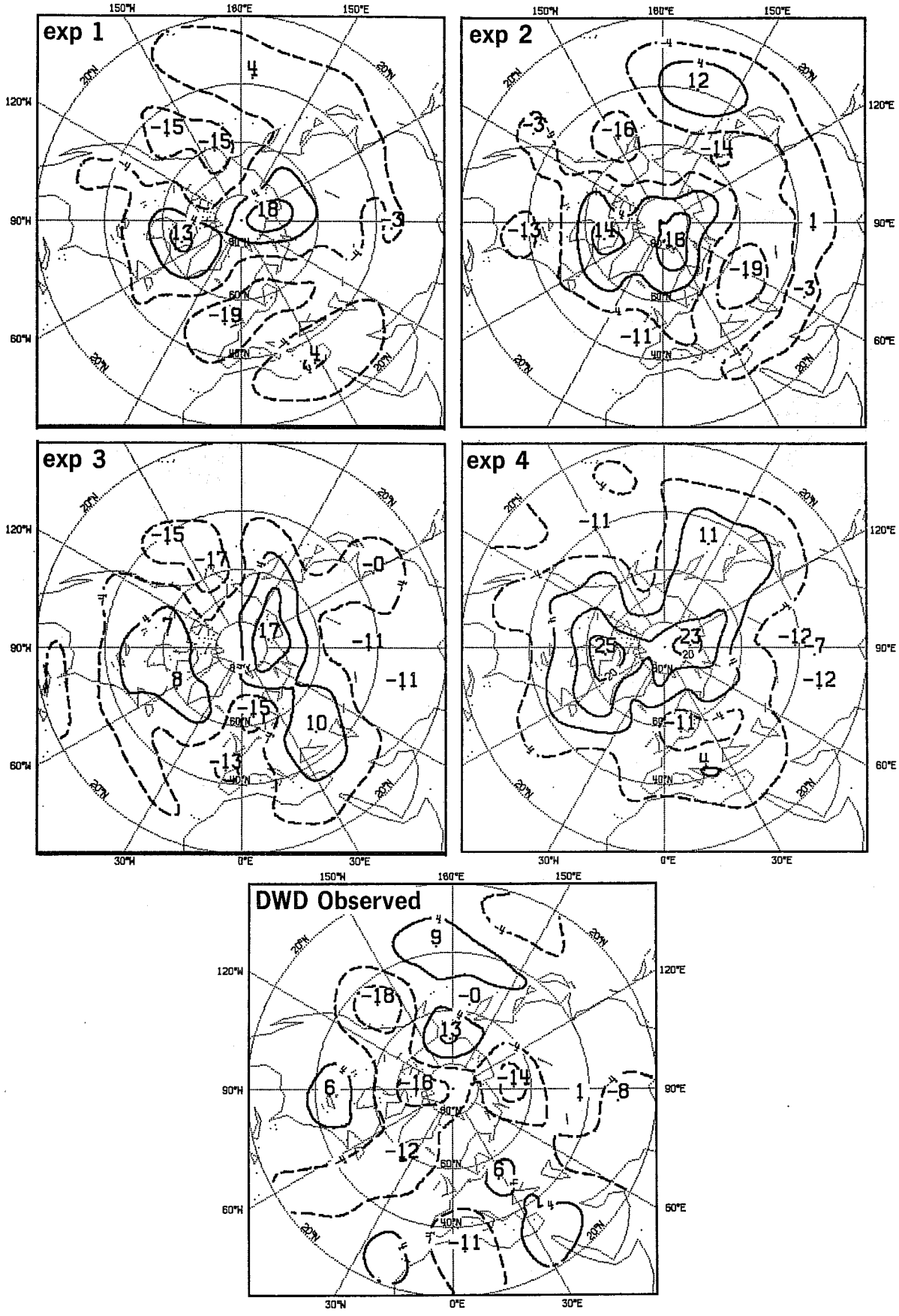

Fig. 48 The 24 day mean difference of the 500 mb height field to climate.

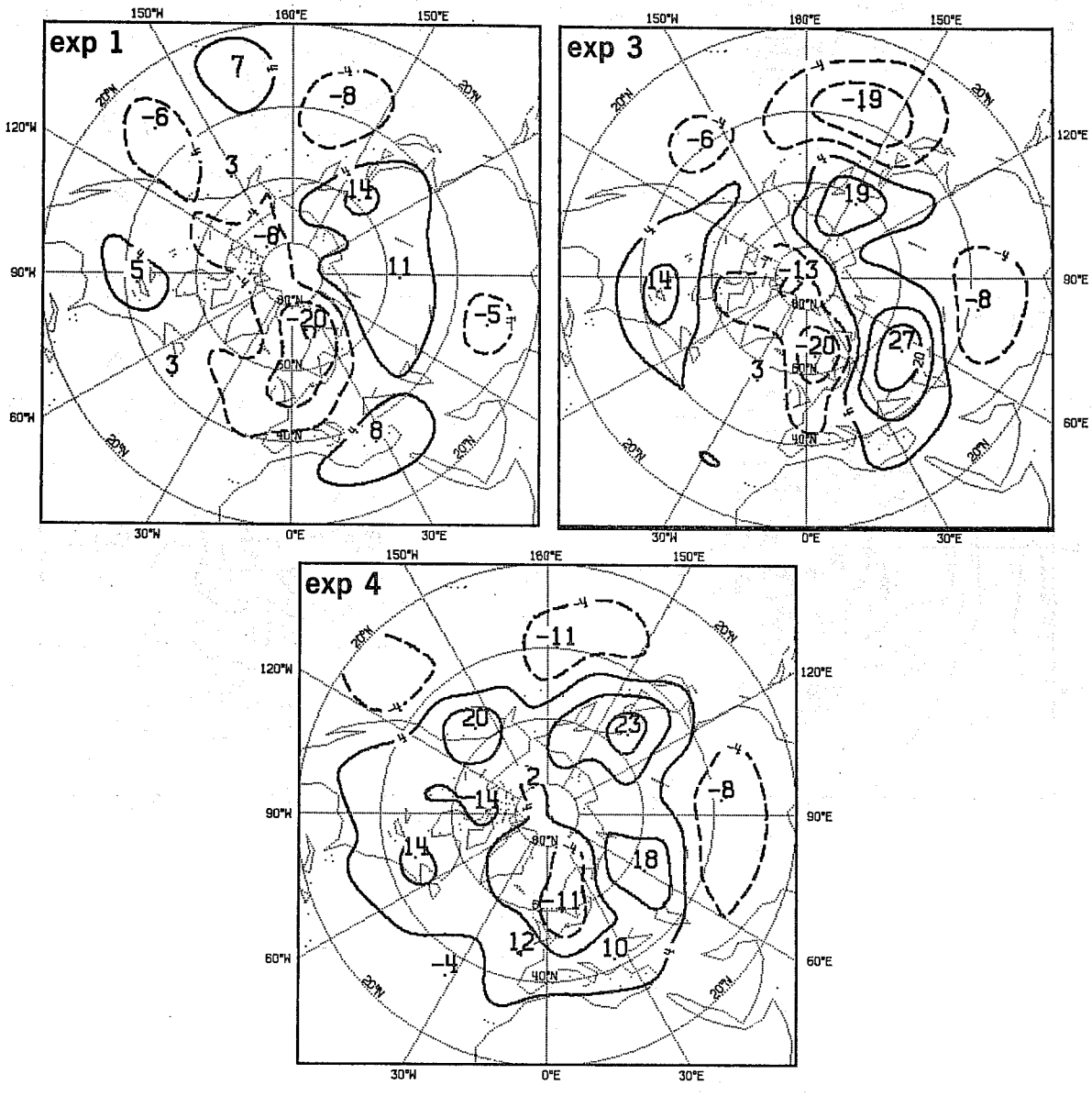

Fig. 49 The 24 day mean difference of the 500 mb height fields to the one of experiment 2.

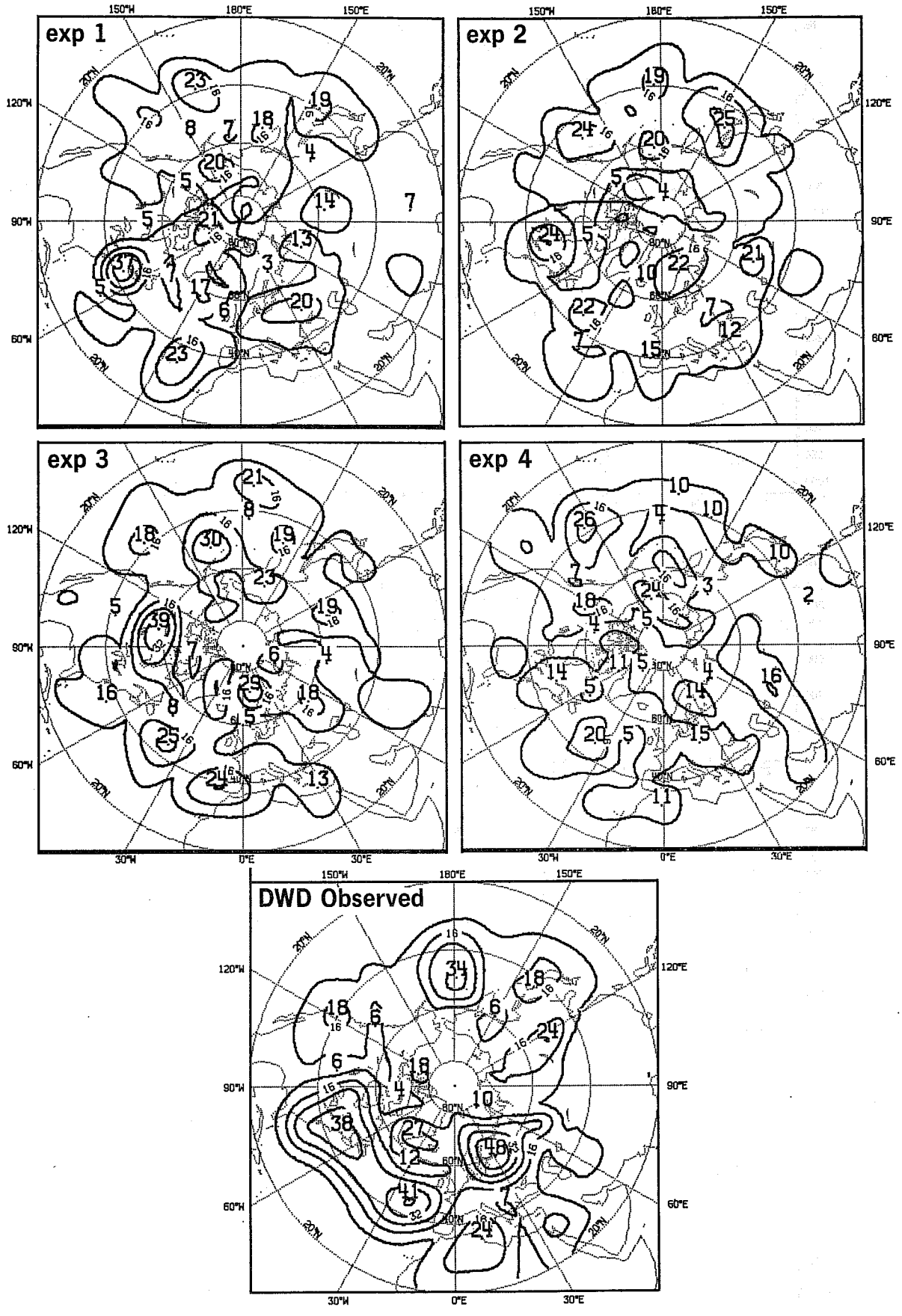

Fig. 50 The 24 day mean variance by transient waves in 500mb.

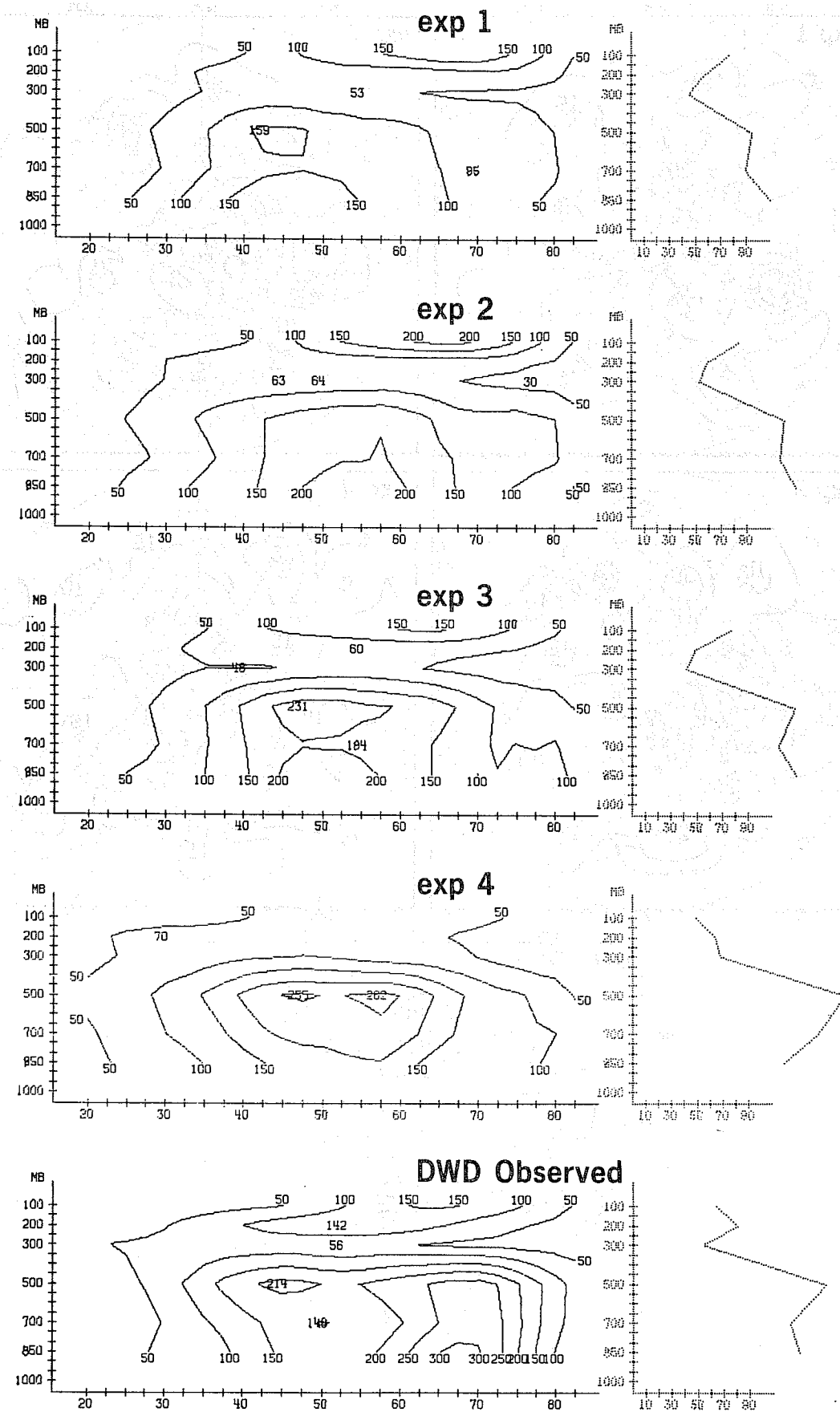

Fig. 51 The 24 day mean available potential energy (wavenumber 1...20, unit: 1/10 Watt/m^2/bar

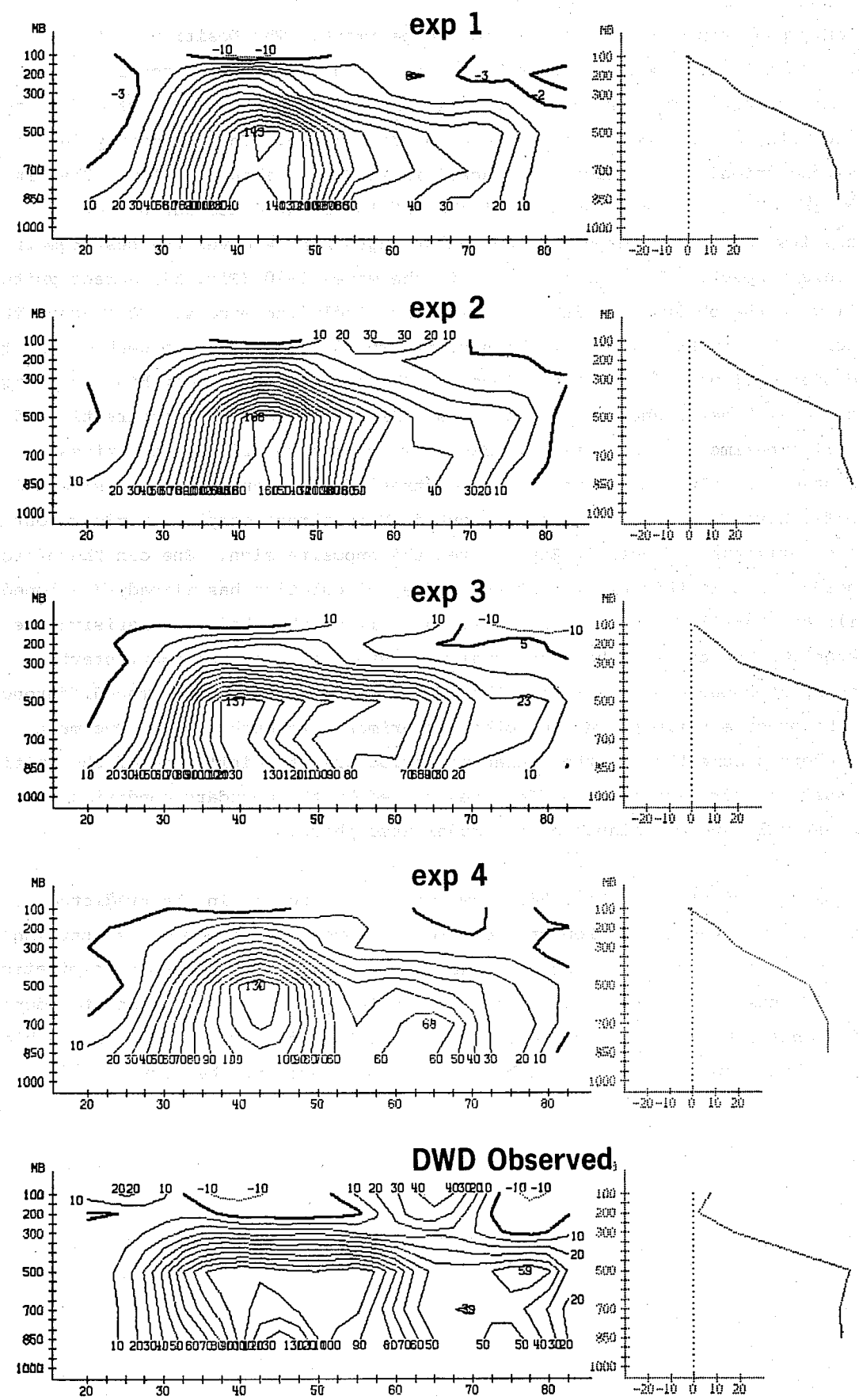

Fig. 52 The 24 day mean conversion of available potential energy (wavenumber 1...20, unit: 1/10 Watt/m^2/bar).

is only poor reproduced in the 1 and 4 experiment. The position of the jet stream in the model can be seen in Fig. 53 displaying the zonal kinetic energy. The strength of the jet in the predictions with real data agrees quite well, but is too low compared with observation. This is mainly due to the resolution. The maximal wind speed is in Exp. 4 about 15% lower than in the other experiments. The core of the jet is situated too far north. Since its position is dependent on the strength Exp. 4 gives the best result in this respect. The kinetic energy in the waves 1-20 (Fig. 54) agrees quite well with the observation in all experiments including exp. 4. It reaches its lowest level in Exp. 1 and its highest in Exp. 3, but it is too weak in the mid and high latitudes for all experiments. The conversion of eddy kinetic energy into zonal kinetic energy and vice versa (Fig. 55) seems to be overestimated in all experiments, especially in Exp. 2 where one records up to 3 times the observed value. The axes of the centres of main conversion are situated too far north. A third centre at about 48°N is almost completely missed out in all experiments and gets in Exp. 4 even the opposite sign. One can therefore conclude that in this experiment the Hadley circulation has already developed while the Ferril Circulation is still not well established. Summarising the energetics one can say that the zonal mean state of the experiment starting from an atmosphere at rest shows the same order of magnitude in the difference to the other experiments as the other experiments to each other. One must therefore assume that in the averaging period used the influence of the initial dataset is overshadowed by differences caused by the boundary conditions or the natural random variance of the model atmosphere.

The main precipitation (Fig. 56) shows major differences in the predicted rainfall over the inner tropical convergence zone. The experiments starting from a too dry atmosphere (Exp. 1, Exp. 4) get not a high enough precipitation over the Amazonas region and show thereby a high inertial of land regions to adopt to a reasonable hydrological cycle once it is disturbed. Over sea we find a high variability, but a relation to the used dataset could not be found.

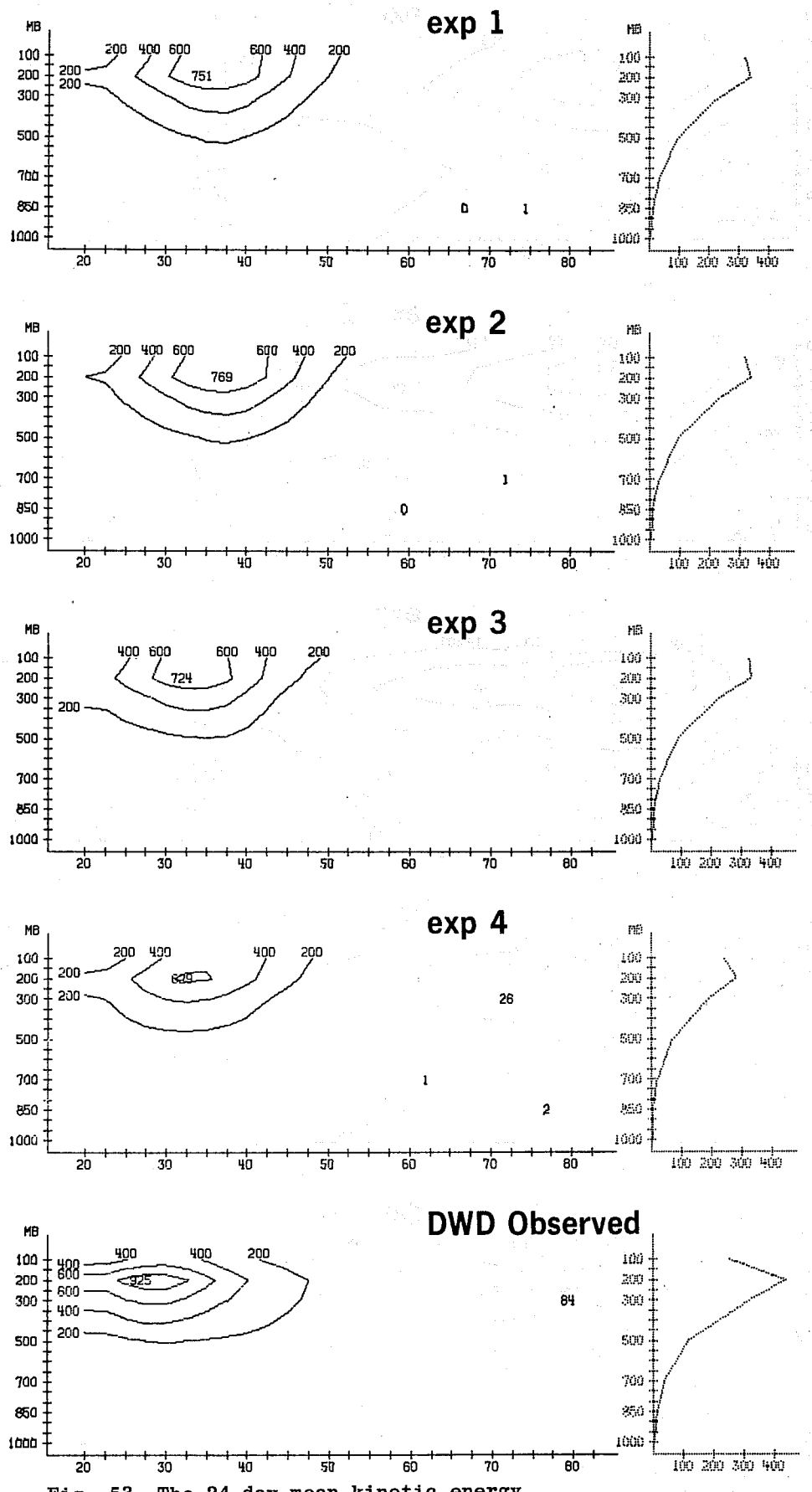

Fig. 53 The 24 day mean kinetic energy
(zonal part, unit: 10* kJ/m^2/bar)

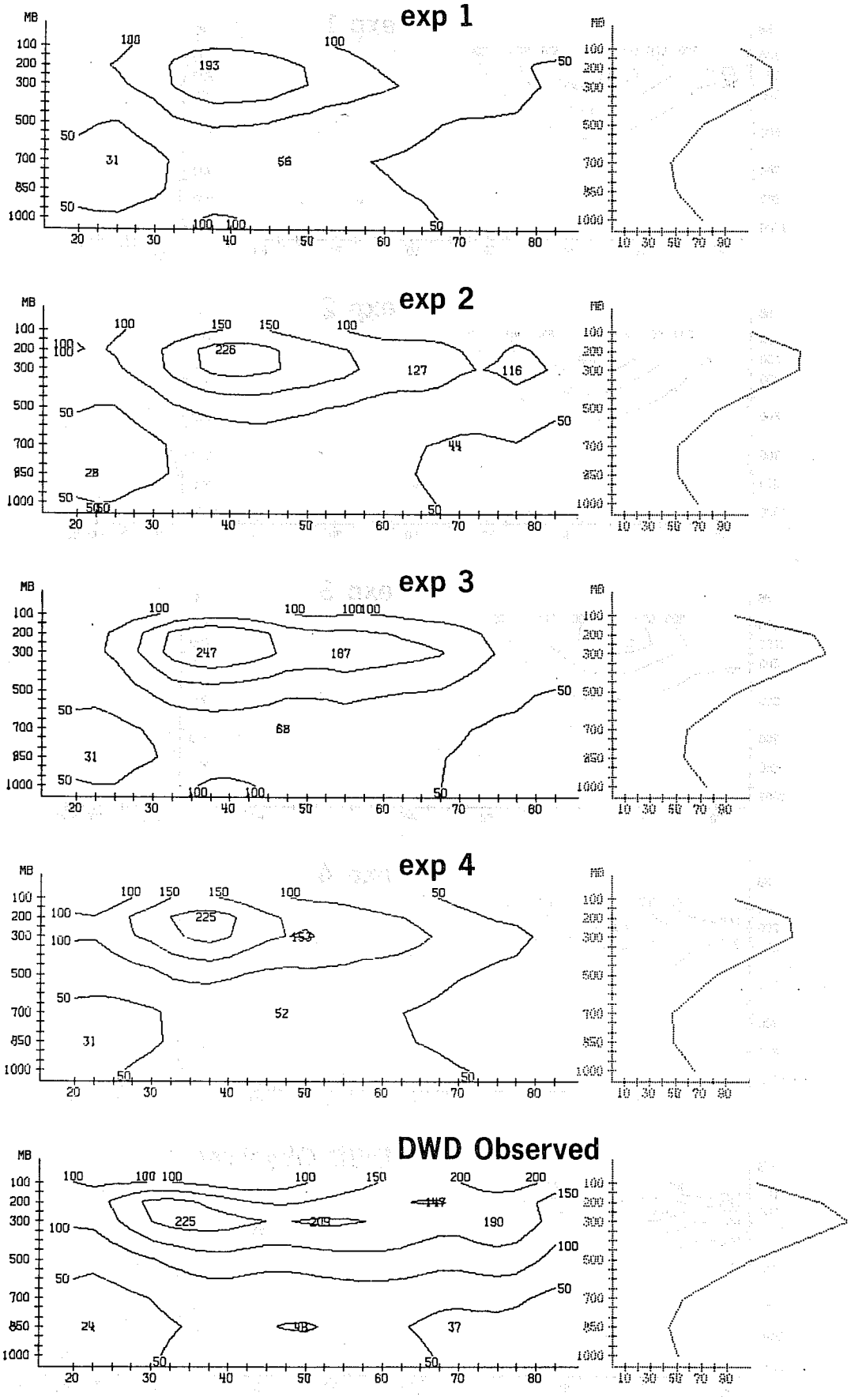

Fig. 54 The 24 day mean kinetic energy (wavenumber 1...20, unit: 10*kJ/m^2/bar)

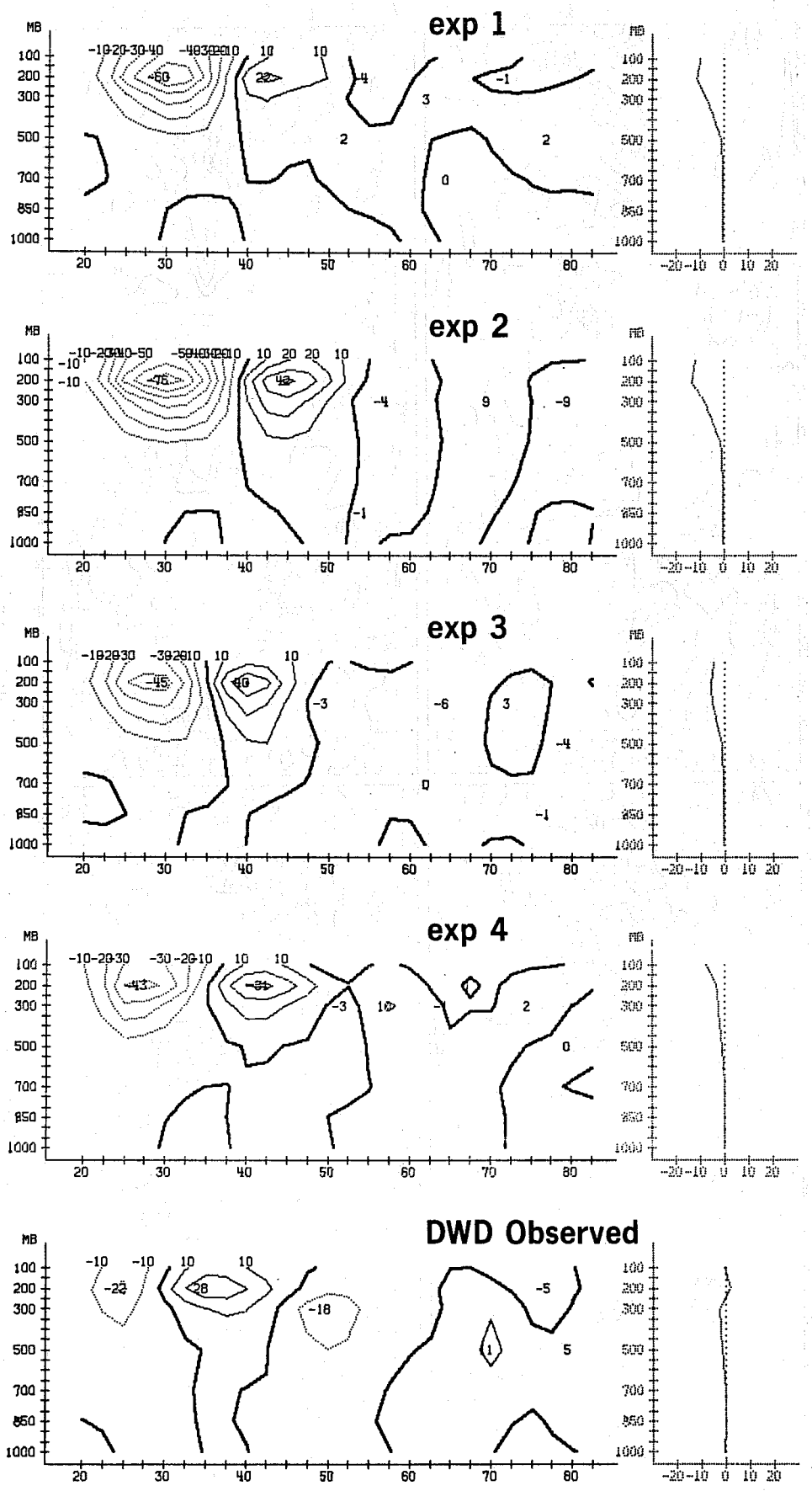

Fig. 55 The 24 day mean conversion of kinetic energy (wavenumber 1...20, unit 1/10 Watt/m^2/bar)

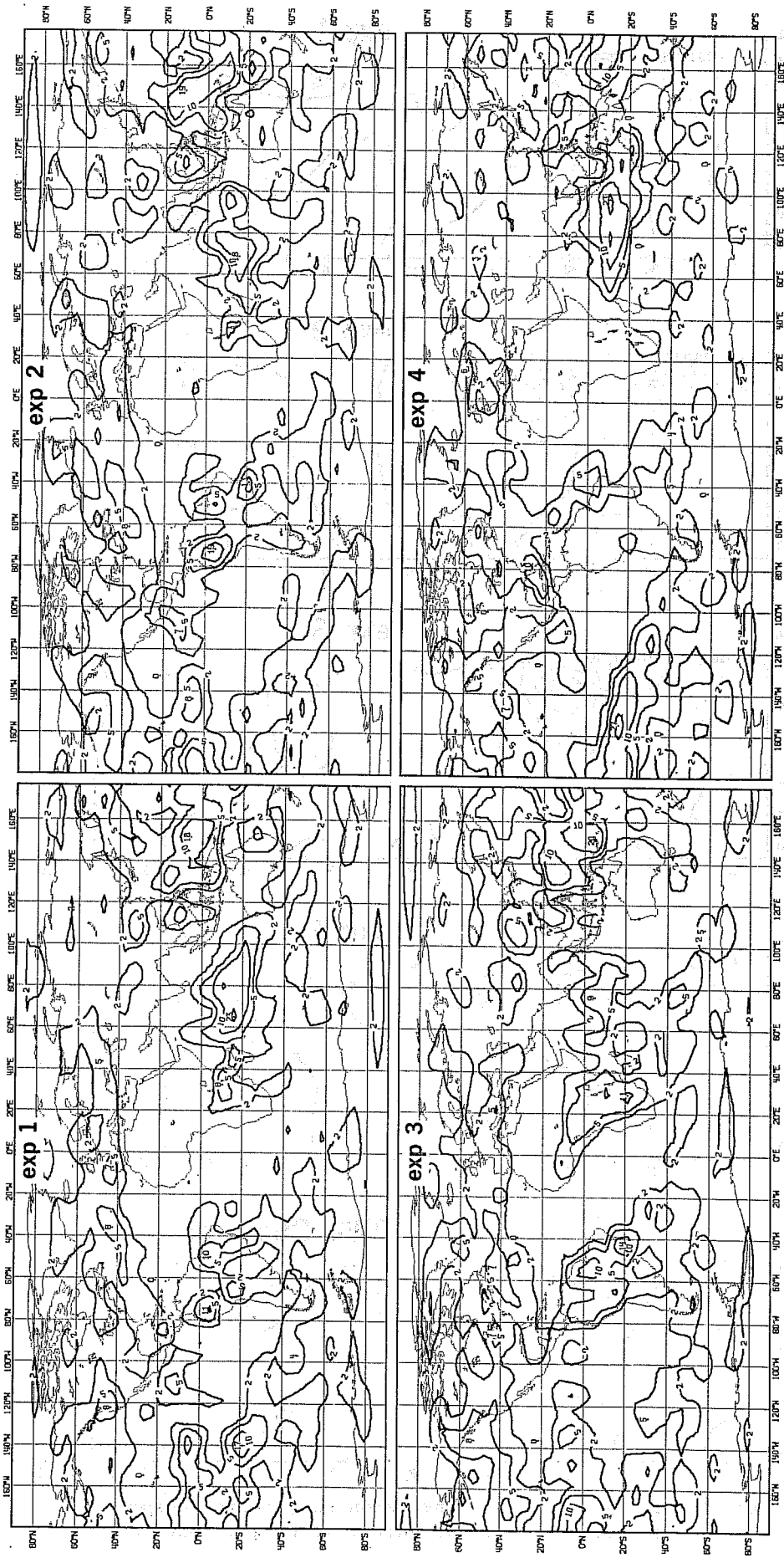

Fig. 56 The 30 day mean precipitation (convective and large scale, unit: mm/day)

5.4 Summary and conclusions

The comparison of four model integrations starting on the same date but with different initial and boundary conditions (one of them starting from an atmosphere at rest) leads to the following conclusion:

The difference in the height field between the models reach the same order of magnitude like the difference of each model run to climate.

The systematic error is independent from the initial data and is produced even in an integration starting from an atmosphere at rest.

The mean state of the model atmosphere seem to be subjected to considerable variance, what makes the evaluation of other experiments testing physical parameterisation in respect of statistical significance difficult.

References

Arpe, K. 1980 Confidence limits for verification and energetic studies ECMWF Tech. Rep. No.18.

Baede, A., Jarraud, M., Cubasch, U. 1979 Adiabatic formulation and organisation of ECMWF's spectral model. ECMWF Tech. Rep. No.15.

Bengtsson, L. 1979 Numerical prediction of atmospheric blocking. Proceedings of the ECMWF Seminar 1979 on Dynamical Meteorology and Numerical Weather Prediction. Vol. 2, 270-329.

Businger, J.A., Wyngaard, J.C., Izumi, Y., Bradley, E.F. 1971 Flux Profile Relationships in the Atmospheric Boundary Layer. J.Atm.Sci., 28, 181-189.

Hollingsworth, A., Arpe, K., Tiedtke, M., Capaldo, M., Savijärvi, H., Åkesson, O., Woods, J.A. 1979 A comparison of medium range forecasts made with two parameterisation schemes. ECMWF Tech. Rep. No.13.

Holloway, J.L., Manabe, S. 1971 Simulation of climate by a global general circulation model: I Hydrologic cycle and heat balance. Mon.Wea.Rev., 99, 335-370

Manabe, S., Smagorinsky, J., Strickler, R.F. 1965 Simulated climatology of a GCM with a hydrological cycle. Mon.Wea.Rev. 93, 12, 769-798.

Manabe, S., Smagorinsky, J., Holloway, J.L., Stone, H.U. 1970 Simulated climatology of a general circulation model with a hydrologic cycle III. Effects of increased horizontal computational resolution. Mon.Wea.Rev. 98, 175-212.

Manabe, S., Hahn, D.G., Holloway, J.L. 1979 Climate simulations with GFDL spectral models of the atmosphere effect of spectral truncation. Rep. of the JOC Conference on Climate Models GARP Publication Series No.22, 41-94.

Mintz, Y. 1964 Very long-term global integration of the primitive equations of atmospheric motion. WMO-IUGG Symposium, Tech.Note No.66, 141-167.

Pruitt, N.O., Morgan, D.L., Lourence, F.G. Momentum and mass transfers in the surface boundary layer. Quart.J.Roy.Met.Soc., 99, 370-386.

Smagorinsky, J., Manabe, S., Holloway, J.L. 1965 Numerical results from a nine level GCM of the atmosphere. Mon.Wea.Rev. 93, 727-768

Sutton, O.G. 1953 Micrometeorology, McGraw Hill, New York.

Tiedtke, M.,Geleyn, J.-F., Hollingsworth, A., Louis, J.-F. 1978 ECMWF model parameterisation of subgrid processes. ECMWF Tech.Rep. No.10.

Williamson, L. 1978 The relative importance of resolution, accuracy and diffusion in short range forecasts. Mon.Wea.Rev. 106, 1, 69-87.